2003

Energy absorption and load management characteristics of aluminum foam-filled braided tubes.

Christopher Richard. Powell
University of Windsor

ENERGY ABSORPTION AND LOAD MANAGEMENT CHARACTERISTICS OF ALUMINUM FOAM FILLED BRAIDED TUBES

by

Christopher Powell

A Thesis Submitted to the
Faculty of Graduate Studies and Research
through the Department of
Mechanical, Automotive & Materials Engineering in Partial Fulfillment
of the Requirements for the Degree of
Master of Applied Science at the
University of Windsor

Windsor, Ontario, Canada
2003

Your file Votre référence
ISBN: 0-612-84592-3
Our file Notre référence
ISBN: 0-612-84592-3

ABSTRACT

The work in this thesis presents the test results of an energy absorber that functions under tensile loading. Unlike conventional energy absorbing devices that function in compression, the aluminum foam filled braided tube design has the capability of absorbing energy in tension under quasi-static and dynamic loading.

A series of quasi-static tests were performed with various aluminum foam densities to understand the relationship between foam density and energy absorption. It was determined from an analysis of the data that a linear relationship exists between foam density and energy absorption per unit volume of aluminum foam.

A numerical model was developed to estimate the energy absorption for a tensile loading condition only. As the dynamic test involves a bending and tensile loading condition, the numerical model is applicable to the quasi-static tests only. The results of this model were compared to the quasi-static test results, with differences ranging from 7% to 59%.

Dynamic tests were performed to investigate the energy absorption capabilities of the aluminum foam filled braided tube in an impact loading condition. The tests that were performed used high density aluminum foams in the braided tube assembly.

This work outlines the procedures and testing of a unique alternative, namely, an aluminum foam filled braided tube, for energy absorption in tension and bending loading conditions.

ACKNOWLEDGEMENTS

The author wishes to express sincere gratitude to **Dr. William Altenhof** for his leadership and guidance throughout the course of this study. I am truly grateful to **Dr. Robert Gaspar** for his support and counseling at the onset of this investigation. Credit is given to **Dr. Murty Madugula** and **Dr. Nader Zamani** for their assistance as committee members.

I am indebted to **Mr. Robert Tattersall** for his assistance and technical expertise in the design and fabrication of the clamping and machine mounting details employed in this study. Special thanks must be given to **Mr. Michael Powell Sr.** for his fabrication skills and collaboration with **Mr. Stan Coulthard** of Propower to provide the required materials to perform the dynamic experimental tests.

The dynamic test segment of this study would not have been possible without the cooperation of **K.S. Centoco**.

The teamwork of **Mr. Mike Powell** and **Dr. Malcolm Matthew** was greatly appreciated for their assistance in the review of this manuscript.

TABLE OF CONTENTS

LIST OF FIGURES

LIST OF TABLES

NOMENCLATURE

C_p	Constant for foam density and plateau stress relationship	$\frac{kg}{m - s^2}$
d	Displacement	m
D	Distance between tows	m
E	Energy	$\frac{kg - m^2}{s^2}$
F	Force	$\frac{kg - m}{s^2}$
H	Height of foam	m
k	Stiffness	$\frac{kg}{s^2}$
ℓ	Length of tow in unit cell of braid	m
L	Length of braided tube	m
n	Constant for foam density and plateau stress relationship	
r	Radius of individual strand of braid	m
R	Radius of braided tube	m
w	Width of tow	m
W	Width of foam	m
U	Energy associated with compression of foam	$\frac{kg - m^2}{s^2}$
x	Displacement	m

Subscript Notation

d_{max}	Maximum displacement	m
E_1	Energy from Region 1 of the braided tube	$\frac{kg - m^2}{s^2}$
E_2	Energy from Region 2 of the braided tube	$\frac{kg - m^2}{s^2}$
E_{EXP}	Energy – experimental test value	$\frac{kg - m^2}{s^2}$
E_{THEO}	Energy – theoretical value	$\frac{kg - m^2}{s^2}$
E_{foam}	Modulus of elasticity for foam	$\frac{kg}{m - s^2}$
F_{COLUMN}	Force required to crush column	$\frac{kg - m}{s^2}$
F_{FOAM}	Force required to crush foam	$\frac{kg - m}{s^2}$
F_{max}	Maximum force	$\frac{kg - m}{s^2}$
F_{TOTAL}	Total force	$\frac{kg - m}{s^2}$
F_{TUBE}	Force constant for braided tube	$\frac{kg - m}{s^2}$
k_1	Stiffness in Region 1 of the braided tube	$\frac{kg}{s^2}$
k_2	Stiffness in Region 2 of the braided tube	$\frac{kg}{s^2}$
ℓ_x	Length of unit cell of braid along its axis	m
ℓ_y	Length of unit cell of braid along its circumference	m
L_{FOAM}	Length of foam	m

L_o	Initial length of braided tube	m
L_{UC}	Length of unit cell of braid	m
R_{eq}	Equivalent radius	m
R_o	Initial radius	m
σ_{pl}	Foam plateau stress	$\frac{kg}{m-s^2}$
ε_D	Densification strain	
θ_L	Braid lock angle	° (degrees)
ρ_f	Foam density	$\frac{kg}{m^3}$
ρ_{fo}	Density of base material of foam	$\frac{kg}{m^3}$

Greek Symbols

δ	Displacement of tube	m
ε	Strain	
θ	Braid angle	° (degrees)
ρ	Density	$\frac{kg}{m^3}$
σ	Stress	$\frac{kg}{m-s^2}$

List of Abbreviations

LVDT	Linear Variable Differential Transformer

Units

mm	Millimetre, unit of length .i.e. 10^{-3} m	
cm	Centimetre, unit of length .i.e. 10^{-2} m	
m	Metre, base unit of length (SI)	
g	Gram, base unit of mass (SI)	
kg	Kilogram, unit of mass .i.e. 10^{3} g	
J	Joule, unit of energy (SI)	$\frac{kg - m^2}{s^2}$
MJ	Megajoule, unit of energy .i.e. 10^{6} J	
N	Newton, unit of force	$\frac{kg - m}{s^2}$
kN	Kilonewton, unit of force .i.e. 10^{3} N	
Pa	Pascal, unit of pressure (SI)	$\frac{kg}{m - s^2}$
MPa	Megapascal, unit of pressure (SI) .i.e. 10^{6} Pa	
in	Inch, unit of length	
G	Gravitational acceleration	
s	Seconds, unit of time	

1. INTRODUCTION

As the levels of impact energy rise in a vehicle crash-impact, the severity of injury increases. In an effort to prevent injury to the occupants, vehicle safety standards have been revised to mandate improvements to occupant crash protection. These changes have required automobile manufacturers to invest countless hours of research to improve the crashworthiness of their products.

Crashworthiness is the ability of a vehicle to prevent occupant injuries in the event of an accident. One example of a method to improve this characteristic is the inclusion of crumple zones into the design of the vehicle to compress, crush and therefore absorb energy in the event of an accident. These methods are grouped in a category known as 'passive' safety devices that provide occupant safety and a means of protection for the structure of the vehicle that function only in the event of an accident.

Automotive applications require these light weight, high energy absorption capacity materials to meet crashworthiness and occupant safety requirements. Several areas of an automobile use these materials within the design of energy absorbing devices to provide protection to the structure of the vehicle and the occupants in the passenger compartment in the event of a front or side impact.

One area where an energy absorbing device is used to protect the structure of the vehicle is in the automobile bumper. In this area, the energy absorber is incorporated into the design of the bumper mount to create a 'crash box'. An impact to the bumper area will result in axial compression of the 'crash box', thus minimizing any plastic deformation of the vehicle body frame. Following impact, the resulting deformed structure can be exchanged to reduce the cost and time to repair the vehicle. An example of this type of device can be seen in Figure 1-1.

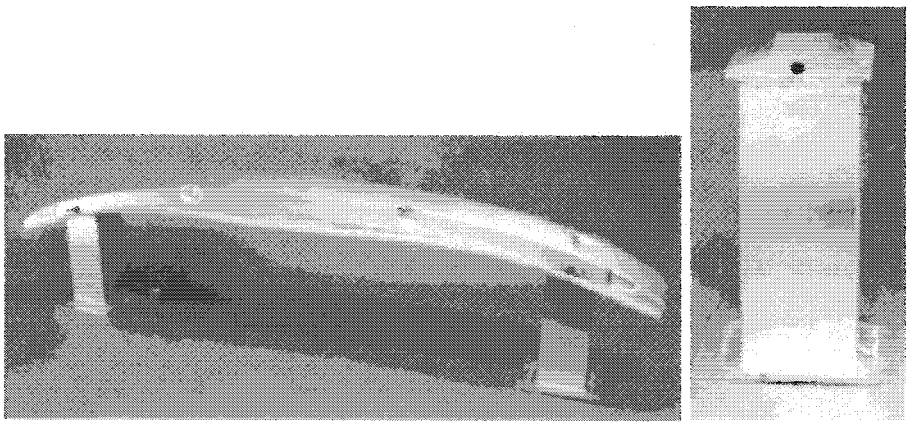

Figure 1-1: Automobile bumper and bumper mount energy absorber [1]

This application in the bumper is mainly for impacts below 15 km/h where contact is localized to the bumper of the vehicle. These are considered 'low speed' impacts and represent a large number of motor vehicle accidents. Due to the high number of these types of accidents, it is beneficial that a device such as this is used to protect the vehicle structure. Through deformation of the energy absorber in the bumper, the vehicle body and frame are protected in the front impact scenario.

Although the bumper provides protection to the vehicle and contributes to the overall energy absorption to protect the occupants in a frontal impact, there are no axial-type energy absorption devices to provide protection for an impact to the side of a vehicle. A side impact presents a special case where the structure is subjected to a bending load. This represents the most severe type of accident, as intrusion into the passenger compartment by the impacting mass is possible. Devices that are used to strengthen the vehicle structure and absorb side impact energy are side impact beams, which are mounted in the doors of the vehicle as shown in Figure 1-2.

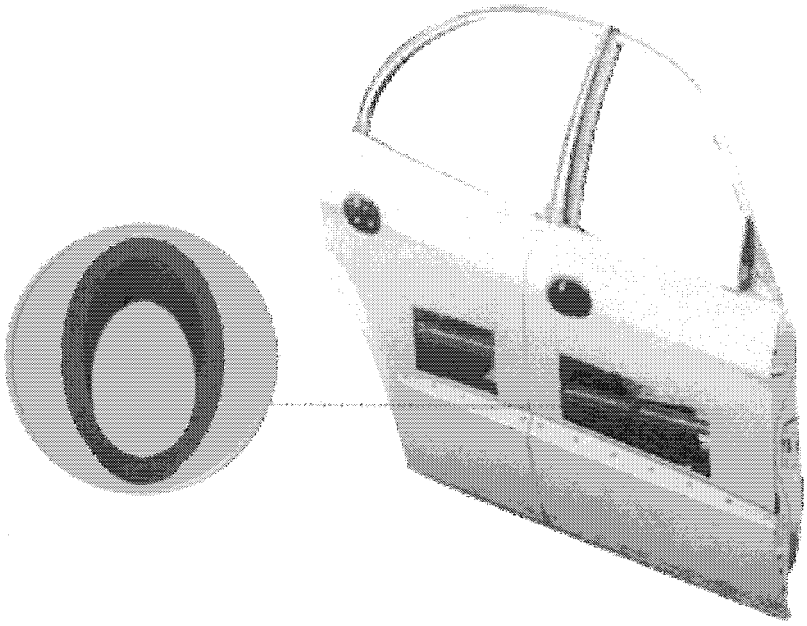

Figure 1-2: Side impact beam mounted in doors of vehicle [2]

The drawback of the side impact beam is that any energy absorption is localized to the immediate area that undergoes bending. It would be beneficial if the overall length of the beam could deform and contribute to the absorption of impact energy. This type of device is primarily used to stiffen the body of the vehicle to prevent intrusion of the impacting vehicle into the passenger compartment.

In each of these cases, the devices function under compressive and bending loading and function in a satisfactory manner for their respective applications. As requirements for occupant safety increase, there has been research into the introduction of materials that have the capability to provide additional energy absorption without excess weight to enhance these existing devices. The limitation of these materials is that energy absorption is difficult under tensile loading conditions.

There are application areas within an automobile where a device that absorbed energy in both tensile and bending loading situations would enhance crashworthiness. Through the literature reviewed for this study, it was observed that little research has been performed on energy absorbing structures under tensile loading conditions. The need exists for an energy absorber to control the energy absorbed under these loading conditions to satisfy a number of applications.

1.1 Layout of the Thesis

This thesis is comprised of ten chapters, which are outlined below.

Chapter 2 reviews the literature that was examined for this thesis. The citation of each reference is done by numerical notation.

Chapter 3 presents the proposed research for this study.

Chapter 4 presents the experimental work performed to show the stress – strain relationships of aluminum foams of various densities under quasi-static compression.

Chapter 5 details the quasi-static experimental work and analysis that was completed for this study.

Chapter 6 investigates the theory behind the numerical prediction for the energy absorption of a braided tube and compares the results of the numerical solution to the quasi-static experimental work.

Chapter 7 presents the dynamic impact test work that was performed and the analysis of the test results.

Chapter 8 summarizes the results of the research and discusses how the objectives of the study have been satisfied.

Chapter 9 provides a list of recommendations for further development of the energy absorbing device as well as future research opportunities.

Chapter 10 provides a listing of the cited references and additional references used for background material in the research and preparation of this thesis.

2. LITERATURE REVIEW

The fundamental basis of this study was to investigate the use of a stainless steel braided tube filled with aluminum foam for the purpose of acting as an energy absorber. For that consideration, literature was reviewed for this study considering topics of crashworthiness, energy absorbers, aluminum foam, and braided tubes.

2.1 Crashworthiness

The automotive industry is driven to make changes to vehicles to improve crashworthiness to comply with Federal Motor Vehicle Safety Standards. Constraints on vehicle fuel economy call for the changes that are performed to incorporate high strength, lightweight materials in order to reduce the overall weight of the vehicle. Early work with non-structural energy absorbing devices by Lin and Mase [3] concluded that "... it was possible to absorb extra crash energy without increasing the vehicle crush distance and passenger compartment deformation by inserting add-on energy absorbing devices in the unutilized space along existing load paths." This early work supports the use of a 'crash box' to absorb impact energy without detrimental effects to the vehicle structure. In addition, Lin and Mase also performed theoretical work with several different types of energy absorbing media, including honeycomb foam, glass/epoxy tubes, Kevlar/epoxy tubes, graphite/epoxy tubes, steel tubes, and aluminum tubes.

Experimental work by Fuganti et al. [1] dealt with the integration of aluminum foams to an automotive bumper application. Their work was the use of aluminum foams in a crash box application attached to an automobile bumper in static and dynamic testing. The results of the experiments showed that aluminum foam filled crash boxes met the design constraints of energy absorption, maximum force transmitted and size. The advantages of the crash box in this case were found to be a weight savings of 10%, crash box size reduction of 30% and crash box volume reduction of 60%.

This work was further validated by experimental tests using a similar test arrangement and numerical simulations by Hanssen et al. [4]. The finite element model was able to predict the whole crushing of the bumper with an acceptable accuracy when compared to the experimental results.

2.2 Energy Absorbing Structures Containing Aluminum Foam

Typical energy absorbing devices that were found in the literature review were extruded tubes filled with aluminum foam in axial compression. Figure 2-1 shows a typical plot of the force – displacement profile of a foam filled extruded tube energy absorber under axial compression. The maximum force required to initiate crush and the energy absorption capacity of the structure are important attributes. An ideal energy absorber would have two significant characteristics: the maximum force equal to the average force required to crush the structure and a high deformation capacity. For a practical application, an energy absorber

would be selected such that the maximum force in deformation would not cause damage to the item that the absorber is protecting.

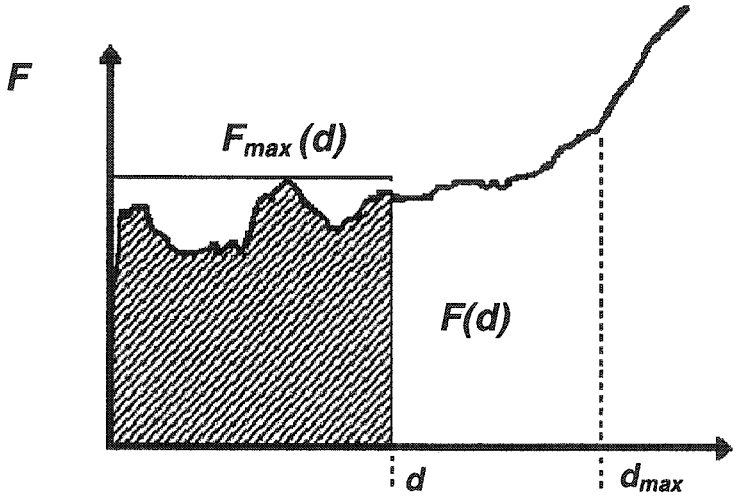

Figure 2-1: Force – displacement curve of energy absorber under axial compression [5]

An ideal energy absorber has a flat force – displacement curve such that the absorber folds at a constant force. The force – displacement plots contain peaks of variation due to the folding stage of the absorber.

The energy absorbed by the structure during the crushing process is identified as the area under the force – displacement curve. This value is defined as E(d) and can be obtained by integrating the force – displacement curve.

$$E(x) = \int_0^d F(x)\, dx \qquad \text{Equation 2-1}$$

Figure 2-2 shows the corresponding energy – displacement curve for the specimen under axial compression.

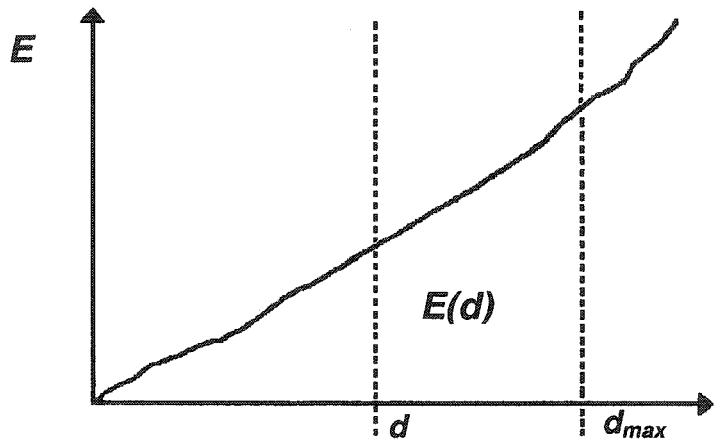

Figure 2-2: Energy – displacement curve of energy absorber under axial compression [5]

2.3 Aluminum Foam

Metal foams are materials that are gaining acceptance for their mechanical, acoustic, and thermal properties. Aluminum foams in particular are used in various areas such as furnishings, wall coverings and ceiling tiles, in addition to their application as an energy absorbing media [6]. Of particular interest to the automotive industry is the high strength to weight characteristic of aluminum foam. Low weight and high energy absorption are properties that make aluminum foams favorable for integration into an automobile to improve the vehicle crashworthiness.

In quasi-static compression, aluminum foam exhibits a stress-strain relationship as shown in Figure 2-3. The curve is characterized by a short elastic

region with slope E_{foam}, followed by a long horizontal plateau of stress σ_{pl} and a rise in the stress at the densification strain ε_D. It is this type of deformation behavior that is desirable for materials used in energy absorbers.

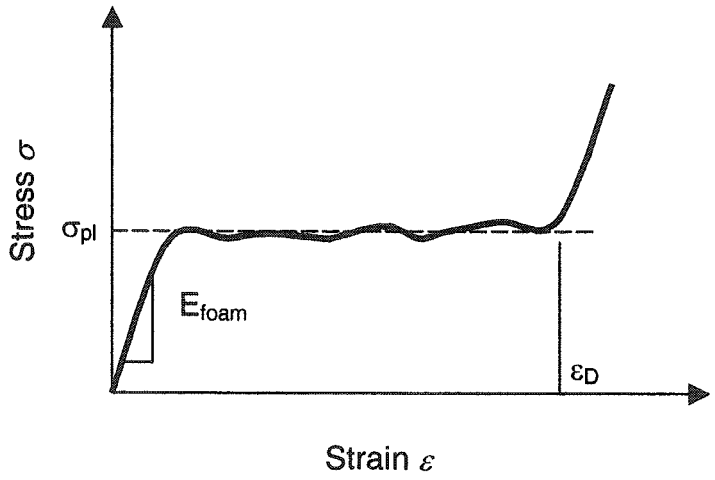

Figure 2-3: Stress – strain relationship for aluminum foam in compression

2.3.1 Open Cell and Closed Cell Aluminum Foams

There are two types of aluminum foams that are available. These foams vary by their basic cellular structure. These two types are open cell and closed cell foams.

Open cell foams resemble a lattice-type structure as shown in Figure 2-4. This type of foam is produced by filling an open cell polymer foam with a slurry of heat resistant material. After drying, the polymer is removed and a molten alloy is cast into the cavity. Once solidified, the mold material is removed leaving the open celled, continuously connected structure. This type of foam can be cast for complex three-dimensional structures.

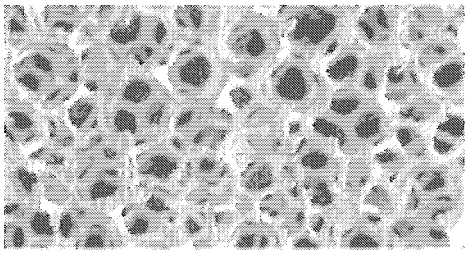

Figure 2-4: DUOCEL open-cell aluminum foam [7]

The closed cell foam under consideration in this study is the product of Cymat Aluminum Corporation [8]. As seen in Figure 2-5, a closed cell foam resembles the cellular structure of a sponge. The Cymat foam casting process is a method that uses a metal matrix composite additive to stabilize the walls of the cellular structure when a gas, typically air, is introduced to the molten metal. This is a continuous production method that yields an average of 900 kg/hour of aluminum foam. [7]

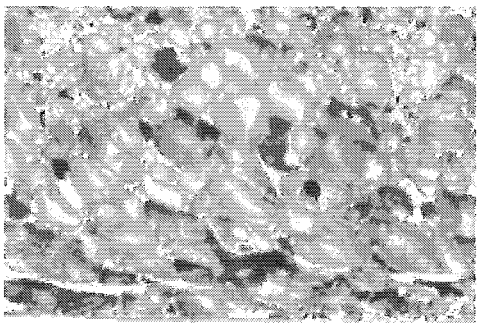

Figure 2-5: Cymat closed-cell aluminum foam

2.3.2 Research on Aluminum Foams

A significant amount of work has been done with aluminum foams and their inclusion in extruded tubes in axial compression and bending.

Hanssen, Hopperstad and Langseth [9] performed research with aluminum foams included in circular and square cross-section tubes in axial compression. The experiments utilized both quasi-static and dynamic testing methods and revealed that the aluminum foam had the effect of increasing the stiffness of the tube wall, resulting in an increased buckling load and higher energy absorption of the structure. As seen in Figure 2-6, the tube with foam filler had a higher number of sidewall lobes than the tube without the foam. The increased number of lobes is due in part to initial buckling taking place in the sidewalls in the early stages of loading. The foam filler forms an elastic foundation for the sidewalls, offering resistance for lobes moving inwards. The foam provides internal support to the wall that reduces the buckling length of the sidewall resulting in an increased buckling load compared to the tube without foam filler. [5, 9, 10]

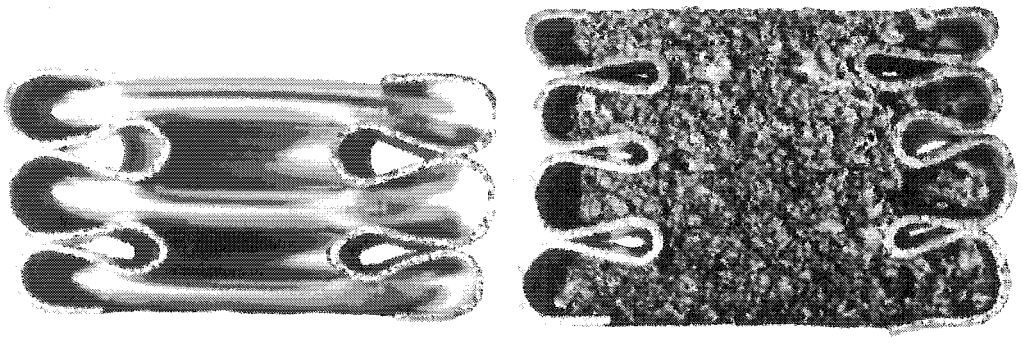

Figure 2-6: Non-filled and filled square tubes under quasi-static compression [5]

Gradinger et al. [11] performed similar work with aluminum foam filled tubes in compression. Their work involved single tube foam filled specimens and double tube specimens, where the foam was inserted between the inner and outer tubes. The experiments revealed that the foam created an 'interaction effect' between the tube wall and the aluminum foam that affected the buckling mode of the tube. This change in the buckling mode resulted in a higher number of folds in the tube that led to higher energy dissipation due to the increased plastic deformation of the tube wall.

The summation of individual energies of crushing the foam and the tube alone does not equal that of the foam-tube assembly. The differential between the two is known as the 'interaction effect'. The addition of the foam to the tube results in additional energy absorbing ability due to the deformation of the tube wall interacting with the foam core and is illustrated in Figure 2-7.

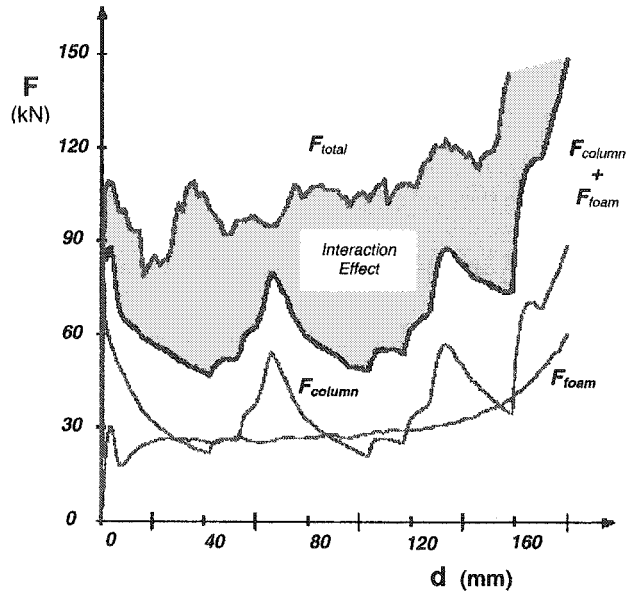

Figure 2-7: Force – displacement curve for compression of tube and foam [9]

2.3.3 Effect of Foam Density

It can be seen in the work of Langseth, Hopperstad and Hanssen [12] that the energy absorbing capacity of aluminum foam holds a relationship to the foam density under axial compression. Through experiments in quasi-static testing of square cross-section tubes in compression, Langseth et al. found that as foam density increased the specific force required to crush the test specimens increased and the force – displacement curve tended to be more stable. Regarding the energy absorbing capacity, Langseth et al. found the mass specific energy increased with higher foam densities.

2.3.4 Aluminum Foam Filled Sections in Bending Loading

Santosa, Banhart and Wierzbicki [13] conducted research on foam filled sections in bending with an application for use in automobile structures. Their work involved a thin walled stainless steel extrusion filled with aluminum foam placed in three point bending. Their conclusions were that the foam filler increases the number of folds in the crushing failure mode and prevented a drop in the load carrying capacity of the beam. In the fail mode, there are additional plastic hinge lines formed due to the addition of the foam and this produces a limited amount of crush over the section. As a result, more bending energy can be dissipated with this structure.

Additional work by Santosa, Banhart and Wierzbicki [14] involved partial filled stainless steel structures in bending. Aluminum foams were inserted into the areas that were subjected to bending loads. The advantage of this type of

structure was a reduction in overall weight. Testing was performed on the beams targeting these areas in the test. Similar to the previous work, their conclusion was that partial foam filling offers a significant reduction in foam weight while maintaining higher crush resistance.

2.4 Braided Tubes

Braided fibre architecture resembles a mixture of strand winding and weaving. Tubular braid features seamless fibre continuity from end to end of the tube. Like woven materials, braided fibers are mechanically interlocked with one another. When used as a composite reinforcement, braid exhibits remarkable properties because it is highly efficient in distributing loads. In general, all the fibres within a braid are continuous and mechanically locked; it has a natural mechanism that distributes load evenly through the structure. As all of the fibres of a braided structure are subject to loading during an impact or loading occurrence, braid absorbs high amounts of energy as it fails.

2.4.1 Braid Manufacturing Process

Braid is manufactured on machinery that is designed to interweave the strands. The filaments of the braid are woven around a molding tool or core mandrel in a continuous spiral pattern. Figure 2-8 shows a typical wire braid manufacturing machine producing braided tube coverings for medium pressure hose applications.

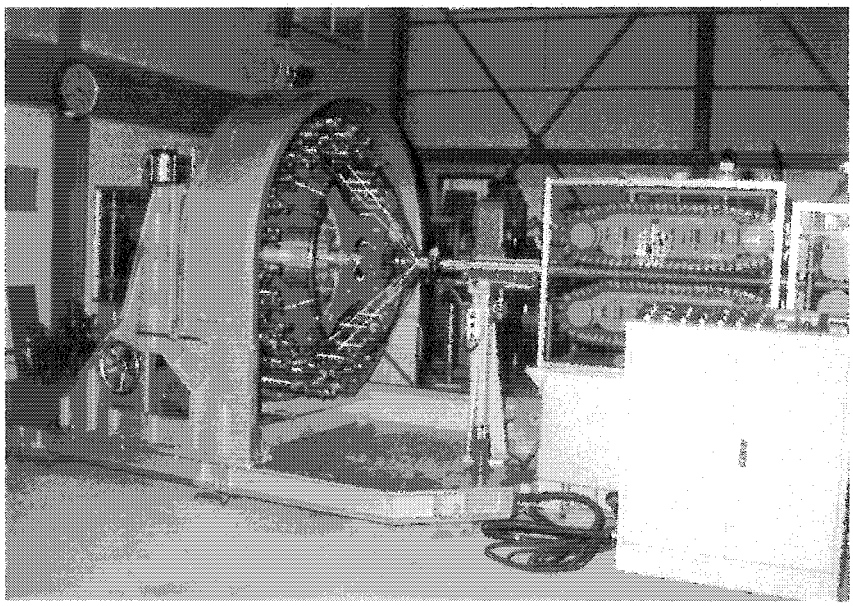

Figure 2-8: Wire braid manufacturing machine [15]

This manufacturing process is similar to the production methods used in the textile industry. This sector of industry performs a great deal of research on cloth and yarn materials and was a source of information and research papers for this study.

2.4.2 Research on Braided Tubes

Research on braided tubes was carried out in the areas of the textile industry and was published in engineering journal papers. The specific topics included the manufacture of braided tubes and the mechanics and energy absorption of braided tubes.

The construction of a braided tube is similar in nature to the manufacture of a fabric. The strands of the braid are interwoven to form a cloth-like arrangement. The starting point for an investigation into the physics of braid

construction is with the textile industry. Papers that dealt with friction between the fibers of a braided structure [16] and strand interaction in braided textile structures under tensile loading [17, 18] were produced by this industry.

The textile industry provided good information regarding the mechanics of the individual strands of the structure, which would benefit a computational analysis. For the braided tube as a whole structure, the mechanics and energy absorption properties are best defined by Harte and Fleck [19] and Harte, Fleck and Ashby [20].

Harte and Fleck [19] performed experimental tests on braided composite tubes in tension. The focus of their study was to determine the effects of braid angle and to determine the stresses and mechanics of deformation in the neck of a braided tube under tensile loading. In their tests, four different helix angles of braid were placed under axial tension. It was found that the braids with small helix angles failed at low strains, whereas the braids with the largest helix angle stretched by a nominal strain of up to 60%. For the specimen with the largest helix angle, the diameter of the braid decreased and neck propagation at a constant stress occurred. This is significant as the amount of energy absorbed can be determined as being the product of the yield stress and the strain at failure. The large strain of this specimen at the constant stress suggests that braided composites with initial helix angles over 45° have potential as energy absorbers as they deform in tension at constant stress over large strains.

Harte, Fleck, and Ashby [20] also studied foam filled tubes with braided composite walls as energy absorbing devices. Their work involved quasi-static tests on glass fibre/epoxy braided tubes with polyurethane foam cores in both tension and compression. In a comparison between the tension and compression tests, they observed a pronounced load peak that occurred in the compression test, but not in the specimen under tension. This peak load reduces the crashworthiness of the braided tube and foam core structure, as it leads to an increased acceleration rate of the crashed body. The crush force efficiency, expressed in Equation 2-2, is a measure of the average crushing force (F_{AVG}) and the peak force (F_{PEAK}). As a result of the high load peak in the compression test, the crush force efficiency of the structure is reduced. This draws the conclusion that there is a benefit to an energy absorber in tension, in that there is no peak load at the onset of loading as in compression.

$$\eta = \frac{F_{AVG}}{F_{PEAK}} \qquad \text{Equation 2-2}$$

In addition to their experimental work, Harte, Fleck and Ashby [20] developed models to provide a theoretical prediction of energy absorption for the glass fibre/epoxy braided tube and polyurethane foam core specimen in both tension and compression. They found that their analytical model for energy absorption consistently exceeded the measured experimental values in excess of 50%. It was concluded that this was due to material property changes over the large plastic strains that were not considered in the analytical model.

3. PROPOSED RESEARCH

From the literature that was reviewed, there has been little work with energy absorbers under tensile loading. For energy absorbers that were tested under compression, reduced crush force efficiencies have been realized that reduce the crashworthiness of these structures. In specimens under bending loads, the addition of aluminum foam enhances energy absorption, however it is localized to the immediate area subjected to the bending load.

Based on these concerns with current energy absorbing devices, investigation is required for a device capable of energy absorption under tensile loading which, at the same time can also maximize energy absorption through deformation along its entire length.

3.1 Proposed Energy Absorption Device

The proposed research study is to investigate the use of an aluminum foam core within a stainless steel braided tube as an energy absorber. As aluminum foams have demonstrated excellent energy absorption properties under compressive loading, their inclusion within a stainless steel braided tube may result in an effective energy absorber.

The device under study is an assembly that consists of a stainless steel braided tube with an aluminum foam core. The tube is comprised of continuous stainless steel strands processed to form a fabric-like braid as shown in

Figure 3-1. This material is also commonly known as overbraid and is used as reinforcement for high-pressure hoses.

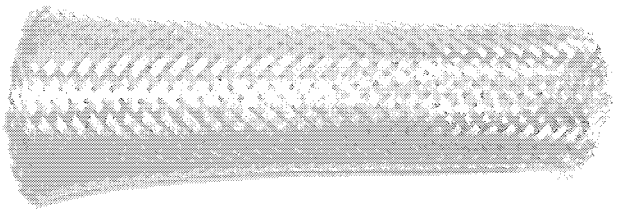

Figure 3-1: Stainless steel braided tube

The braided tube is the essential component, as it has the advantage that the diameter of the tube reduces as the tube is elongated. When an aluminum foam core is installed into the tube, any tension placed on the tube will result in a decrease in tube diameter and crushing of the aluminum foam core. In the event of an impact in one region of the tube transverse to the tube axis, a stretch in the tube due to impact would give rise to a decrease in tube diameter where the internal aluminum foam would be crushed.

The aluminum foam is a material that resembles a sponge but that, unlike a sponge, undergoes plastic deformation when compressed. A sample of aluminum foam can be seen in Figure 3-2.

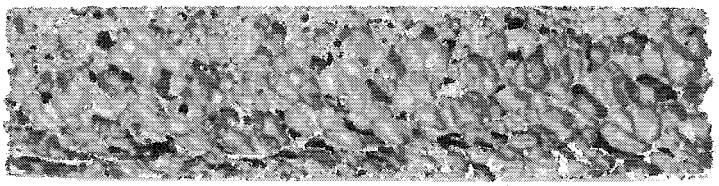

Figure 3-2: Sample of aluminum foam

Aluminum foam is commonly used in compression and is considered an excellent material for the application of absorbing mechanical energy due to its high strain capacity and deformation under an almost constant stress.

3.2 Types of Testing

Experimental testing is required to evaluate the effectiveness of any device or system as an energy absorber. Tests must be carried out in a standardized procedure to ensure the validity of the data that are collected. There are two types of tests to investigate the functionality and capability of this energy absorbing device, quasi-static tensile testing and dynamic impact testing. These two distinctively different methods of testing each have advantages and disadvantages of obtaining the desired test results.

3.2.1 Quasi-static Tensile Testing

Quasi-static tensile testing requires that the specimen be placed in a test fixture and secured in a standard test machine as seen in Figure 3-3. The test sample is then placed under a tensile load at a slow rate of increase of force. The machine fixture is equipped with a load cell for monitoring force and a linear variable differential transformer (LVDT) to measure the elongation of the sample. This test method is inexpensive and is used to determine the load management or force – displacement relationship of the sample under tensile loading. The limitation of this type of test is that any effects relating to the materials that vary with the rate of loading are not captured. This type of test provides valuable

information on the energy absorbing capacity and strength of a test specimen as it can be loaded until failure.

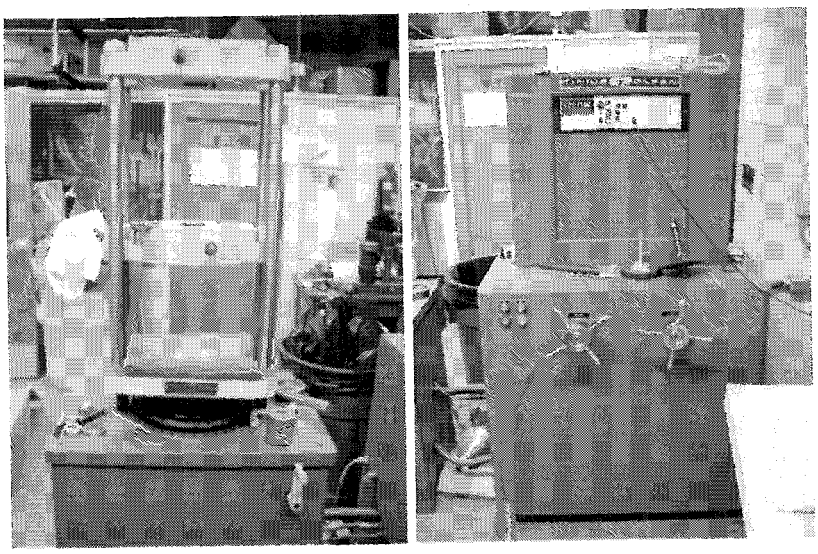

Figure 3-3: Tinius Olsen test fixture and test machine

3.2.2 Dynamic Impact Testing

Dynamic impact testing is a method where a mass is impacted on to the test specimen in a direction perpendicular to its axis. Test equipment that is commonly used for dynamic impact testing includes drop towers and impact sleds. For this investigation, a drop tower tester was used. A cylindrical impactor was fastened to a vertical translating crosshead, which served as the impacting entity in this research. The crosshead was instrumented with an accelerometer to determine the acceleration of the impacting mass and a LVDT was fastened to the translating crosshead to determine the displacement at impact. The crosshead traverses in the vertical direction and impacts the test specimen. Figure 3-4 shows the drop tower test machine used in this study.

This type of test is typically more expensive to perform due to the unavailability of lab environment test machines. This test can validate data gathered from quasi-static tensile testing and can precisely define the test specimen's interaction in a dynamic environment.

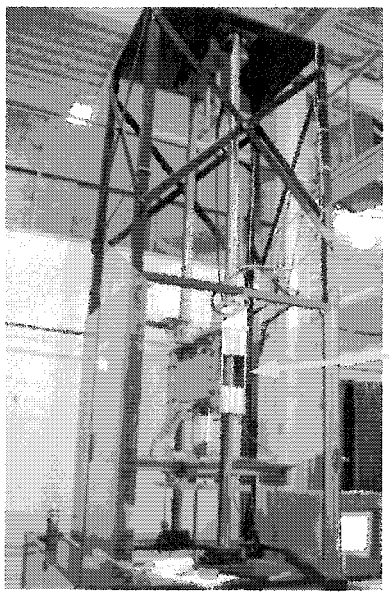

Figure 3-4: Drop tower test machine

3.2.3 Testing Standards

A review of the testing techniques and standards of the various test standard organizations such as Society of Automotive Engineers and American Society for Testing and Materials did not reveal a test method for a braided tube – aluminum foam assembly. In addition, no standards were available from any previous literature studied to test the braided tube-aluminum foam in tension or impact. Testing standards needed to be developed for this study to gather data in quasi-static tensile and dynamic impact testing.

3.3 Objectives of the Study

The objectives of this research were to determine the energy absorbing capabilities and load management characteristics of an aluminum foam filled stainless steel braided tube. This investigation used quasi-static tensile testing methods to determine the load management characteristics and the feasibility of this device as an energy absorber. A theoretical model was developed and compared to the quasi-static tensile test results. Dynamic testing methods were the third area of study to validate the quasi-static testing methods and to place the device into a real-life impact situation to determine its effectiveness as an energy absorber.

It is believed that this structure is an effective energy absorber in both quasi-static and dynamic loading conditions and that the theoretical approximation of energy absorption for the structure provides a suitable estimate for the energy absorbing capability.

This research determined the energy absorbing capabilities of the stainless steel braided tube – aluminum foam structure by focusing on the following aspects:

i. Developing a testing procedure to standardize trials.

ii. Performing quasi-static test studies on structures with various densities of aluminum foam.

iii. Establishing a mathematical model for estimating energy absorption of this device for quasi-static cases.

iv. Performing dynamic test studies using a drop tower test machine.

4. MECHANICAL CHARACTERISTICS OF ALUMINUM FOAM

The mechanical characteristics of aluminum foam are important for the present research. The deformation behavior of the aluminum foam during compression provides information for levels of energy absorption and the plateau stress to compress the foam to densification.

In preparation for testing, the geometry and mass of the foam specimens were measured to determine the density for each specimen. A sample of parts was separated from the collection for quasi-static compression testing to determine the plateau stress of the foam samples, rather than make use of the power law calculation that relates foam density and plateau stress, which will be discussed later in Chapter 6, Section 6.2.1.

4.1 Test Procedure

The testing was carried out using the Tinius Olsen test machine. It was determined that the low density foam specimens required the 60 kN force range setting on the tester to complete the compression of the specimens and the high density foams required the 150 kN force range. Each test was performed with a nominal crosshead speed of approximately 0.1 mm/s on the Tinius Olsen test machine. Detailed dimensions for each of the foam specimens can be found in Appendix A.

4.2 Low Density Foam Test Results

All test specimens were positioned as shown in Figure 4-1. This provided a ratio of length to width to height ratio of 1.53: 0.95: 1 respectively for the two low density foams available for test. Although not a perfect cubic specimen, this ratio was sufficient for the compression test. To minimize any effects of friction, teflon plates were placed on the top and bottom of the specimen for the low compression foam test with Foam #27.

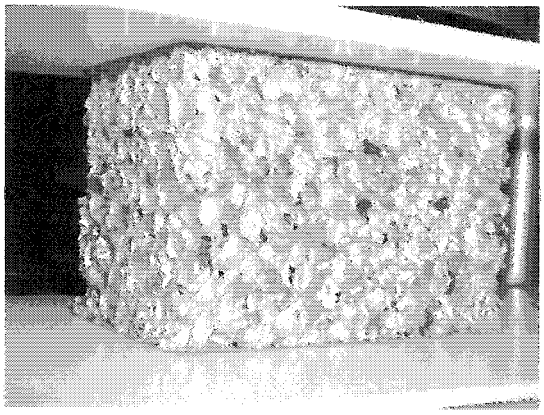

Figure 4-1: Position of Foam #27

Figure 4-2 shows the stress – strain curve for the low density foam specimens. The densities for Foam #27 and Foam #28 were 240.0 kg/m^3 and 231.1 kg/m^3 respectively.

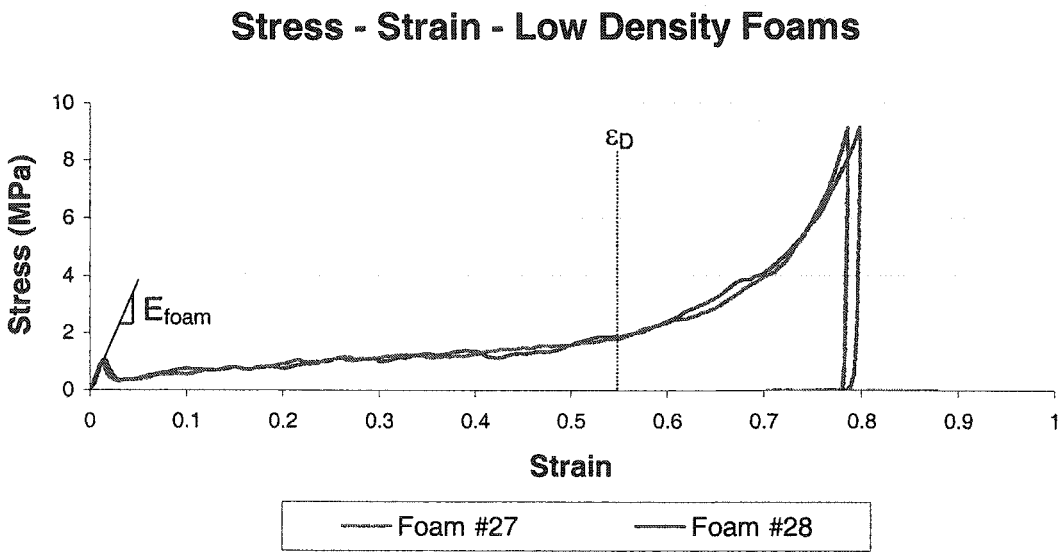

Figure 4-2: Stress – strain for low density foam specimens

The modulus of elasticity (E_{foam}) was calculated to be approximately 72 MPa for the two low density foams. The densification strain ε_D was determined to be in the region of 0.55. The results indicated a plateau stress of approximately 1 MPa for each foam brick and that friction effects were negligible, as the two specimens are very similar in their stress – strain relationship. The strain of the low density foam is very high, indicating that it was able to compress over a large displacement. Measurements indicated that both Foam #27 and Foam #28 were identical in size prior to compression testing. To illustrate this, Figure 4-3 shows Foam #27 after the compression test, in comparison to Foam #28 prior to its test. The height of the compressed Foam #27 is approximately 20% of the original sample and the width of the sample is very similar to the original size, indicating negligible Poisson's effects.

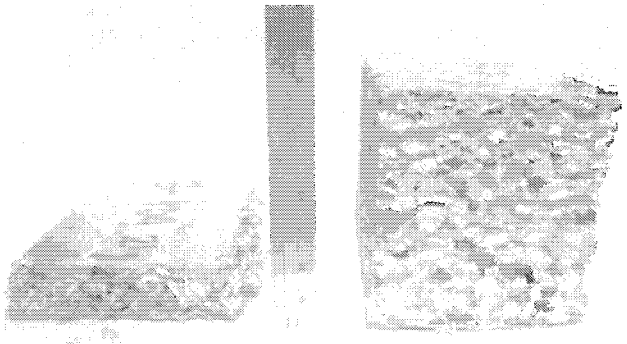

FOAM #27 - AFTER **FOAM #28 - BEFORE**

Figure 4-3: Foam #27 and Foam #28 compression

4.3 High Density Foam Test Results

There were two sets of tests carried out with the high density foams, each with different length / width / height ratios. The first test pieces were similar in size to the low density foam, with a greater length to height ratio. The specimens in the second set of tests had a shape that was closer to a cubic form.

4.3.1 High Density Foam – Test Set #1

The dimensions of the high density foam blocks were slightly different from the low density, providing a length to width to height ratio of 1.65: 1.02: 1. Foams #32 and #33 with this profile ratio were tested and the results can be seen in Figure 4-4. The densities for Foam #32 and Foam #33 were 418.6 kg/m^3 and 416.5 kg/m^3 respectively.

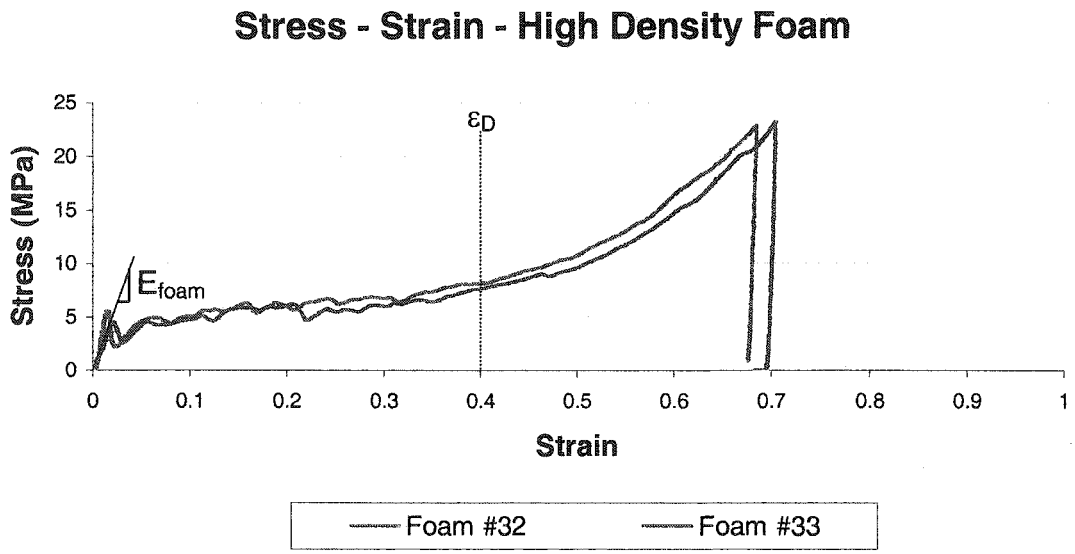

Figure 4-4: Stress – strain for high density foam specimens

The modulus of elasticity (E_{foam}) was calculated to be approximately 120 MPa for Foam #32 and approximately 142 MPa for Foam #33. The densification strain ε_D was determined to be in the region of 0.40. The results indicated that the high density foams had a plateau stress of approximately 6 MPa. The strain is not as high as the low density foam, as can be seen in Figure 4-5 that shows an uncompressed and compressed brick of high density foam. The height of the compressed brick is approximately 40% of the original sample as can be seen with the compressed Foam #32 and uncompressed Foam #33. Similar to the low density foam specimens, the width of the compressed sample is very close to the original width, indicating negligible Poisson's effects in the high density specimens.

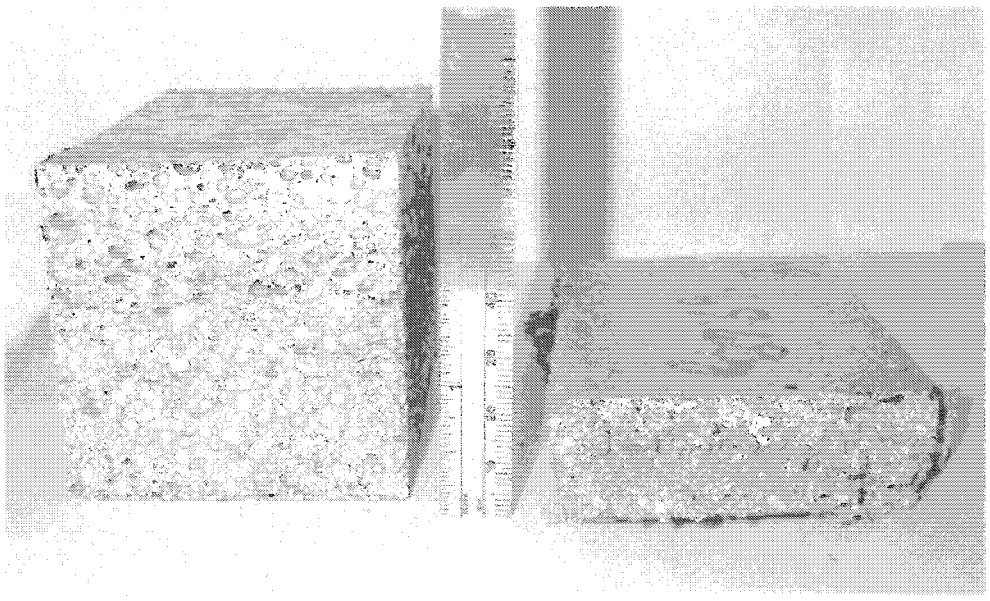

FOAM #33 - BEFORE **FOAM #32 - AFTER**

Figure 4-5: Foam #33 and Foam #32 compression

4.3.2 High Density Foam – Test Set #2

The second set of tests with the high density foam used Foams #34 and #35, two smaller test specimens with a profile ratios of 0.77: 1.03: 1 and 0.84: 1.02: 1, length to width to height. Results from these specimens can be seen in Figure 4-6. The densities for Foam #34 and Foam #35 were 426.9 kg/m^3 and 422.0 kg/m^3 respectively.

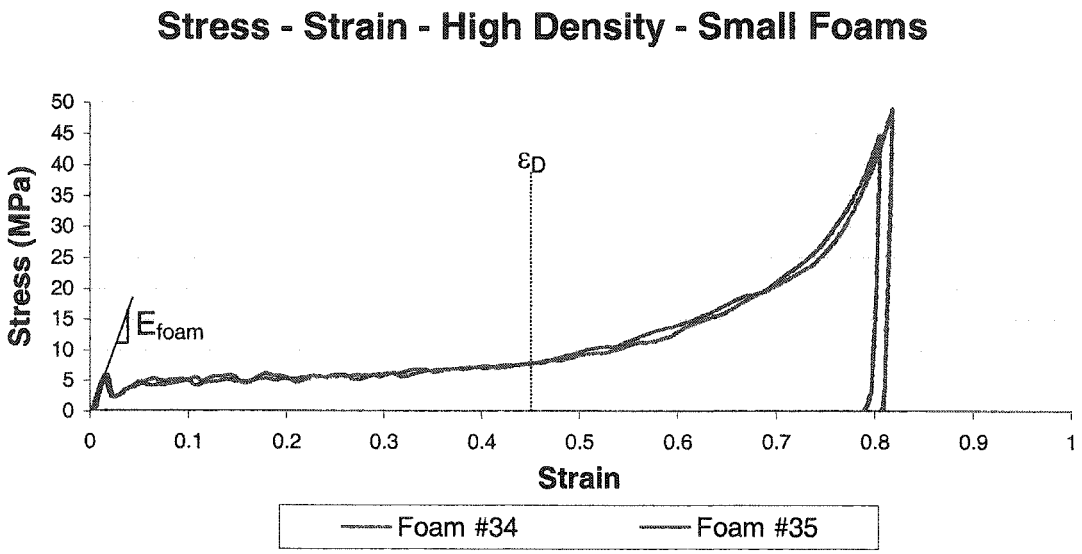

Figure 4-6: Stress-strain relationship for reduced profile foams

As can be seen in the plots, the high density foams with the reduced profile ratio were able to crush significantly more. This was due to the smaller cross sectional area using the same range of compressive force that the larger profile foams used. The modulus of elasticity (E_{foam}) was calculated to be approximately 160 MPa for the two foam specimens. The densification strain ε_D was determined to be in the region of 0.45. The plateau stresses remain similar to the previous samples, at approximately 6 MPa, as can be seen with the two sets of foams overlaid in Figure 4-7. Foam #32 and #33 are larger profile foams and #34 and #35 are reduced profile foams.

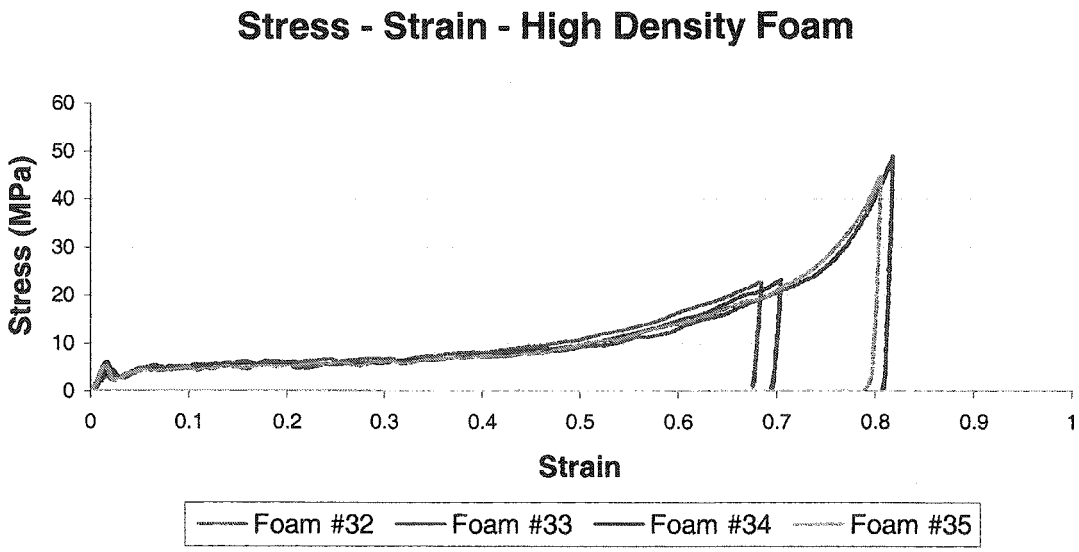

Figure 4-7: High density foams – Large and reduced profile

5. QUASI-STATIC TENSILE TESTING

Quasi-static tensile testing is a method of experimental investigation where tensile loading conditions are applied at a slow rate of increase on a test specimen. This testing method is often used to characterize mechanical properties and can be used to develop material models that can be used in finite element analysis models. Quasi-static tensile testing is used to qualify the test component against a specification or to support the product development process.

The advantages of this test method are:

i. Slow rate removes element of time dependency

ii. Proves the functionality of the design

iii. Provides an accurate estimate for dynamic tests in most cases

iv. Less expensive than dynamic tests

v. Determine energy absorption capacity

The early experimental tests carried out were performed to develop an improved clamping mechanism and then determine the energy absorbing abilities of the tube/foam specimens. To minimize errors in testing, procedures were written to ensure the assembly of the test specimens and the steps and process parameters, such as rate of speed of the test, in the testing process were similar.

Following the successful gripper redesign, the experimental testing was carried out following standardized procedures to assemble test specimens and perform tensile tests.

5.1 Clamp Development

Testing started with investigation into the maximum tensile force that the braided material could withstand. During this study, failure of the material at the clamping points was evident, requiring a clamp design that would not induce material failure of the braided tube through the tensile loading process due to high contact stresses or stress concentrations. This material failure mode occurred with the both the upper and lower gripper jaws of the Tinius Olsen tester as shown in Figure 5-1.

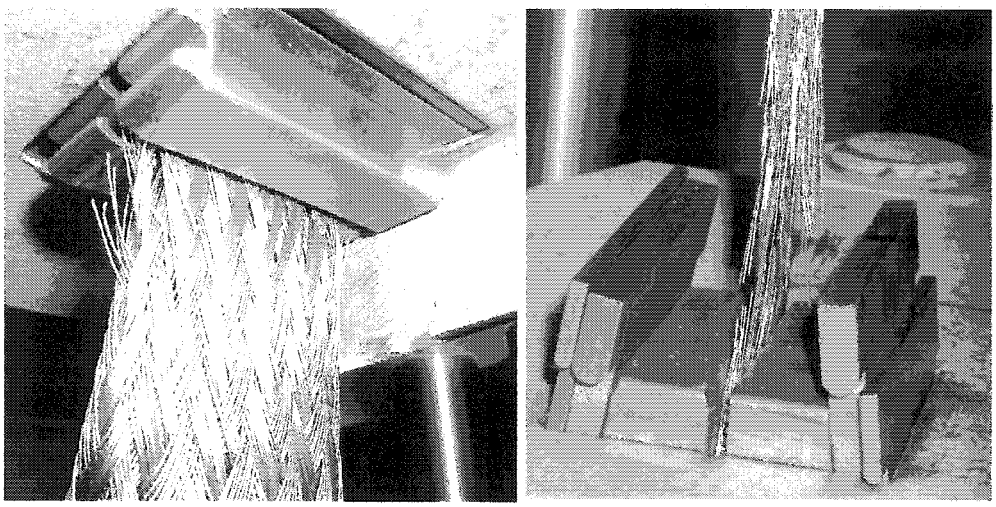

UPPER JAW LOWER JAW

Figure 5-1: Tinius Olsen gripper jaws

The second clamp design also proved to induce material failure, as the clamp consisted of two plates that were bolted together. Figure 5-2 shows deformation of the tube material as a result of clamping the tube as well as the material failure during the tensile test.

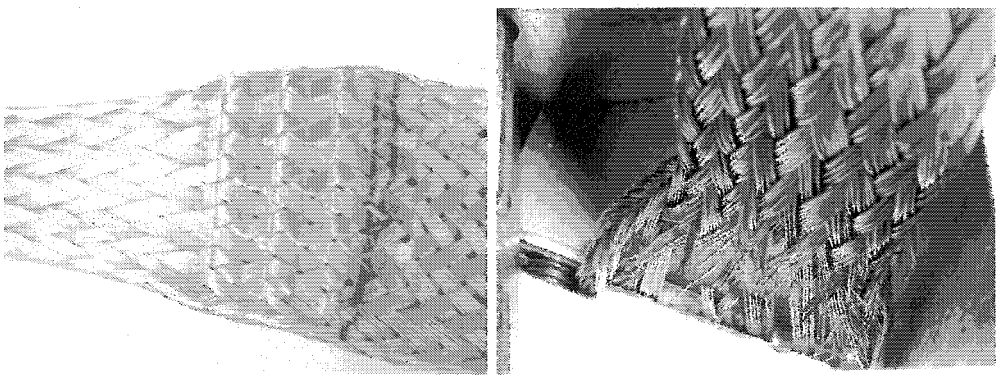

MATERIAL DEFORMATION MATERIAL FAILURE

Figure 5-2: Second clamp design – material deformation and material failure

Unacceptable levels of slippage and strand failure at the grip points on the jaws rendered these two styles of flat-grip clamping undesirable for this study. The ideal grip style would make use of mechanical advantage of the tensile test and provide a uniform grip around the entire tube diameter.

The most suitable design was found to be a circular or annular wedge clamp as shown in Figure 5-3 that was fastened to the Tinius Olsen test fixture. This design makes the most of the tensile load acting upon the braided material; any slippage would tend to pull the wedge in for greater grip action.

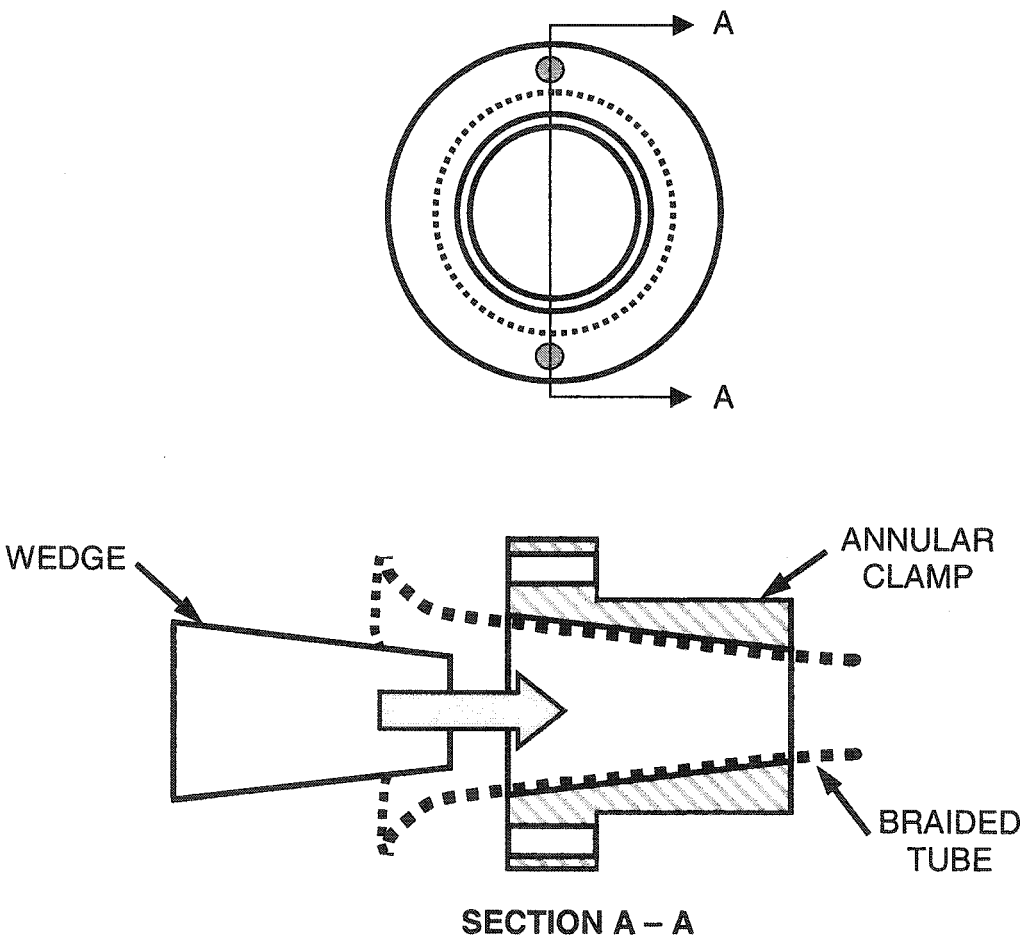

Figure 5-3: Annular wedge clamp for braided tube

Through the use of the annular wedge clamps, the load capacity of the braided material far exceeded that of the stock Tinius Olsen jaws and the clamp jaws. With the stock jaws and the clamp jaws, the maximum force was 15 000 N, compared to 50 000 N with the annular wedge clamps. When failure of the braided material was observed with the circular clamps, it was not at the clamping points or associated with contact stresses at the clamping areas. Complete drawings of the annular clamps can be found in Appendix B.

5.2 Material Selection

The device under study was an assembly consisting of a braided tube with an aluminum foam core. The tube was comprised of continuous strands processed to form a fabric-like braid. There are many types of stainless steel braids available, varying by the grade of stainless steel. For this study, 304 stainless steel was the braid material selected for its material properties and cost effectiveness. The braid weave consists of forty-eight tows, with each tow consisting of eight strands of stainless steel wire of 0.51 mm diameter. The nominal tube diameter of the braid that was selected for this study was 64.5 mm. The braid length of each specimen that was used for each test was approximately 406 mm between clamp points. The braid that was selected is commonly known as standard braid, which consists of a '2 over, 2 under' weave. Figure 5-4 shows the construction of the braid material, where the standard braid weave can be seen in the close-up picture. Mechanical properties for this braid strand material can be found in Appendix C.

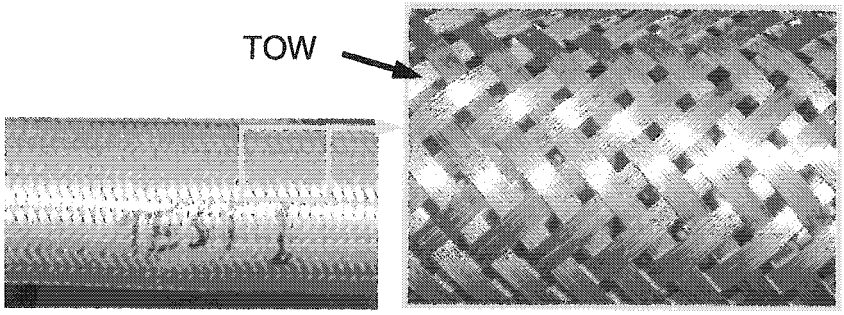

Figure 5-4: Stainless steel braided tube

The aluminum foam used in this study is a closed-cell foam, essentially resembling a sponge. Similar to other aluminum foams, this material has the characteristics of:

i. High strength to weight ratio
ii. Inflammable
iii. Strain rate insensitive
iv. High mechanical energy absorption in every direction
v. Negligible Poisson's effects
vi. Recyclable

A sample of aluminum foam can be seen in Figure 5-5. A detailed list of the physical characteristics of the foam specimens used in this study can be found in Appendix A.

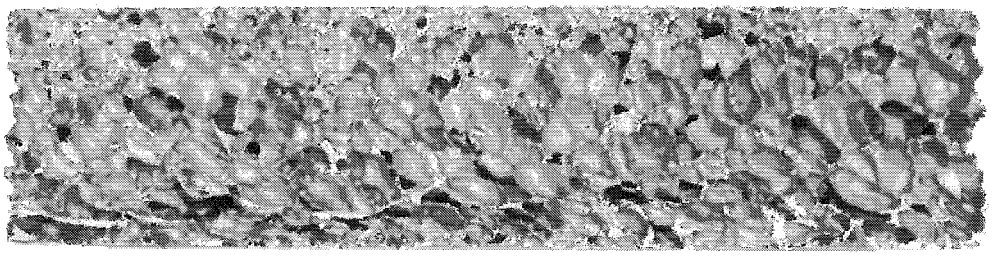

Figure 5-5: Aluminum foam

5.3 Tensile Testing of Empty Tube

To determine the force – displacement relationship of the stainless steel braided tube, a tensile test of an empty tube sample was performed. The Tinius Olsen test machine was used for this test with the annular wedge clamps. The empty stainless steel tube was inserted into the wedge clamps and a preload of 27 kN was applied to press in and secure the wedges. The braided tube specimen was 185 mm in length, measured between the clamp points. For this test, the crosshead speed was 0.3 mm/s. Figure 5-6 shows the force – displacement relationship for the empty braided tube. As can be seen in the force – displacement plot, the tube was able to withstand tensile loading in excess of 50 kN. The braided tube was loaded until the strands of the braid failed.

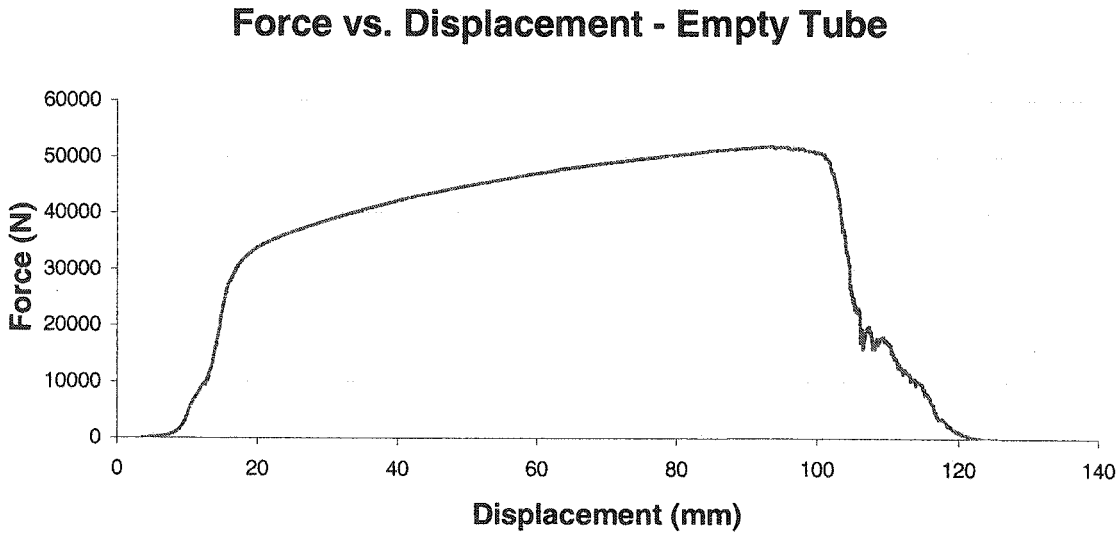

Figure 5-6: Force – displacement relationship for empty braided tube

5.4 Aluminum Foam Filled Specimen Preparation and Test Procedures

Errors may be introduced at any level of testing; the errors may come from the testing machine, the data collection equipment, or human errors from improper specimen preparation or testing errors.

Standardized assembly and test procedures were written to carry out the experimental testing of the braided tube and aluminum foam specimens. This was done to ensure that test results for different foam densities were performed in the same manner – reducing the possibilities of error. The rate of speed of the crosshead on the quasi-static tensile test machine was 0.5 mm/s for all tests, which required approximately five minutes to complete each stage of loading. In addition to this, to minimize error in the test specimens, the length of each braided tube was verified to be 405 mm between clamp points prior to the start of the first stage of loading.

5.4.1 Assembly of Foam Specimens

The procedure to assemble the foam and tube specimen began with compressing the braided tube along its length. This increases the angle between the braid lengths, consequently increasing the diameter of the tube. The next step prior to insertion of the aluminum foam is to bend the edge of the tubing so that it is 'bell-mouthed'. This is easily done by pulling the edge of the steel braid away from the centreline of the tube. Once complete, the aluminum foam brick was able to slide freely into the compressed tube as shown in Figure 5-7.

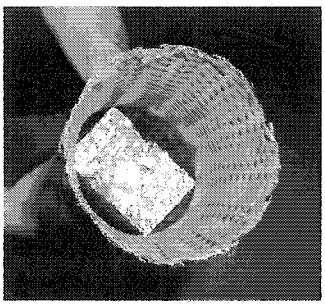

Figure 5-7: Aluminum foam insert in braided tube

To complete the preparation of the test specimen, the tube was released and it was ensured that the foam is in the centre of the test specimen as shown in Figure 5-8.

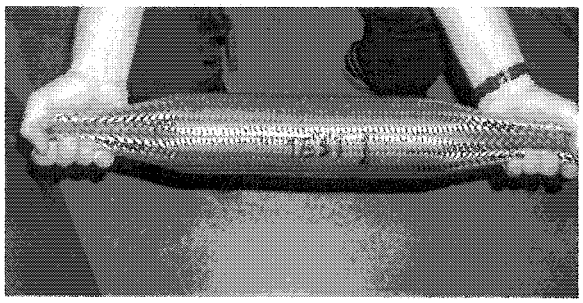

Figure 5-8: Braided tube and foam insert test specimen

5.5 Testing Method

The experimental testing required that the stock gripper jaws that are used in the Tinius Olsen test fixture be removed and that the centre holes in the upper and lower plates of the test fixture be cleared of obstructions. Following this, the specially designed annular wedge clamps were secured to the upper and lower plates of the test fixture. The comprehensive test procedure and exact steps that were followed for the testing process can be found in Appendix D.

During tube insertion, care was taken to ensure that any slack was taken from the braided tube, to make certain that tensile loading would begin the compressive loading on the foam and any displacement would not be wasted in stretching the tube only. To achieve this, a preload of 500 N was placed on the tube assembly at each intermediate step in the testing process, to guarantee that the braid was firm and tight on the aluminum foam.

For the quasi-static experimental testing, there were six foam specimens of various densities available for testing. The foam segments and the associated physical characteristics are listed in Table 5-1.

Table 5-1: Aluminum foam physical characteristics

Specimen Number	**Length** (mm)	**Width** (mm)	**Height** (mm)	**Volume** (m^3)	**Mass** (kg)	**Density** (kg/m^3)
1	304.8	49.85	73.46	$1.12x10^{-3}$	0.311	278.5
2	304.8	49.9	73.05	1.11×10^{-3}	0.276	248.9
3	304.8	49.49	73.59	1.11×10^{-3}	0.415	373.4
4	304.8	48.12	73.65	1.08×10^{-3}	0.312	288.2
5	304.8	49.9	73.54	1.11×10^{-3}	0.332	298.2
6	304.8	49.13	73.59	1.10×10^{-3}	0.250	226.9

5.6 Quasi-static Tensile Loading Test Description

Illustrations of the deformation of the braided tube and aluminum foam throughout the first quasi-static test stage can be seen in Figure 5-9. During the first stage of loading, the braid weave 'scissors' and begins to compress and conform to the square foam shape at the ends of the foam. At approximately

75 mm elongation, deformation in the foam is evident at each end, and the centre of the braided tube is conforming to the shape of the foam brick. Following this, the aluminum foam fails in tensile fracture, breaking into smaller pieces. This can be seen as a steep drop in the force-displacement curve in each tensile test. The braid conforms around these smaller pieces and continues the radial compressive loading. Throughout the tensile test, the foam is broken into smaller pieces, as a result of being subjected to tensile loading from the braid.

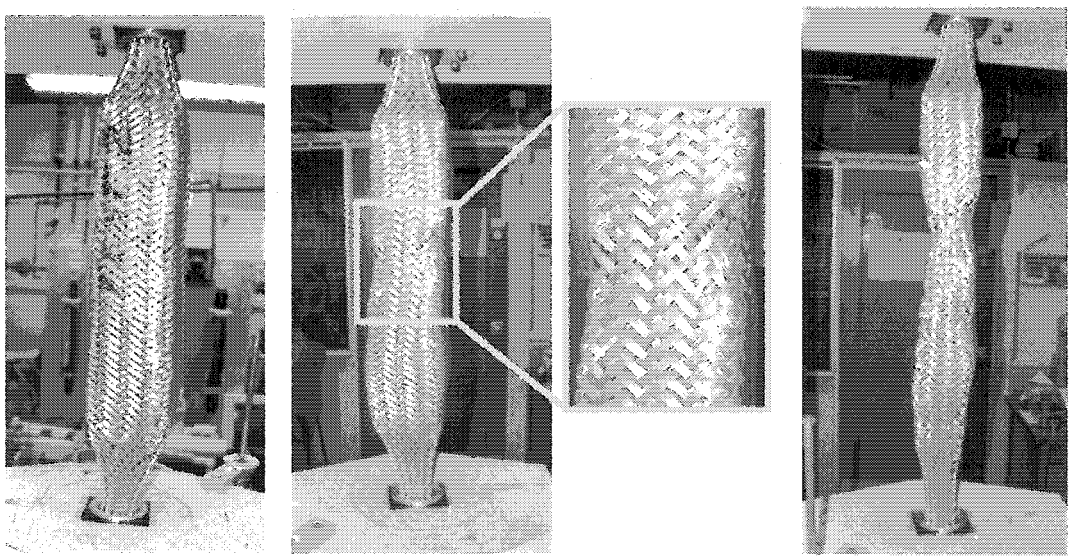

Figure 5-9: First stage quasi-static loading – beginning, middle, and end of stage

After 150 mm of elongation, the test fixture is reset and the test procedure is repeated. At this stage, damage is evident on the pieces of the foam as seen in Figure 5-10. The solid brick has fractured into a number of pieces. At the end of this stage of the test, the foam is almost completely compressed.

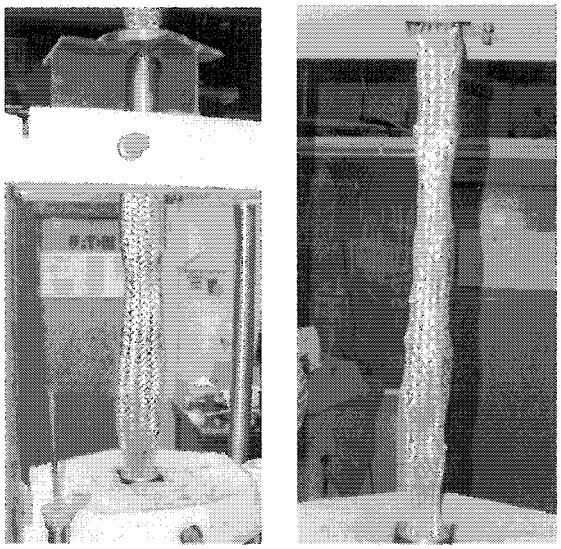

Figure 5-10: Intermediate stage quasi-static loading – beginning and end of stage

After completion of the intermediate loading stage, the test fixture is reset and the test procedure is repeated. As can be seen in Figure 5-11, after a total of 300 mm of elongation, the braid strands have locked and tensile elongation in the strands is occurring. In the final loading stage, each test ended with either braid strand breakage or when the force had reached approximately 40 000 newtons. Oftentimes, the test fixture had not moved through the full 150 mm stroke in this stage when the test had ended. At the end of the test, the aluminum foam was pulverized or had reached a stage of densification that resulted in braid strand deformation also shown in Figure 5-11. Compared to a compressive loading test, where the foam maintains its cross-sectional shape, the tensile loading test has broken the foam into a number of small pieces.

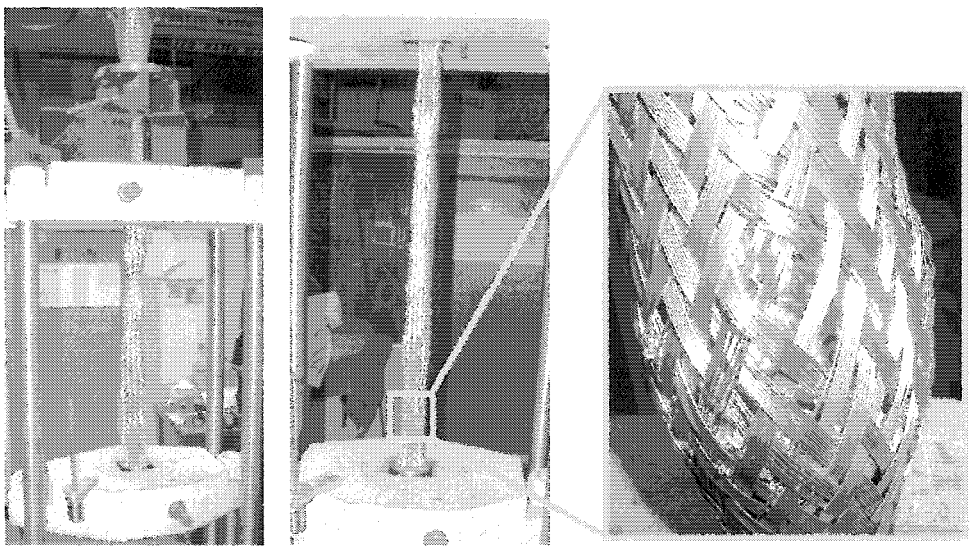

Figure 5-11: Final stage quasi-static loading – beginning and end of stage

5.7 Test Results

The six foam specimens were tested in order of increasing density. Table 5-2 shows the test order and foam specimen used in each test.

Table 5-2: Test sequence and foam specimen used

Test Number	Specimen Number	Density (kg/m^3)
1	6	226.9
2	2	248.9
3	1	278.5
4	4	288.2
5	5	298.2
6	3	373.4

5.7.1 Force – Displacement Results

The three data files from the first, intermediate, and final loading stages were processed and yielded a force – displacement curve for each of the test specimens. Further analysis of the force – displacement curve involved numerical integration to determine the energy capacity associated with the structure.

In each of the test cases in the first stage, the curve is flat with the exception of several drops in the force. These drops are coincident with tensile fracture of the foam specimen. Once fractured, the braid conformed to the new pieces of the foam to continue compression. At the early part of Stage 2, foam crushing is still evident, though in much smaller pieces. This stage illustrates densification of the foam specimen and the early phase of braid locking and braid material elongation. Stage 3 shows the rise in force associated with elongation of the braided tube. This portion of the curve had a similar shape for each of the loading cases with the exception of Test 1. The results for Stage 3 of Test 1 were affected by problems that were encountered during the setup of the specimen in the Tinius Olsen machine fixture. The force – displacement and subsequent energy-displacement results for Stage 3 of this test cannot be considered valid in the analysis of results.

The force – displacement curves are shown with their respective energy – displacement curves in Figures 5-12, 5-14, 5-16, 5-18, 5-20, and 5-22 in the pages following the energy – displacement discussion. For the test illustrated in Section 5.6, the force – displacement curve is shown in Figure 5-14.

5.7.2 Energy – Displacement Results

The amount of energy applied and the energy absorption characteristics of the specimen throughout the sequence of elongation are important factors to understand the effectiveness of an energy absorber. Ideally the absorber will exhibit a characteristic such as a long slope corresponding to the crush of the aluminum foam. The energy – displacement curves were obtained by numerical integration of their corresponding force – displacement curves. Each of the figures shows the energy – displacement curve that was obtained from the force – displacement curve. The energy – displacement curves are shown in Figures 5-13, 5-15, 5-17, 5-19, 5-21, and 5-23.

In each of the tests, Stage 1 of the energy curve shows a steady slope indicative of the foam crushing at its plateau stress. Stage 2 shows an increase in the slope and the shape of the curve becomes parabolic – indicating densification of the foam and interaction with the braid. Stage 3 is the steepest of the curves, shows energy absorption through deformation of the braided tube and elongation of the strands of the tube. As previously discussed, due to problems during the setup of the specimen, the total energy of Test 1 is significantly lower than the other five tests and cannot be considered in the analysis of Stage 3 energy absorption. Table 5-3 summarizes the test number, foam specimen, density, energy absorbed by the braided tube structure and total displacement of the specimen.

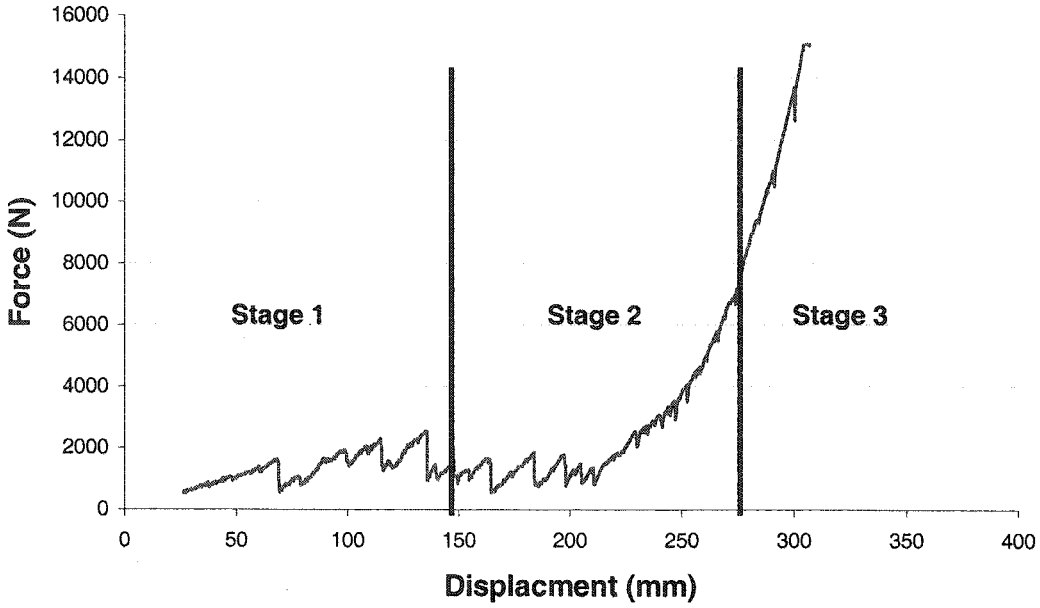

Figure 5-12: Force – displacement plot for Test 1 (ρ_f = 226.9 kg/m^3)

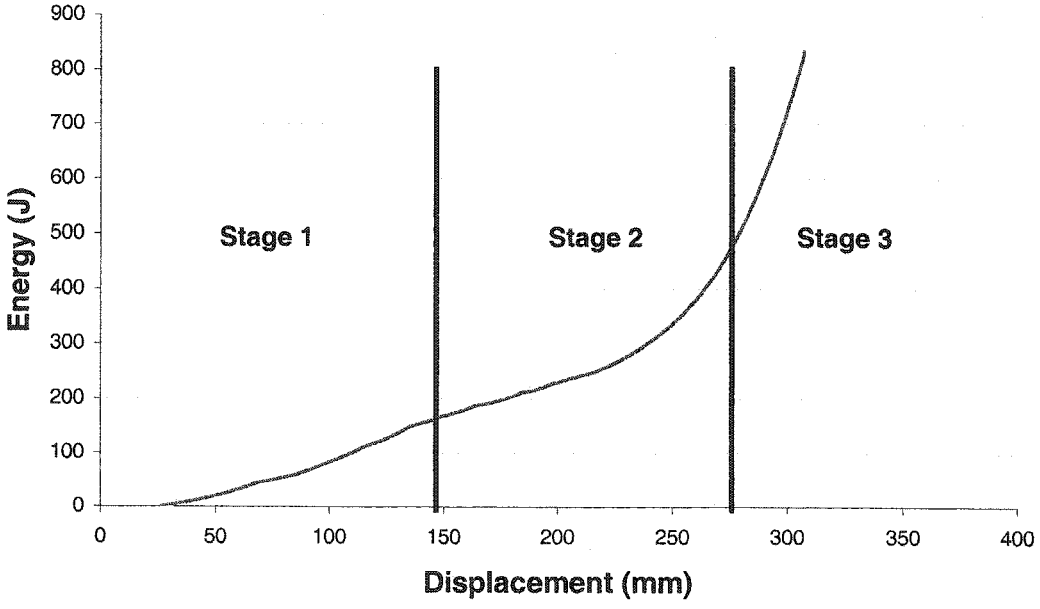

Figure 5-13: Energy – displacement plot for Test 1 (ρ_f = 226.9 kg/m^3)

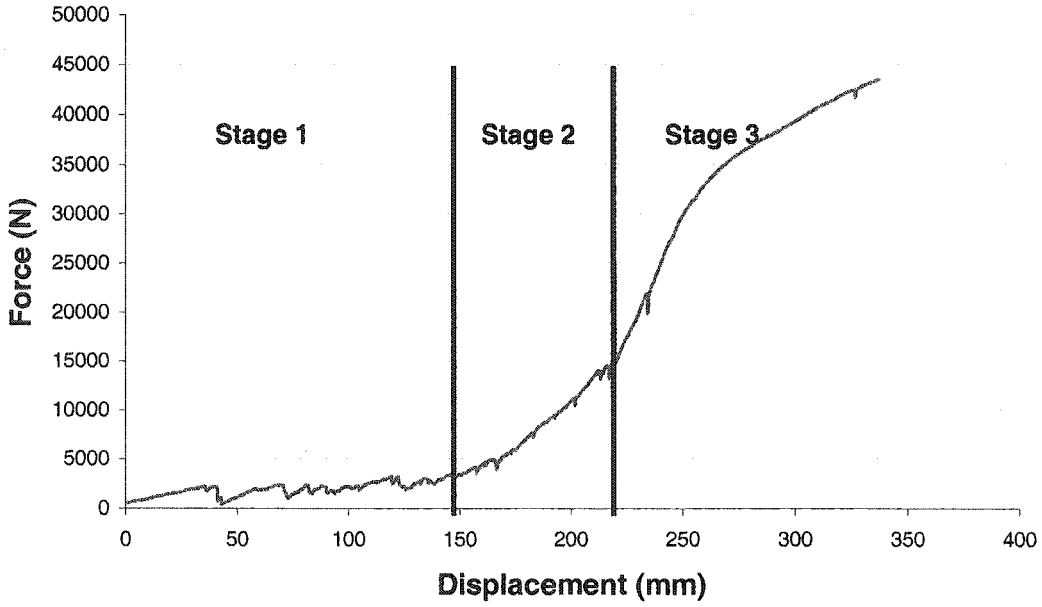

Figure 5-14: Force – displacement plot for Test 2 (ρ_f = 248.9 kg/m^3)

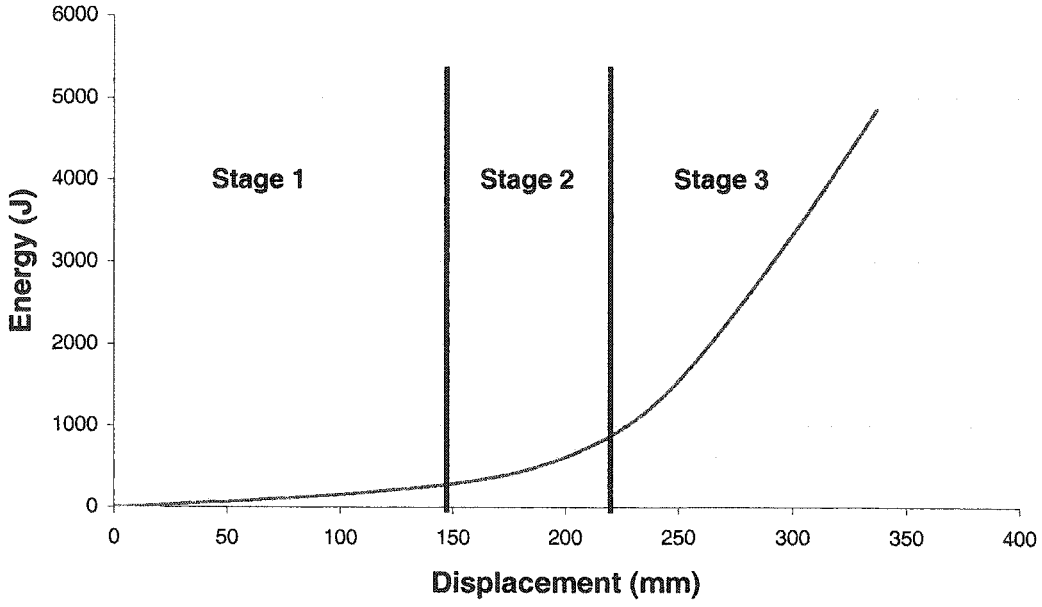

Figure 5-15: Energy – displacement plot for Test 2 (ρ_f = 248.9 kg/m^3)

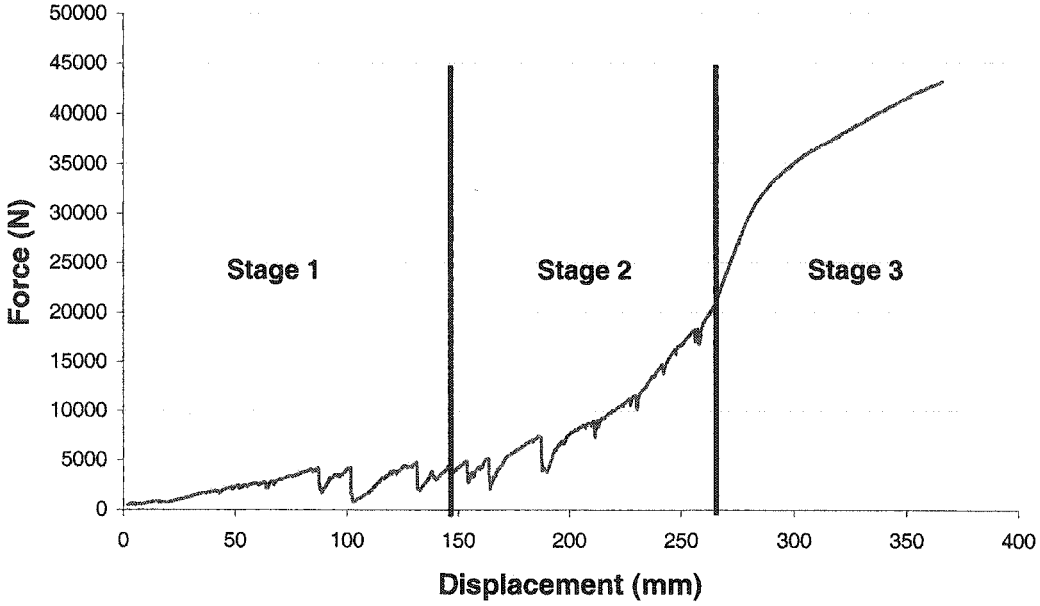

Figure 5-16: Force – displacement plot for Test 3 (ρ_f = 278.5 kg/m^3)

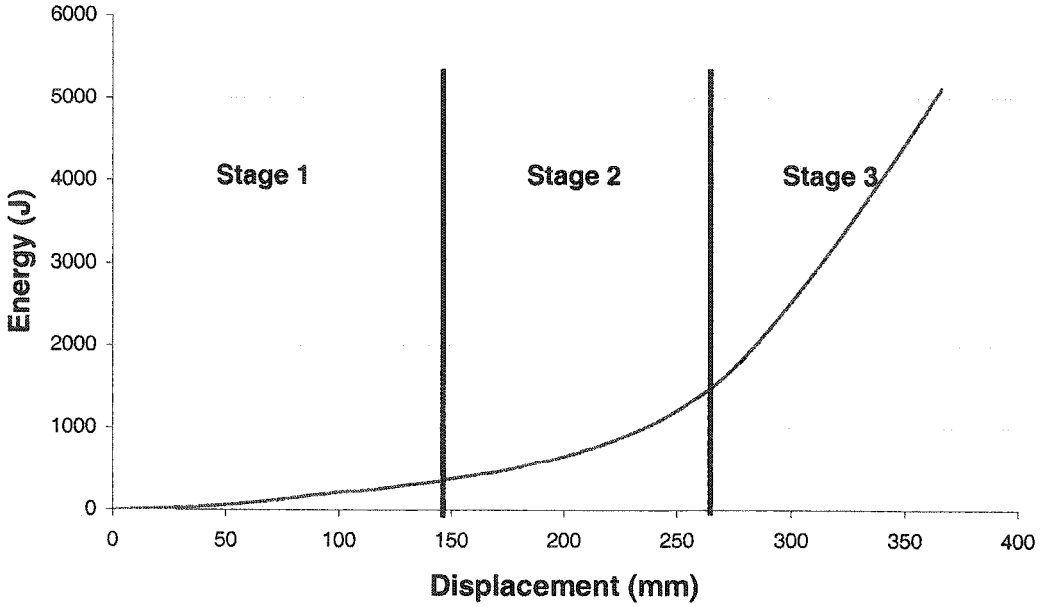

Figure 5-17: Energy – displacement plot for Test 3 (ρ_f = 278.5 kg/m^3)

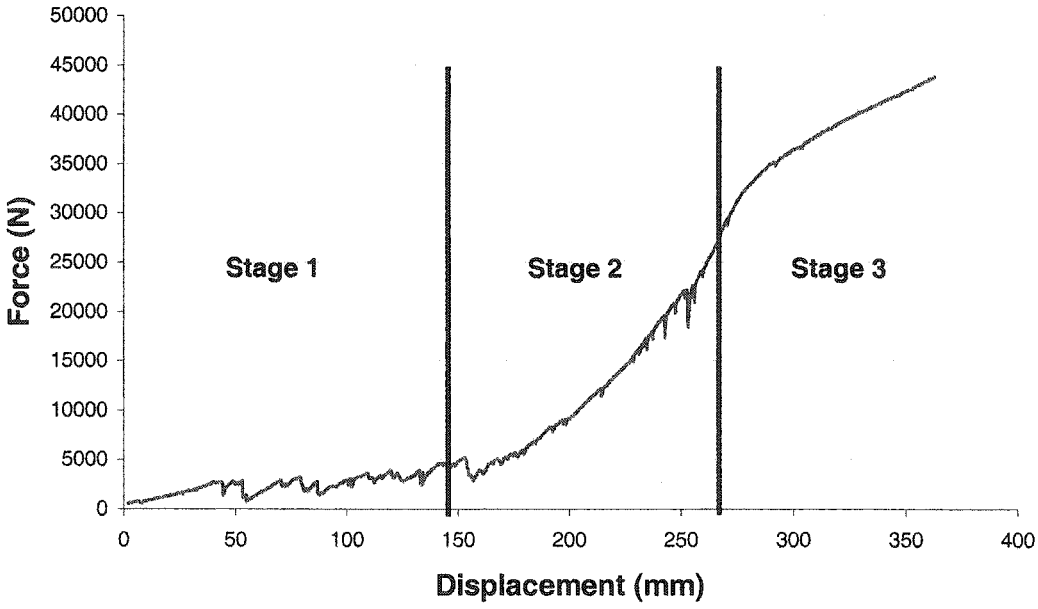

Figure 5-18: Force – displacement plot for Test 4 (ρ_f = 288.2 kg/m^3)

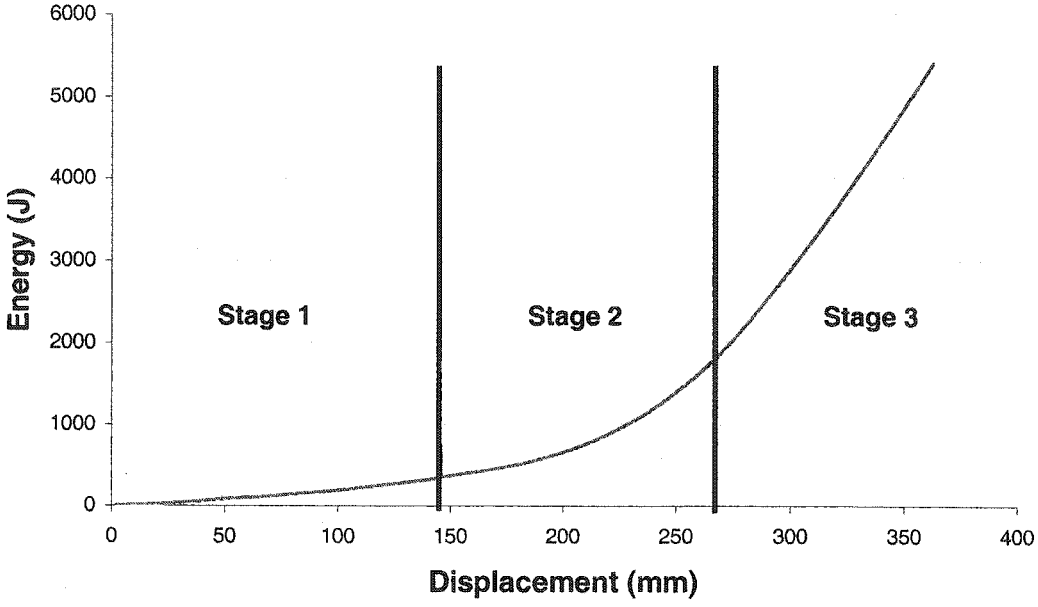

Figure 5-19: Energy – displacement plot for Test 4 (ρ_f = 288.2 kg/m^3)

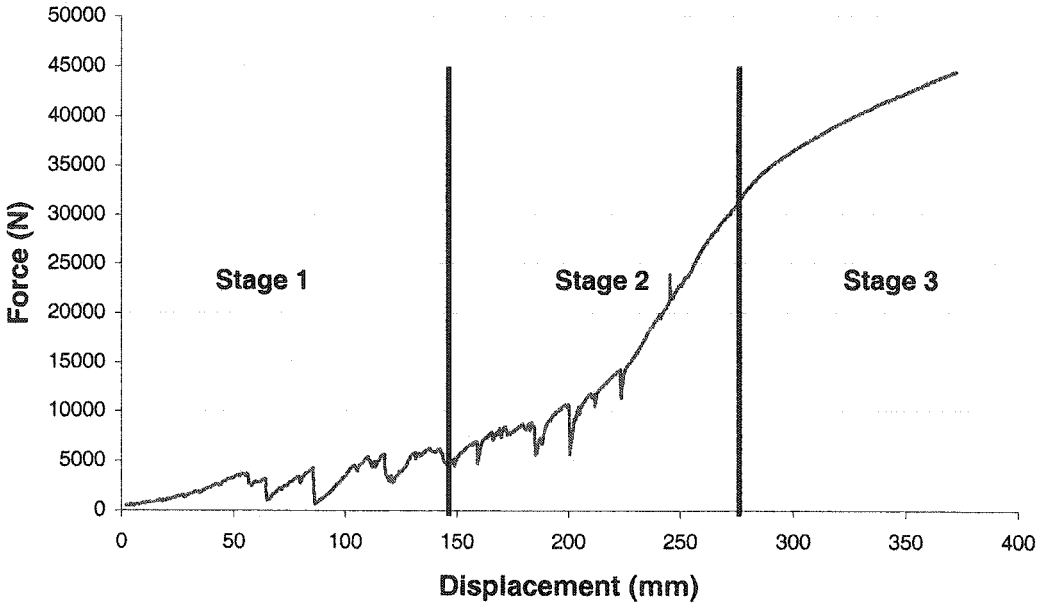

Figure 5-20: Force – displacement plot for Test 5 (ρ_f = 298.2 kg/m^3)

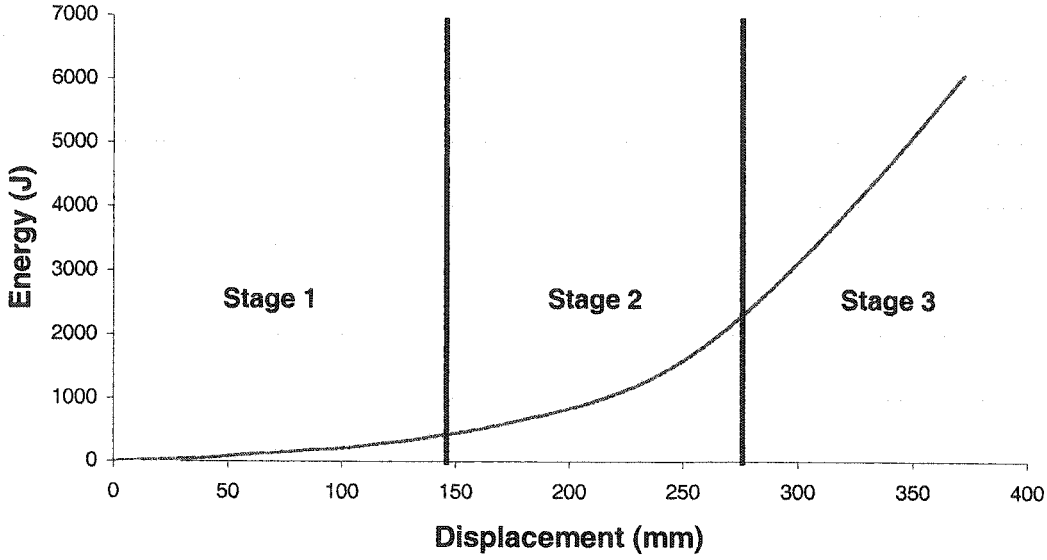

Figure 5-21: Energy – displacement plot for Test 5 (ρ_f = 298.2 kg/m^3)

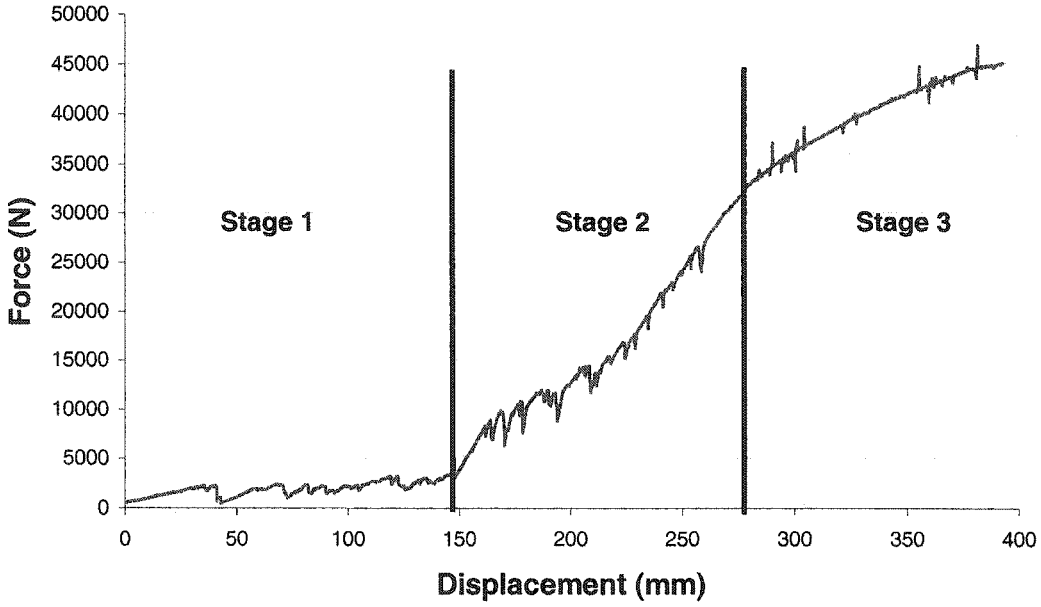

Figure 5-22: Force – displacement plot for Test 6 (ρ_f = 373.4 kg/m^3)

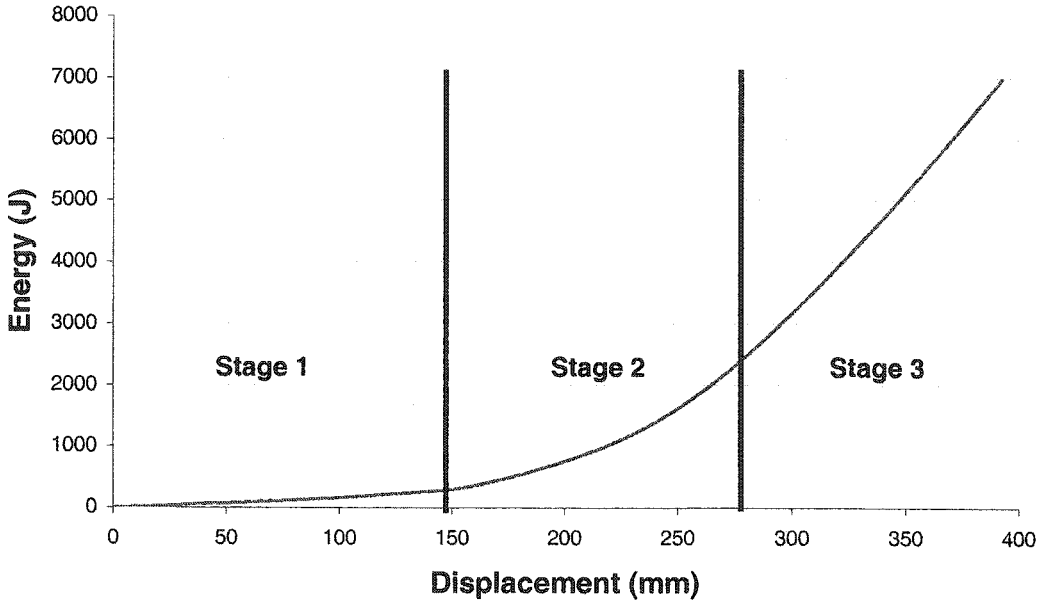

Figure 5-23: Energy – displacement plot for Test 6 (ρ_f = 373.4 kg/m^3)

Table 5-3: Energy absorbed and total displacement for quasi-static tests

Test Number	Specimen Number	Density ρ_f (kg/m^3)	Total Energy (J)	Total Displacement (mm)
1	6	226.9	835.2	306.9
2	2	248.9	4854.6	337.2
3	1	278.5	5124.2	366.3
4	4	288.2	5406.8	362.8
5	5	298.2	6060.8	372.4
6	3	373.4	6977.7	392.6

5.7.3 Effect of Foam Density

From the experimental test results, it is useful to examine the first and second loading stages to determine the effects of foam density on the average crushing force and the energy absorption. It was observed that the foam had reached a stage of densification prior to the third stage of loading. Prior to the foam density analysis, the results from each loading stage are presented to show the change in energy absorption at each stage.

For the first loading stage, the increase in foam density corresponds with an increase in the average force as shown in Figure 5-24. The higher density foams required more force to start and sustain the crushing. The highest density foam had a lower average force; this was due to foam breakage in the first stage. The force – displacement curves have been plotted individually for clarity of viewing the average force in the first loading stage.

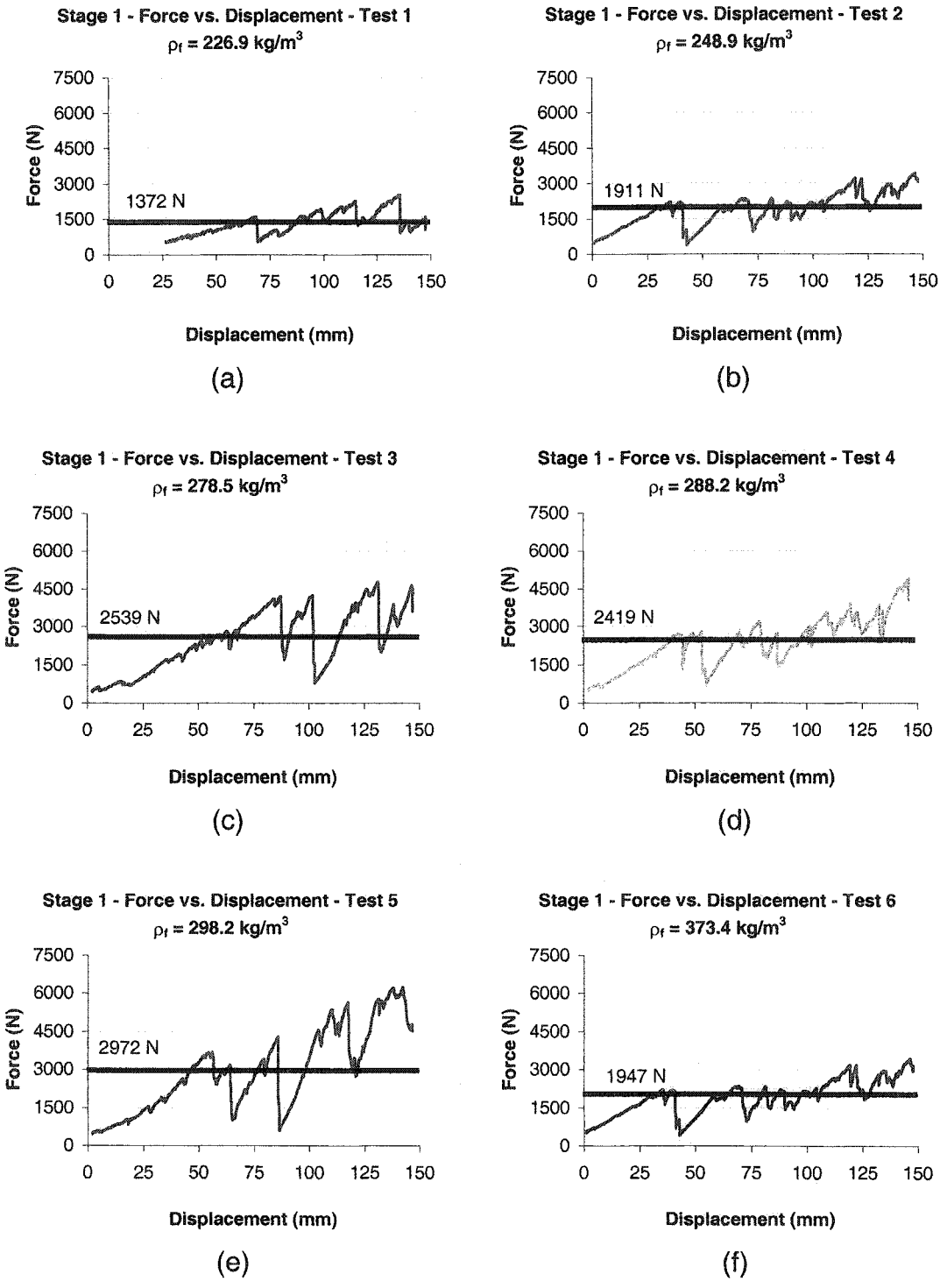

Figure 5-24: Average crush force for the first loading stage

This force acting upon the tube increases in the second stage of loading with foam densification and braid locking. The force – displacement data for the second loading stage shown in Figure 5-25 clearly shows that as foam density increases, the average force required rises.

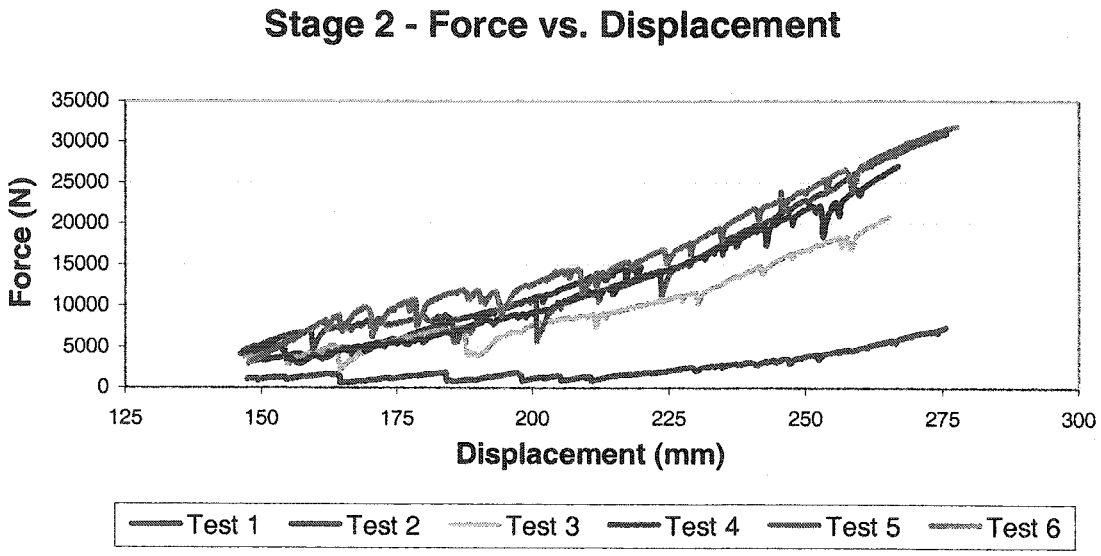

Figure 5-25: Force – displacement data for the second loading stage

In the third loading stage, the foam densification is complete and the braid will no longer scissor. Braid lock has occurred and elongation and yielding in the strands occurs through this phase. Figure 5-26 shows the force – displacement data for the quasi-static test cases, note that the shape of each curve for Tests 2 through 6 is approximately the same after 300 mm, indicating that the foam no longer has any effect. The shape of the curve prior to 300 mm suggests that there was energy absorption from crushing the aluminum foam. Figure 5-26 clearly shows the effect of the setup errors encountered in Test 1 that were previously presented.

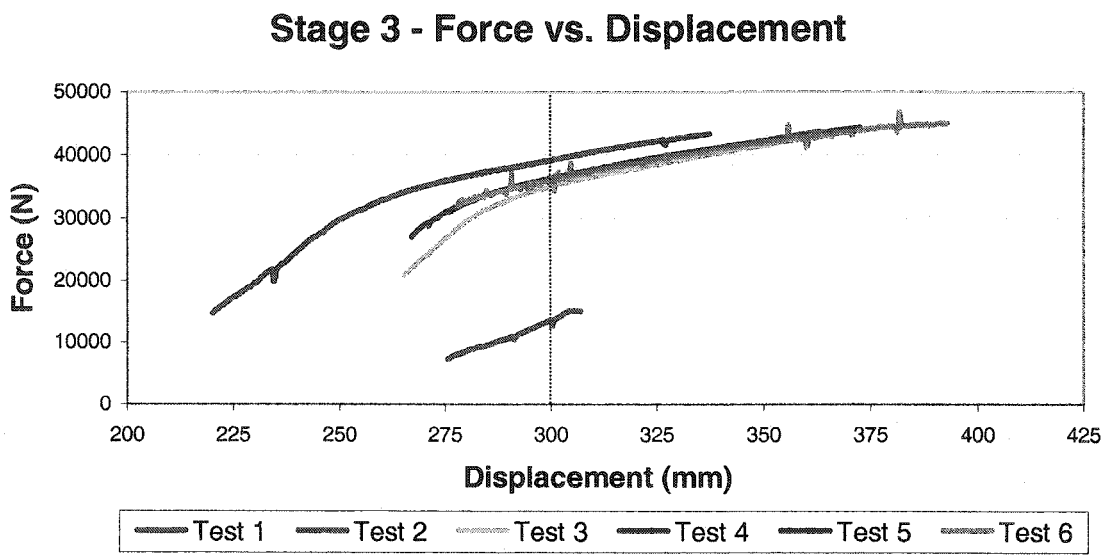

Figure 5-26: Force – displacement data for the third loading stage

5.7.4 Energy Absorption

The increase in foam density corresponds with an increase in the total energy. This energy is absorbed by the foam and the braided tube and is the product of the force acting upon the structure and the elongation of the tube structure. This relationship between foam density and energy absorption was reviewed in the literature for tubes in axial compression and was expected in the outcome of this study. The length of the braided tube specimens was identical for each of the test cases and therefore it was not necessary to normalize the data for the length of the tube. The energy related to the individual stages of the test procedure can be found in Table 5-4.

Table 5-4: Energy associated with each loading stage

Test Number	Specimen Number	Density ρ_f (kg/m^3)	Stage 1 Energy (J)	Stage 2 Energy (J)	Stage 3 Energy (J)	Total Energy (J)
1	6	226.9	164.7	308.8	361.8	835.2
2	2	248.9	280.4	591.9	3982.3	4854.6
3	1	278.5	369.3	1118.4	3636.4	5124.2
4	4	288.2	347.7	1444.0	3615.2	5406.8
5	5	298.2	430.6	1852.4	3777.9	6060.8
6	3	373.4	284.4	2102.5	4590.8	6977.7

5.7.4.1 Stage 1 Energy Absorption

The energy in the first stage of loading is the result of work input to crush and compact the foam and to fracture the foam in tension. As foam density increases, the energy input also increases. This effect can be seen in Figure 5-27, which shows the energy required to crush the foam through the first loading stage of each test. Similar to the results for the force – displacement, the highest density foam required less energy input through the first stage of loading. This was due in part to braid conforming to the shape of the foam brick and tensile fracture of the foam during the test that created voids between the foam pieces in the braided tube structure. These concerns created inefficiency in the device, in that tube elongation occurred with minimal increase in force. Areas where the foam fracture occurred can be seen as horizontal flat areas on the energy – displacement graphs. For the first loading stage, the energy – displacement plots were plotted individually for clarity and comparison between tests.

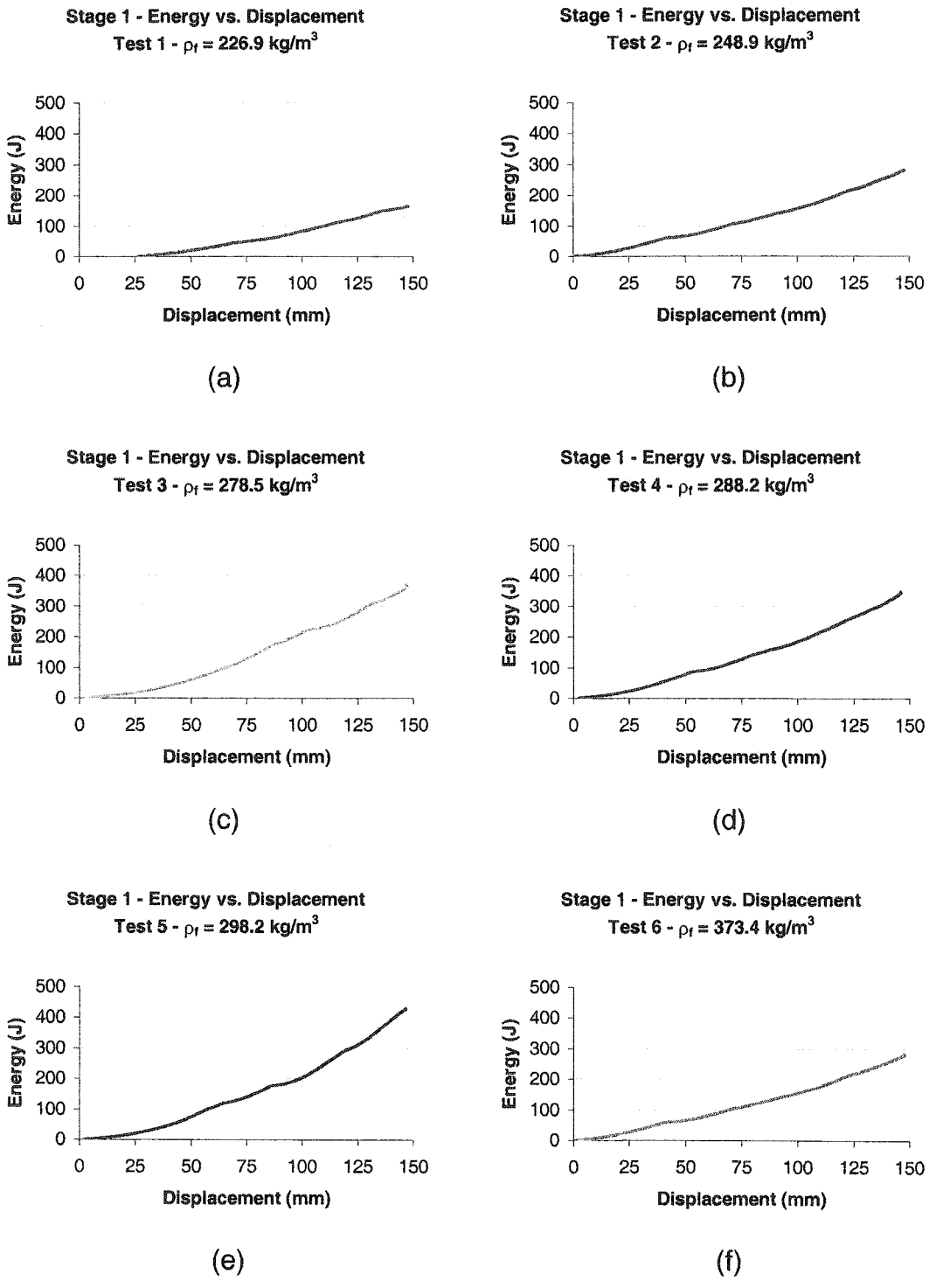

Figure 5-27: Energy – displacement relationship in the first loading stage

5.7.4.2 Stage 2 Energy Absorption

Stage 2 represents a transition from energy absorption due to foam crushing to energy absorption as a result of deformation of the braided tube. During loading stage 2, the foam reaches a state where it no longer contributes to the energy absorption. It can be seen in the graphs in Figure 5-28 that as foam density increases, the energy also increases.

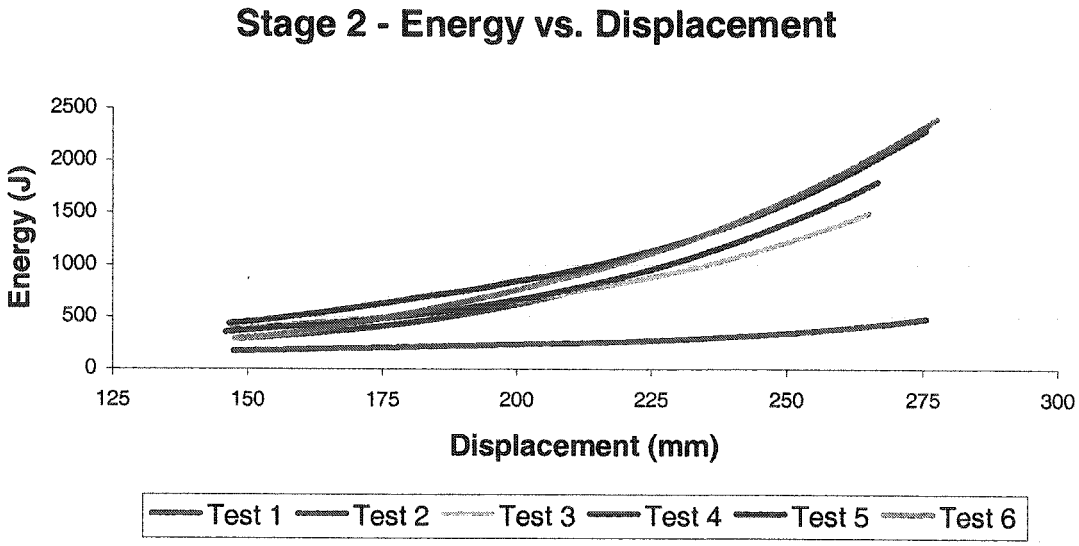

Figure 5-28: Energy – displacement relationship in the second loading stage

During this stage of loading, the foam pieces that remain in the specimen did not break down into smaller pieces as was observed in the first stage. At this point the braid was clamping the foam and completing compression until foam densification was reached.

5.7.4.3 Stage 3 Energy Absorption

The energy absorption in the final loading stage was due to final compaction of the foam and the force required to elongate the strands of the braid. At this point in the test, the foam had collapsed and was contributing little to the energy absorption. It is common to have an elongation of 70% before failure of the braid material [21]. The shape of the energy curves for Tests 2 through 6 followed a common form as seen in Figure 5-29. As previously discussed in Section 5.7.1, improper setup for Test 1 yielded complications, therefore the results from that test cannot be considered for this stage of loading.

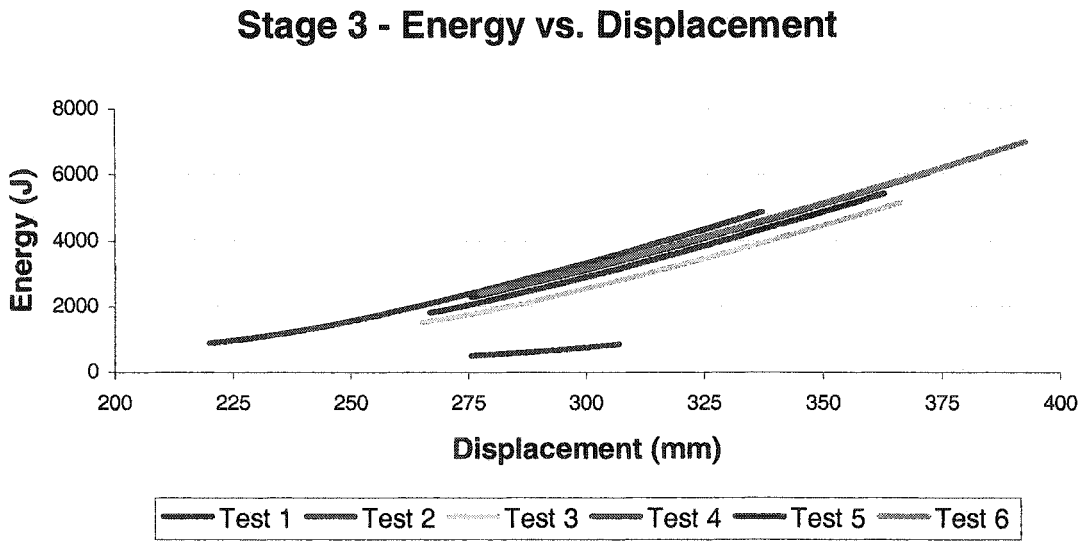

Figure 5-29: Energy – displacement relationship in the third loading stage

5.7.5 Specific Energy and Foam Density

Energy absorption per unit mass or specific energy has a linear relationship to foam density. Stages 1 and 2 are studied, as it was during these stages that the aluminum foam was the primary contributor to energy absorption. It was during Stage 3 that the steel braid absorbed the energy from the forces applied and therefore was not included in the specific energy to density comparisons. Table 5-5 shows the test case, foam density and the total specific energy for loading Stage 1 and Stage 2.

Table 5-5 Specific energy and foam density for loading Stages 1 & 2.

Test Number	**Foam Density** (kg/m^3)	**Stage 1 & 2 Specific Energy** (J/kg)
1	226.9	1894
2	248.9	3166.2
3	278.5	4786.7
4	288.2	5738.9
5	298.2	6868.2
6	373.4	5758.5

Figure 5-30 shows the values from Table 5-5 for specific energy plotted with foam density. A trend can be seen in the data that were collected that indicates a linear relationship exists between specific energy and foam density in the first five tests. It is possible that the foam contributed to energy absorption in the third stage of loading with the test case involving the highest density foam.

This would provide explanation for the relatively low specific energy of the high density foam specimen.

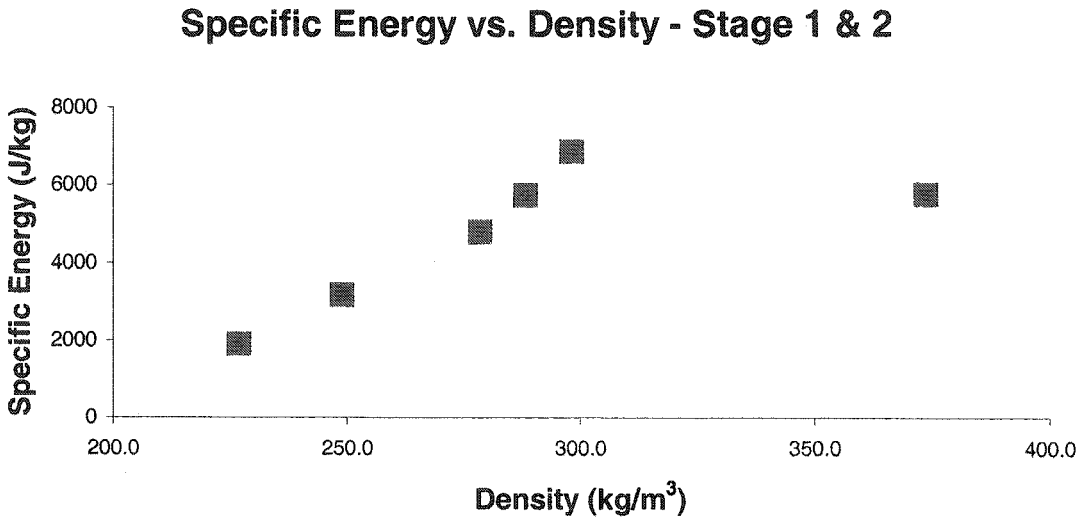

Figure 5-30: Specific energy and foam density for loading Stages 1 & 2

One other useful method to determine if a relationship between energy and density exists is to normalize the energy to the volume of the foam to minimize errors from the size of the foam specimens. The energy and density relationship is further verified by the energy per unit volume and density plot, shown in Figure 5-31.

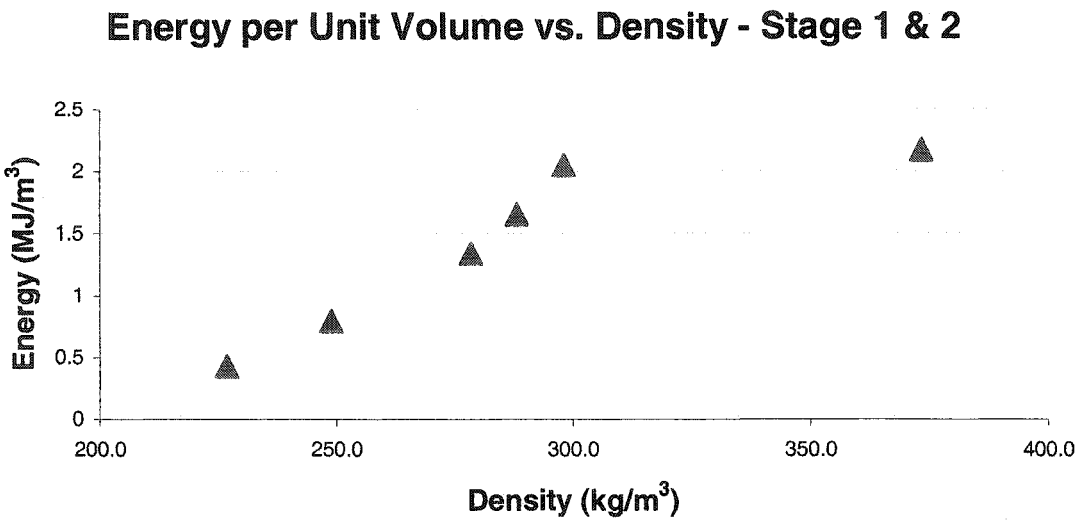

Figure 5-31: Energy per unit volume and foam density for loading Stages 1 & 2

The test with the highest density foam had a significantly higher displacement overall than the other five tests. Energy absorption from the foam core may have contributed in the third stage of testing that is not considered in this data. If we normalize the energy to the volume of the foam and consider the third set of tests, a linear relationship exists between Tests 2 through 5. Test 1 was removed, as the third loading stage was not completed to the same extent as the other five tests. The effect of the tube can be seen in Figure 5-32, where the energy absorption per unit mass is effectively the same for all foam densities.

It can be seen in the energy per unit volume – density plot in Figure 5-33 that the energy absorption increases with the foam density. Selection of appropriate density foam will depend on volume and mass constraints and required energy absorption that apply to a particular application. For example, an automobile requires lightweight and compact energy absorbing devices,

whereas an explosion blast panel may not be concerned with the mass of the absorber, but only have a size or volume constraint.

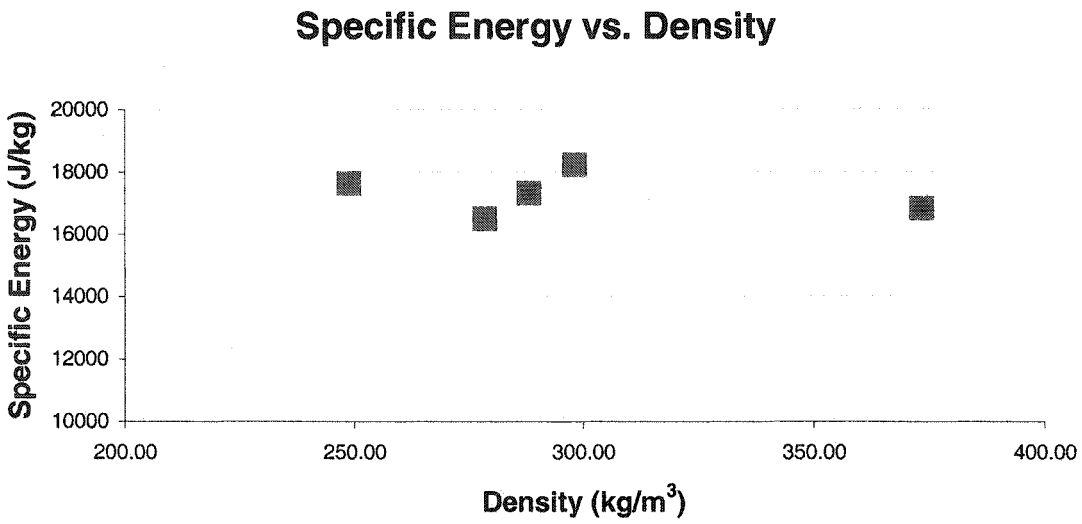

Figure 5-32: Specific energy and foam density for all three loading stages

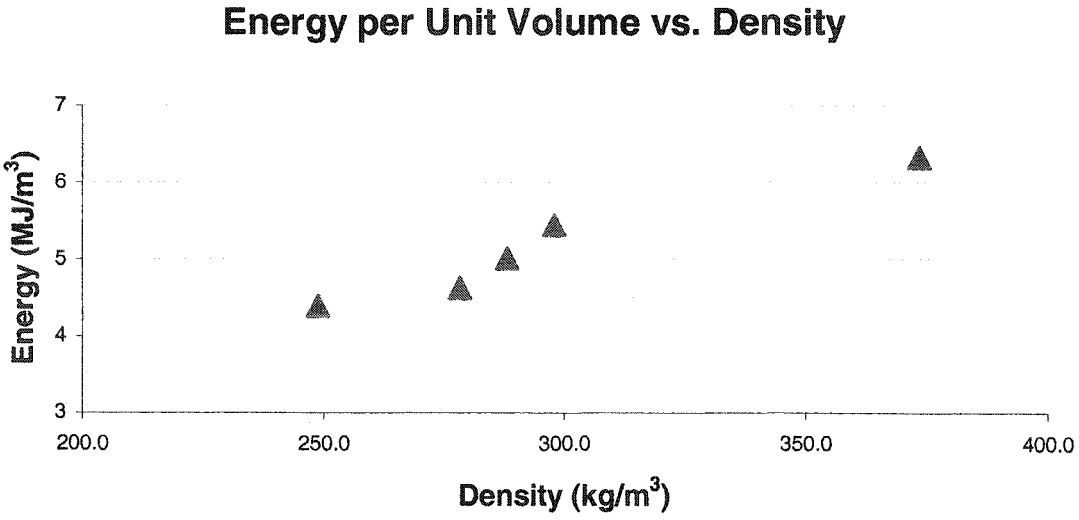

Figure 5-33: Energy per unit volume and foam density for all three loading stages

6. NUMERICAL APPROXIMATION

To eliminate costly experimental testing, it is advantageous to develop a numerical approximation of the energy absorbing capabilities of the braided tube and aluminum foam structure. As this device performs in tension, for a given change in length of the tube, there is a corresponding energy input required to compress the diameter of the tube in order to radially crush the aluminum foam. Each component contributes to the overall energy absorbing ability of the structure and is considered separate in the numerical approximation. It is unknown if any interaction effects between the braided tube and the foam contribute or are detrimental to the energy absorption ability. This numerical model considers a tensile loading condition and therefore is only compared to the quasi-static test results.

6.1 Braided Tube

Harte, Fleck and Ashby [20] investigated the relationships between braid angle, radius, and length of the braided tube with focus on a single 'cell' or 'unit cell' of the braid for their numerical approximation. A unit cell of braid is defined as length 'ℓ' along the length of the 'tow' of the braid and initial angle $2\theta_o$ between the tows as shown in Figure 6-1.

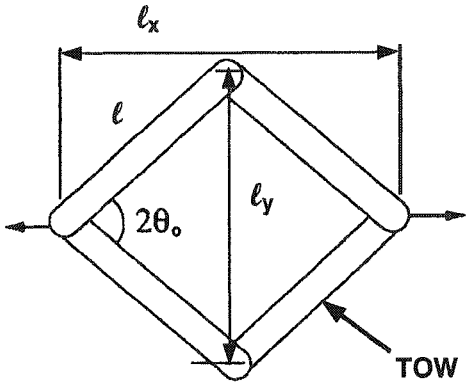

Figure 6-1: Unit cell of braid on braided tube [20]

6.1.1 Radius – Angle Relationship

To determine the relationship between the radius and braid angle, consider that the length of the unit cell along the circumference of the braided tube is defined as

$$\ell_y = 2 \cdot \ell \cdot \sin\theta \qquad \text{Equation 6-1}$$

The circumference is known to be the product of 2π and the radius of the tube. The number of unit cells on the circumference of the tube will remain a constant, with the radius and angle between the strands changing as the tube is loaded axially. This results in the following relationship between the initial (R_o) and final (R) radii and initial (θ_o) and final (θ) braid angles

$$\frac{R}{R_o} = \frac{\sin\theta}{\sin\theta_o} \qquad \text{Equation 6-2}$$

6.1.2 Length – Angle Relationship

The length – angle relationship is similar to the analysis to determine the relationship for the radius and angle. Along the length of the tube, the distance along the unit cell will be

$$\ell_x = 2 \cdot \ell \cdot \cos\theta \qquad \text{Equation 6-3}$$

The number of unit cells along the length of the tube will remain constant, with deviations in the angle between the braids. The relationship between the initial (L_o) and final length (L) and subsequent braid angles is defined as

$$\frac{L}{L_o} = \frac{\cos\theta}{\cos\theta_o} \qquad \text{Equation 6-4}$$

The initial variables that are known include radius, length of the tube, and the braid angle. From these relationships, the changes to the radius and braid angle can be calculated for various length changes to the braided tube. The radial change is significant, as this determines the amount of distance that the aluminum foam is compressed.

6.1.3 Braid Lock Angle

To determine when the contribution of the braided tube to energy absorption will occur, it is necessary to calculate the braid lock angle. This is established from the physical properties and dimensions of the braid. Consider a single cell of braid with pin joints at each of the points where the tows intersect as shown in Figure 6-2.

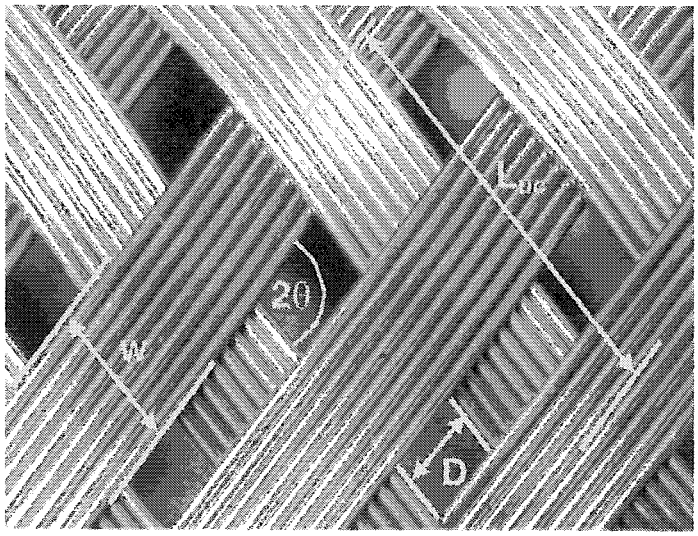

Figure 6-2: Single cell of braid and associated variables

The distance between the tows (D) can be determined from the equation

$$D = \frac{L_{uc}}{2} \cdot \sin(2\theta) - w \qquad \text{Equation 6-5}$$

where the unit cell size (L_{uc}), width of the tows (w), and braid angle (2θ) are known from stated or measured values. When the braid reaches the locking angle, the distance between the tows has a value of zero. Equation 6-5 can be

rearranged to determine the locking angle θ_L from the remaining constants L_{uc} and w when the distance between the tows is zero.

$$\theta_L = \tfrac{1}{2} \sin^{-1}\left(\frac{2\ w}{L_{uc}}\right) \qquad \text{Equation 6-6}$$

For the braid that was used in these experiments, Equation 6-6 was evaluated to determine the braid lock angle of 19.9°.

6.1.4 Energy Associated With Braided Tube

The braided tube will not contribute to energy absorption until lockup when the tows of the braid elastically and plastically deform. When the tows of the tube lock, the energy (E_1) for the first region can be determined from the product of the stiffness of the tube (k_1) and the change in length of the tube from braid lockup length, displacement (δ) in Equation 6-7.

$$E_1(\delta) = \tfrac{1}{2} \cdot k_1 \cdot \delta^2 \qquad \text{Equation 6-7}$$

The values for stiffness were evaluated from the force-displacement relationship of an empty tube under tensile loading. For clarity, the force – displacement plot for the empty stainless steel tube tensile test is shown in Figure 6-3 with the bi-linear approximation for stiffness. Equation 6-7 defines the first region, where k_1 carries a value of 3.391×10^6 N/m. This relationship is valid for displacements up to and including a value of 10 mm. Equation 6-8 characterizes energy associated with the second region (E_2), where k_2 has a

value of 2.68 x 10^5 N/m. This relationship is valid for displacements greater than 10 mm and requires the addition of the energy contribution from Equation 6-7 evaluated at the 10 mm displacement, a value of 169.5 J, and the product of the displacement and a constant value of force F_{tube}, of 33.9 kN. The energy calculation for the second region requires that 10 mm be subtracted from displacement δ.

$$E_2(\delta) = 169.5 + \frac{1}{2} \cdot k_2 \cdot (\delta - 10)^2 + F_{tube} \cdot (\delta - 10) \qquad \text{Equation 6-8}$$

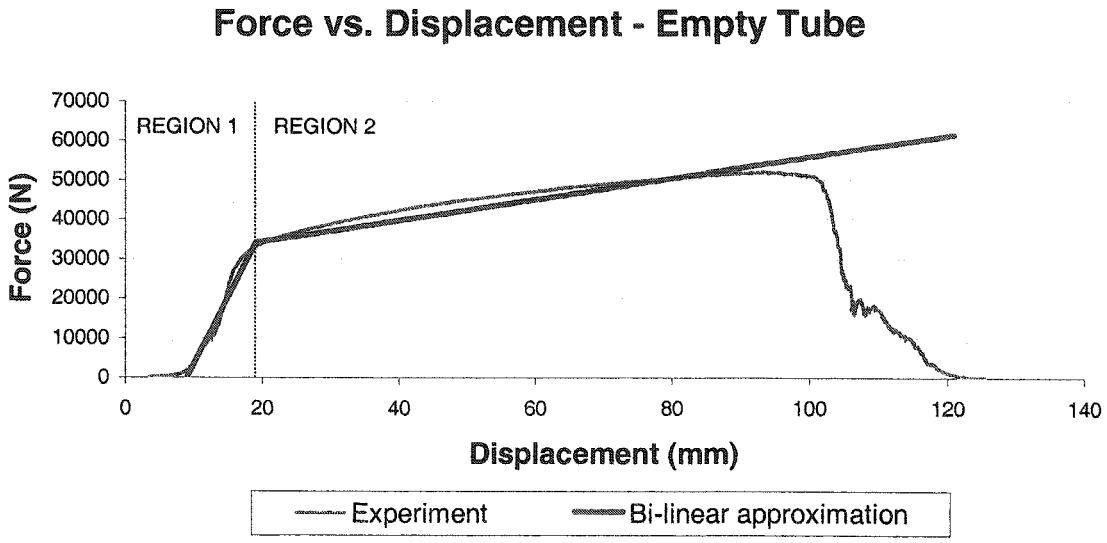

Figure 6-3: Force-displacement plot for tensile test of empty stainless steel braided tube with bi-linear approximation

6.2 Aluminum Foam

The energy absorbed by the aluminum foam is a result of radial compression by the braided tube. The contact area between the tube and the foam is defined as the product of the tube circumference 2π r and the tube length L_{foam}. Consider an infinitesimal radial change (dr) and the associated energy or work (dU) surrounding that as expressed in Equation 6-9

$$dU = F \cdot dr \qquad \text{Equation 6-9}$$

The force (F) acting upon the aluminum foam during radial crushing is the product of the plateau stress σ_{pl} and the contact area 2π r L_{foam}. To determine the total work or energy input to compress the foam through the radial change from initial radius (R_o) to final radius (R), the integral of Equation 6-9 is required.

$$U = \int_{R}^{Ro} \sigma_{pl} \cdot L_{foam} \cdot \pi \, r \, dr \qquad \text{Equation 6-10}$$

Equation 6-10 is evaluated to produce the work or energy to deform the foam as expressed in Equation 6-11

$$U = \sigma_{pl} \cdot L_{foam} \cdot \pi \cdot (R_o^2 - R^2) \qquad \text{Equation 6-11}$$

It should be noted that the quasi-static tensile test cases used rectangular aluminum foam samples. An equivalent radius (R_{eq}) was calculated for each of the aluminum foam bricks, based on the equating the cross-sectional areas of a rectangular cross section, height (H) and width (W), to that of an area of a circle as shown in Equation 6-12.

$$R_{eq} = \sqrt{\frac{H \cdot W}{\pi}} \qquad \text{Equation 6-12}$$

6.2.1 Plateau Stress and Foam Density

As shown in Equation 6-11, the energy absorbed by the foam varies with the length of the foam specimen (L_{foam}) and plateau stress (σ_{pl}) that the foam exhibits in compression. Unless the manufacturer of the foam supplies data, experimental testing to determine the plateau stress of the foam is required. A relationship exists between foam density and plateau stress as detailed in the work of Hanssen, Hopperstad and Langseth [9]. This is referred to as a power law relationship and for the plateau stress σ_{pl} is defined as

$$\sigma_{pl} = C_p \left[\frac{\rho_f}{\rho_{fo}}\right]^n \qquad \text{Equation 6-13}$$

where ρ_f is the foam density and ρ_{fo} is the density of the base material of the foam. The two constants C_p and n are determined through analysis of axial compression test data of foam cubes. For the quasi-static test cases, the data from Cymat was curve-fitted to determine that the values of C_p and n were

287.02 MPa and 1.98 respectively. To determine the error that this estimation for plateau stress presents compared to the actual test data, the sum of squares error was determined for the test data supplied by Cymat and predicted values. This can be seen in Table 6-1.

Table 6-1: Plateau stress predicted values

Density ρ_f (g/cm^3)	Plateau Stress Data (MPa)	Plateau Stress Estimated (MPa)	Sum of Squares Error $(MPa)^2$
0.4	6	6.5	0.294
0.34	5.3	4.7	0.311
0.3	4.7	3.7	0.998
0.25	1.81	2.58	0.592
0.2	1.17	1.66	0.238
		Total Sum of Squares Error	2.433

These values provide a reasonable estimation of the plateau stress based on the variance of 2.433/3 = 0.811 MPa^2 and the calculated correlation of 0.955.

6.3 Evaluation of Quasi-Static Test Cases

The plateau stresses were evaluated using the power law relationship for the various foam densities tested in the quasi-static experiments. Using these plateau stresses and the tube information, the theoretical energy absorption for each foam specimen was determined. The percentage difference was determined as shown in Equation 6-14, where the experimental test values (E_{EXP}) and the values for the theoretical prediction of energy (E_{THEO}) were taken from their respective values in Table 6-2. These values and the variance from the experimental values can be seen in Table 6-2.

$$\% \text{ Difference} = \left| \frac{E_{EXP} - E_{THEO}}{E_{EXP}} \right| \times 100\% \qquad \text{Equation 6-14}$$

Table 6-2: Comparison of experimental and theoretical results

Test	Density ρ_f (kg/m^3)	Plateau Stress σ_{pl} (MPa)	Displacement (m)	Energy (Experiments) (J)	Theoretical Energy (J)	% Difference
2	248.9	2.56	0.3372	4855	5195	7.0%
3	278.5	3.19	0.3663	5124	7342	43.3%
4	288.2	3.42	0.3628	5407	7349	35.9%
5	298.2	3.66	0.3724	6061	8087	33.4%
6	373.4	5.71	0.3926	6978	11122	59.4%

When observing the shape of the plot of predicted values of energy absorption and displacement from the theoretical model, it can be seen that the theoretical model predicts much higher values of energy absorption in the foam crush stage. The assumption was made that a perfect foam crush condition with no braid slippage or foam fracture occurred during the foam compression stages. A plot of the predicted energy and the experimental results for Test 2 can be seen in Figure 6-4. For the second test, the theoretical formulation predicts energy absorption very close to the experimental value and the energy absorption per unit length is similar in this region. The most significant difference from the second test to the remaining four tests is the total displacement of the braided tube test. The plots of the remaining tests against the predicted values for energy can be found in Appendix E.

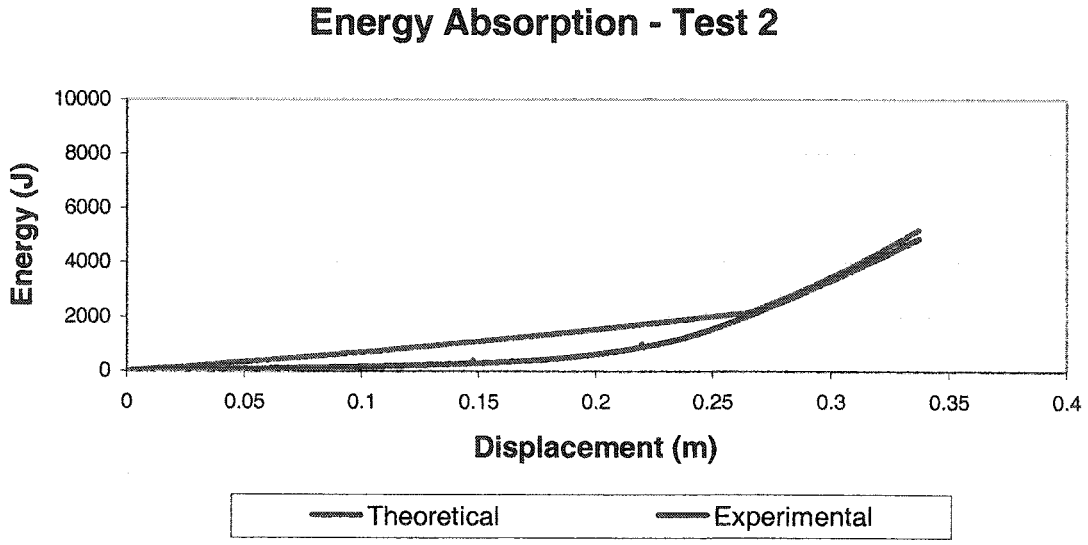

Figure 6-4: Theoretical and experimental energy absorption for Test 2

One other line of reasoning that may affect the comparison of the predicted values to the experimental test is the assumed shape of the aluminum foam. The theoretical model assumes that the foam is cylindrical, similar in shape to the braided tube. This differs from the experimental tests, as the specimens were rectangular in shape. An equivalent radius for each foam brick was calculated and entered into the theoretical model, however the rectangular shape may have influenced the energy absorption and reduced the energy input required to crush the foam.

7. DYNAMIC IMPACT TESTING

Dynamic impact testing was performed on the aluminum foam filled braided tube assemblies. This testing utilized a drop tower impact test machine equipped with a curved impacting nosepiece to strike the tube in a direction perpendicular to its axis. The impact produced tensile and bending loads on the tube, resulting in compression to the aluminum foam core. This test setup can be seen in Figure 7-1. Further details of the test equipment and nosepiece will be reviewed in the next sections.

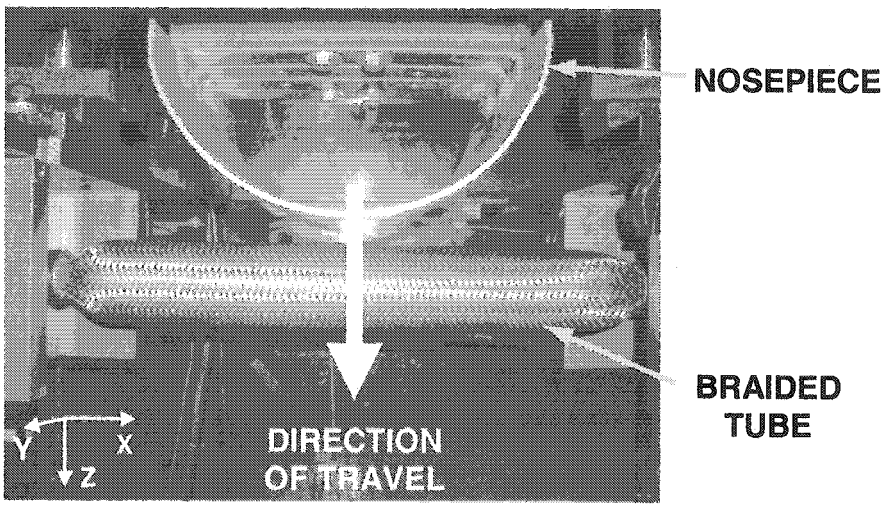

Figure 7-1: Dynamic impact test specimen

From the reviewed literature, no dynamic testing of aluminum foam filled braided tubes has been completed. This investigation represents the first attempt to investigate foam filled braided tubes under impact loading.

7.1 Test Equipment and Instrumentation

The equipment that was used to perform the dynamic testing was a drop tower impact test machine. This device, as illustrated in Figure 7-2, consisted of a crosshead and impact nosepiece that moved in the vertical axis. An accelerometer and LVDT were directly fastened to the mounting plate of the impacting nosepiece to measure acceleration and displacement in the vertical direction. The acceleration and displacement data were recorded at a sampling rate of 23 000 Hz, starting from a position of approximately 2 cm above the braided tube assembly and ending when the crosshead and nosepiece came to rest. The total time duration of impact was approximately 0.1 seconds. The accelerometer that was used had a range of ± 500 G and a resolution of 0.054 G. The LVDT had a range of 400 mm and a resolution of 0.04 mm. The total mass of the crosshead and impact nosepiece was 71.5 kg and remained constant. With the acceleration and displacement information recorded along with the known mass, the impacting forces and the energy absorbed during the tests were calculated.

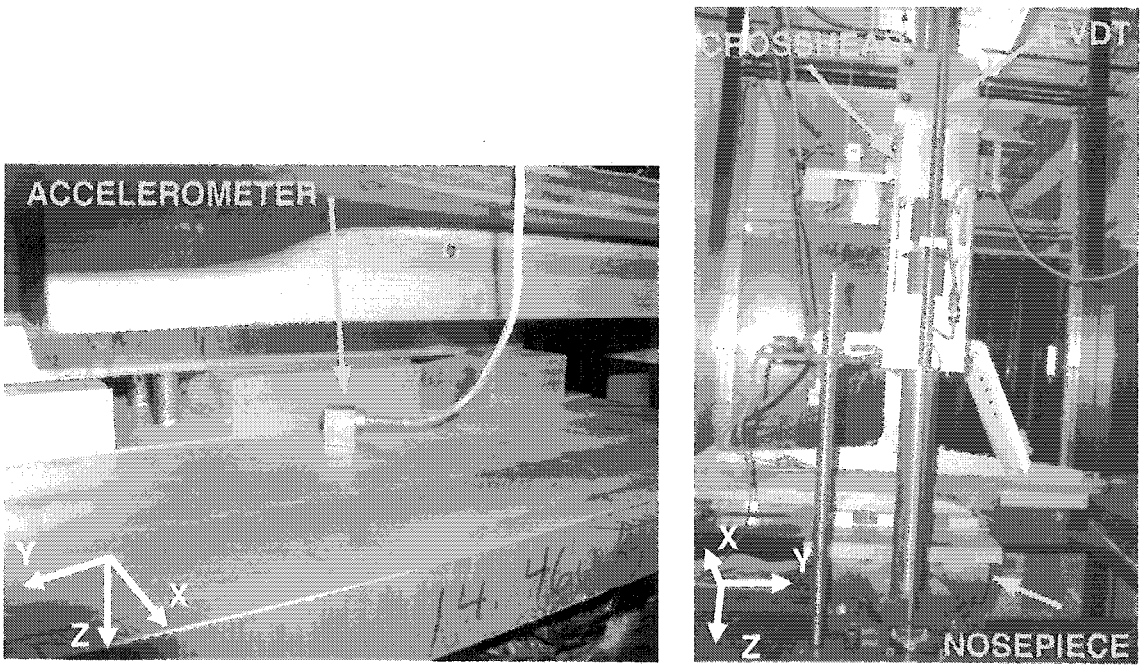

Figure 7-2: Accelerometer and LVDT placement on dynamic impact test machine

7.1.1 Machine Modifications For Braided Tube Tests

Prior to experimental tests, the test machine required modifications to secure the braided tube wedge clamps. Adapters were fabricated to mount to the base plate of the impact test machine that did not interfere with the impact testing machine's capability. Following the modifications to the test machine, an effective length of approximately 590 mm was available for foam inclusion. This is the distance between the mounting wedges for the braided tube assembly as shown in Figure 7-3.

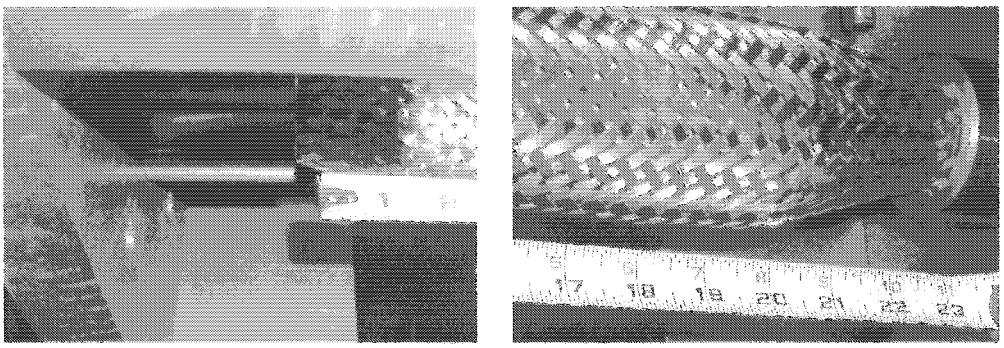

Figure 7-3: Effective length of braided tube between mounting points (dimensions in inches)

7.1.2 Impact Nosepiece

The impact test machine was equipped with a flat plate fastened to the translating crosshead. This plate was not acceptable to impact the braided tube assemblies, as excessive loading would occur at the edges of the plate due to the non-rounded edges. To minimize stress concentrations on impact, a nosepiece was constructed with a radius of 150 mm to provide a curved impacting surface and a thickness of 4.8 mm to ensure no deformation of the nosepiece. The nosepiece was fabricated with an adapter to mount to the flat plate on the crosshead. The material that was selected for the nosepiece was 1018 steel and all joints were welded. The nosepiece is illustrated in Figure 7-4. Complete drawings of the impact nosepiece can be found in Appendix F.

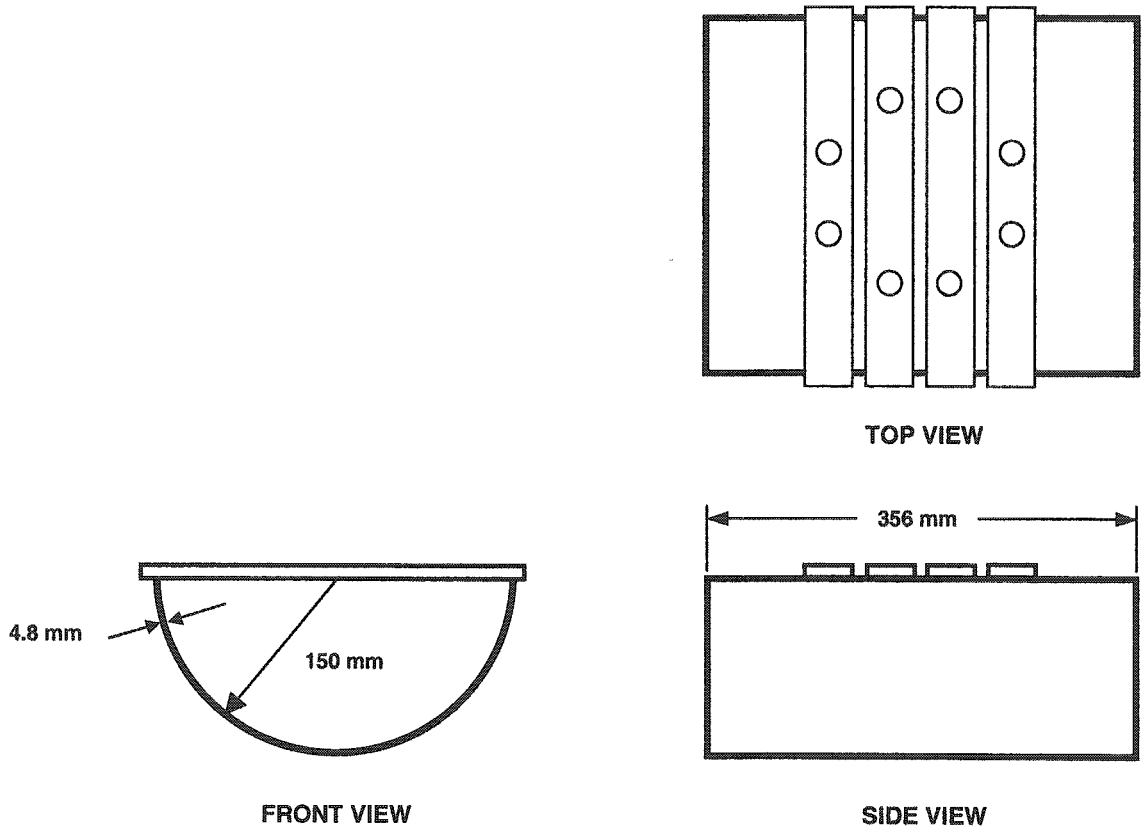

Figure 7-4: Impact nosepiece

During the preliminary tests, it was noted the crosshead had reached the extent of its travel distance and required additional spacing from the mounting plate to permit contact earlier. Two spacers were manufactured and installed for the second set of dynamic tests to add an additional 50.8 mm of height to the impact nosepiece. The resulting mass of the impacting crosshead was 71.5 kg, which was comprised of 57.2 kg for the crosshead and 14.3 kg for the nosepiece and spacers.

7.2 Dynamic Impact Test Procedure

When the braided tube assembly was secured in the annular clamps, the data collection start point was set with the impact test machine computer and the LVDT. Following this, the crosshead was raised to its maximum height of approximately 1.45 metres and released. The setup of the data collection start point allowed acceleration and displacement data recording to begin when the crosshead had reached the preset height.

7.3 Dynamic Tests – High Density Foam

There were three tests that were performed with high density foams. For each test, the length of foam core was approximately 508 mm, to nearly fill all of the tube between the two mounting points. This required the use of three individual foam pieces for each test. The foam specimens were comprised of one long and two short portions of similar length. The longest specimen was selected as the centre piece for the three. The specimens were assembled into the braided tube following the same steps as the quasi-static test specimens, ensuring that the foam pieces were oriented in a similar manner. The tube lengths were the same for all tests, 590 mm between the annular clamps. Any gaps between the foam specimens were minimized or it was noted if gaps were present prior to the start of each test. Figure 7-5 shows the foam samples and tube used in the first high density foam test.

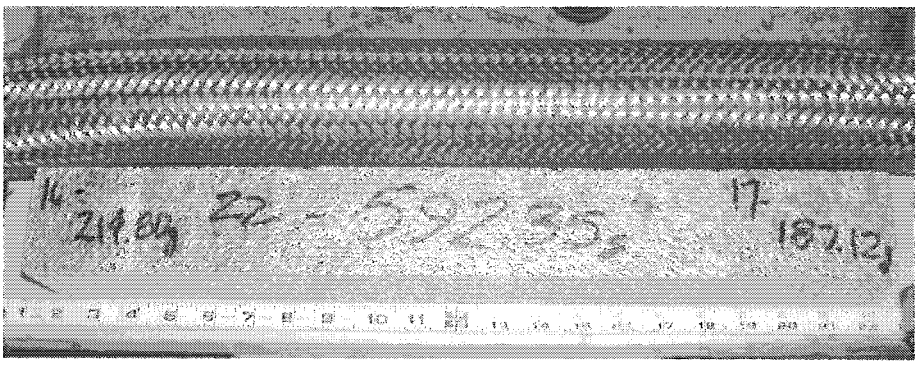

Figure 7-5: Tube and foam specimens from the first impact test

With the foam inserted into the tube, the tube and foam assembly was then secured to the test machine with the annular clamps. All three of the tests were carried out with the high density foams following similar practices in the setup and installation on the test machine.

The physical properties of the foam specimens used for the impact testing are listed in Table 7-1. Effort was made to group the foams with similar densities. A complete table listing all of the physical dimensions for each foam specimen can be found in Appendix A.

Table 7-1: Properties of foam specimens used in dynamic testing

Test Number	Specimen Number	Density (kg/m^3)	Length (mm)
1	37	488.1	304.8
1	30	535.1	100.8
1	31	466.2	100.8
2	36	490.3	304.8
2	20	408.9	100.8
2	22	425.1	100
3	38	531.8	304.8
3	21	429.7	103.2
3	29	429.7	100

7.4 High Density Foam Impact Test Results

Following the impact of the crosshead, the foam specimens had crushed in a number of areas, primarily on the centre segment as highlighted in Figure 7-6.

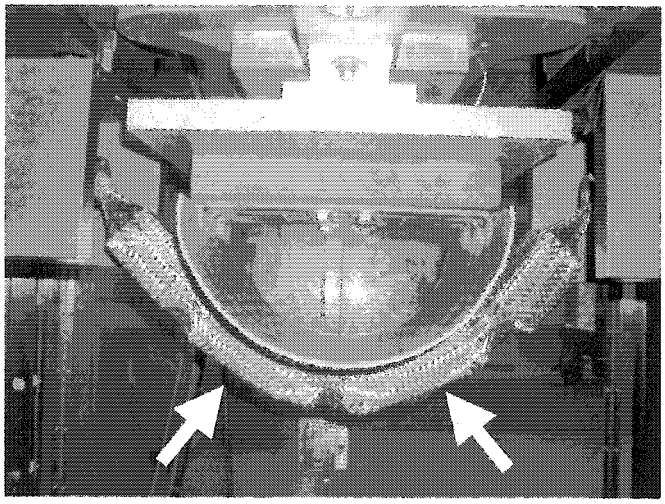

Figure 7-6: Braided tube and foam assembly following test

Fracture of the centre foam specimen occurs, with gaps developing between the individual foam bricks. These spaces caused elongation as the tube diameter decreased and the braid locked in these areas. This event can be seen in Figure 7-7 for the smaller foam pieces at the ends of the tube.

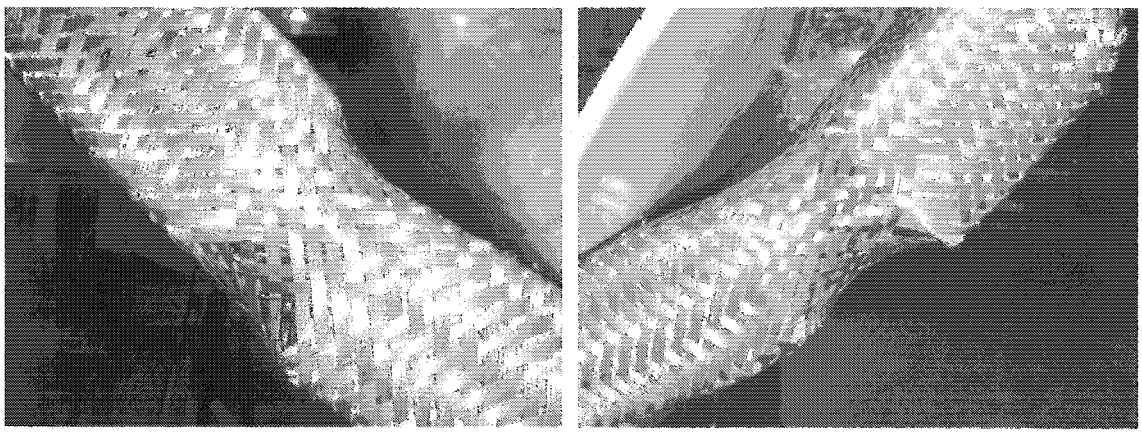

Figure 7-7: Tube elongation due to spaces between the foam bricks within the specimen

One noteworthy observation from these tests was that the high density foam did not permit the tube to conform to the shape of the nosepiece. Figure 7-8 shows that the impact nosepiece strikes the tube with point contact. The lower density foams in the preliminary tests demonstrated a behavior where the tube 'wrapped' around the nosepiece resulting in a high amount of surface contact between the nosepiece and the tube. Through the three tests, strand deformation was noticed, however no strand breakage on the braided tube was observed.

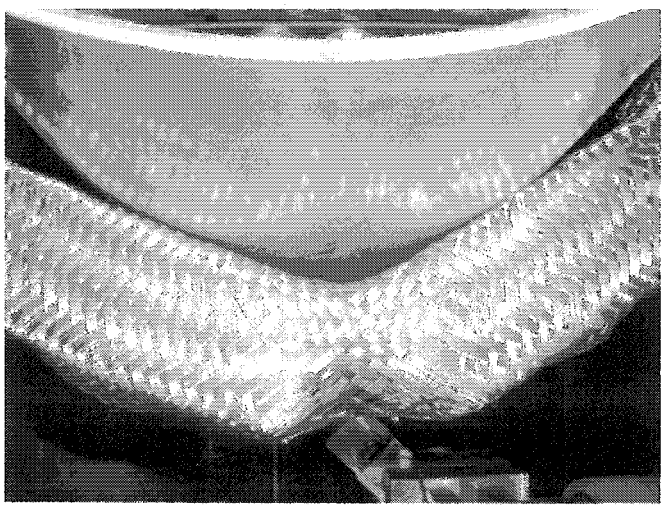

Figure 7-8: Contact points of nosepiece to braided tube with high density foam

7.4.1 Force – Displacement Analysis

The impact tests were carried out in consecutive order in the same test session. In a review of the force versus displacement plots in Figure 7-9 for the three tests, it can be seen that the test specimens respond in a similar manner to the impacting mass. The force response up to 200 mm is principally due to foam compaction and the average force that was calculated in this span for all three tests varies within 10%, between 1.95 and 2.16 kN. As the force rises, the braid has locked in a number of locations. The displacement at which the rise in force begins is attributable to the amount of gap between the foam specimens. It was noted that Test 2 had approximately 5 mm between the centre and one of the end foams prior to the start of the test. This explains the apparent shift in the force – displacement plot for Test 2, compared to the other tests. The maximum force for each of the tests ranged from 16.1 to 18.9 kN, with a minor amount of rebound or bounce in the impact nosepiece at the end of Test 3.

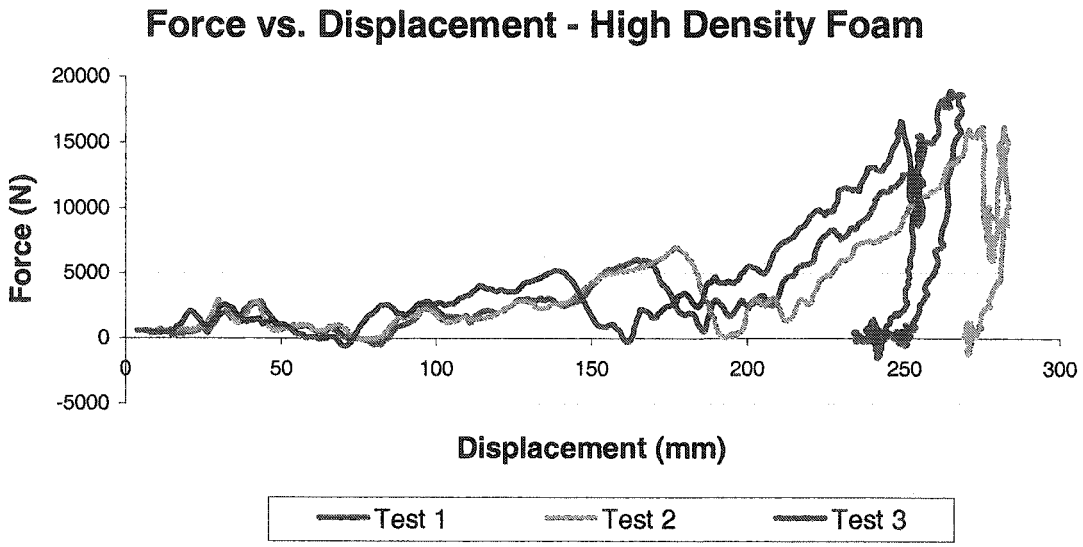

Figure 7-9: Force versus displacement for high density foam tests

7.4.2 Energy – Displacement Analysis

The energy absorbed by the braided tube assembly was determined knowing the mass of the impacting crosshead and from the acceleration – displacement data. The data were analyzed from the start of the test up to the peak acceleration that occurred to determine the energy absorption of the braided tube structure. Figure 7-10 is the plot of energy versus displacement for the three high density foam impact tests. It can be seen in the energy – displacement plots that the energy absorption was consistent between the three tests, including the absorbing capacities and the energy absorbed at a particular displacement. The energy absorbed ranged from a minimum of 901 J to a maximum of 978 J.

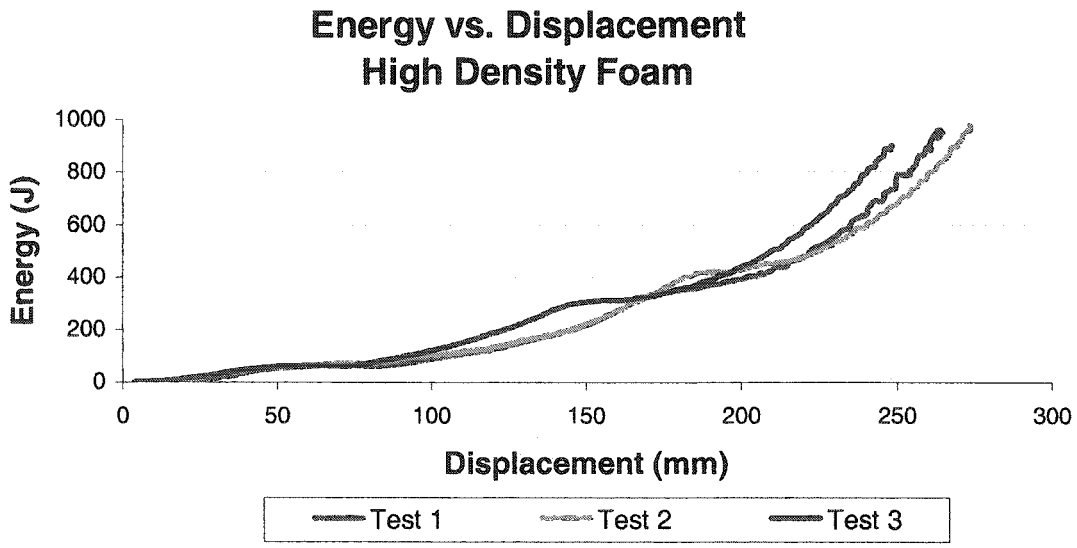

Figure 7-10: Energy absorption versus displacement for high density foam tests

In the initial displacement of the impact nosepiece, the energy absorption was identical for the three tests. This was likely due to initial foam compression and the braid tightening around the foam bricks. The plateau that occurred at approximately 180 mm for Tests 1 and 2 and at 150 mm for Test 3 was due to the fracture of the centre foam core. During the installation of the braided tube for Test 3, the tube was tensioned much tighter than Tests 1 and 2. In addition, the density of the centre foam brick for Test 3 is higher than Tests 1 and 2. The results of the impact testing are summarized in Table 7-2.

Table 7-2: Summary of test results for high density foam impact tests

Test Number	Foam Density ρ_f (LEFT) (kg/m^3)	ρ_f (CENTRE) (kg/m^3)	ρ_f (RIGHT) (kg/m^3)	F_{avg} (0-200 mm) (kN)	Maximum Acceleration (G)	Maximum Force (kN)	Energy Absorbed (J)
1	535.1	488.1	466.2	1.95	26.90	18.9	960.4
2	408.9	490.3	425.1	2.15	22.95	16.1	978.1
3	429.7	531.8	429.7	2.16	23.60	16.6	900.7

8. SUMMARY AND CONCLUSIONS

In this study, quasi-static tensile testing and dynamic impact testing of aluminum foam filled braided tubes has been performed. This device has shown the potential to function as an energy absorber under tensile and bending loading conditions. Further to the work on the braided tubes, development work on clamps that was performed found that the best design to secure the braided tube was an annular wedge and clamp to secure the braid around the entire circumference.

8.1 Quasi-Static Tensile Testing

The aluminum foam filled braided tube was tested in tensile loading conditions only in the quasi-static testing. The quasi-static testing confirmed the load management characteristics and ability to absorb energy in tension at loads up to 45 kN without braid material failure on the 304 stainless steel tubing. The aluminum foam filled specimens were 406 mm in length for all quasi-static tensile tests in this research.

When reviewing the Stage 1 and 2 loading data, the quasi-static test results indicate that changes in foam density affect the energy absorption when normalized on a per unit volume basis. This relationship appears to be linear in the Stage 1 and 2 loading regions, where a foam density (ρ_f) of 226.8 kg/m^3 provided an energy absorption of 0.424 MJ/m^3 (Test 1) and a foam density (ρ_f) of

298.2 kg/m^3 provided an energy absorption of 2.048 MJ/m^3 (Test 5). As the density of the aluminum foam core increased, there was a corresponding increase in the energy absorption per unit volume of foam. Test 6 deviated from the linear relationship for the Stage 1 and 2 loading.

Energy absorption from deformation of the stainless steel tube contributed the highest quantity of energy absorption after the foam core had collapsed. The Stage 3 energy absorption was principally due to braid deformation and contributed between 62% and 82% of the total energy absorbed for the aluminum foam filled braided tube. When Stages 1, 2, and 3 loading are considered, a linear relationship exists between Test 2 through Test 6. Due to complications in setup in the third loading stage, Test 1 was not considered in the analysis for all three loading stages. For all three loading stages, a foam density (ρ_f) of 248.9 kg/m^3 provided 4.386 MJ/m^3 of energy absorption per unit volume (Test 2) and a foam density (ρ_f) of 373.4 kg/m^3 provided 6.332 MJ/m^3 of energy absorption per unit volume (Test 6). Similar to Stage 1 and 2 loading, a linear relationship exists for foam density and energy absorption per unit volume when considering all three loading stages.

8.2 Numerical Approximation

The numerical approximation provided a reasonable estimate of energy absorption for the aluminum foam filled braided tubes provided the foam core has collapsed. Comparison to quasi-static experimental results shows that one of five tests was within 7% of the experimental determination of energy absorption.

Errors may have been introduced with the computation of total tube elongation and the estimation of the foam plateau stresses in the other four tests, as the difference from the experimental results ranged from 33.4% to 59.4%. The error in total tube elongation was influenced by braid slippage in the clamps and excessive slack in the tube. Tube displacement that occurred without significant energy absorption was due in part to the relaxed braid being taken up and due to the tensile fracture of the aluminum foam core.

The foam plateau stresses were calculated for the numerical approximation. The ideal method of determining the plateau stress is through experimental methods as performed in Chapter 4, as the numerical approximation had variations up to 1 MPa from the actual plateau stress. The foam plateau stress is the most significant variable in the determination of energy absorption from the aluminum foam core.

8.3 Dynamic Impact Testing

Dynamic testing indicates that aluminum foam filled braided tubes can function in a combined bending and tensile loading condition with no braid material failure. For the tube length of 590 mm, the device was able to absorb 960.4 J, 978.1 J, and 900.7 J of energy in the three tests that were performed. The average forces of 1.95 kN, 2.15 kN, and 2.16 kN, for each test respectively, were observed in the region where aluminum foam compaction occurred.

The high density foams absorb the energy of the impact but did not conform to the surface of the nosepiece. The braided tube assembly was too

rigid for the impact with the use of the high density foam. Preliminary test results on the dynamic test machine indicate that a low density aluminum foam core would permit for a higher reduction in tube diameter and energy absorption from foam compression.

9. RECOMMENDATIONS

The following recommendations represent areas of possible continued improvement opportunities and research topics for aluminum foam filled braided tubes:

1) Modify the nose of the wedges in the annular clamps to increase the radius on the end of the wedge. Following the experiments performed on the impact tester, deformation of the braid material was evident where strands were subjected to the tensile stresses of bending at the top of the annular clamp. Although no strand failure was noted, the small radius on the wedge clamp has the potential to shear the braid material as it is pulled over during the impact test. A hemispherical shape is ideal for this application to minimize any contact stresses.

2) Further testing should note that spaces or gaps between individual foam specimens increase the elongation of the tube while providing little energy absorption. If possible, the tube should be filled with aluminum foam up to the clamps. Although this causes difficulties to install and secure the braid in the clamp, higher energy absorption occurs.

3) The braid material was selected for its cost effectiveness. Various materials are woven into tubular braid and may yield superior performance to the 304 stainless steel material. Other stainless steels as well as many polymer based materials are available in a variety of configurations, lengths and diameters and should be considered in experimental tests.

4) The characteristics of larger diameter aluminum foam filled tube should be studied. The diameter of the braided tube was chosen based on the size of the aluminum foam specimens that were available for testing. A larger diameter may perform more effectively than those studied in this research.

5) The quasi-static tests in this thesis required three setups to complete each test. A continuous load test of a specimen would be preferred, however this requires the use of an instrumented tensile test machine with a travel of 450 mm or greater and 150 kN capacity. This would provide a continuous test of the specimen and minimize any data collection errors that may have occurred in this study.

6) Impact testing was performed on the high density foam filled braided tubes. Due to problems with the data collector, the low density foam specimens could not be tested. The preliminary dynamic tests that were performed show promise that the low density foams will prove to be a superior energy absorber. When available, these tests should be carried out and compared to the high density specimens.

10. REFERENCES

10.1 Cited References

1. Fuganti, A., L. Lorenzi, A.G. Hanssen and M. Langseth, Aluminium Foam for Automotive Applications, Advanced Engineering Materials, 2, No. 4, (2000).

2. DongWon Pipe Company
www.dwmic.co.kr/edongwonpipe/product/promain9.html

3. Lin, K.H. and G. Thomas Mase, An Assessment of Add-on Energy Absorbing Devices for Vehicle Crashworthiness, Journal of Engineering Materials and Technology, 112, pp. 406-411, (October, 1990).

4. Hanssen, A.G., L. Lorenzi, K.K. Berger, O.S. Hopperstad and M. Langeth, A Demonstrator Bumper System Based on Aluminium Foam Filled Crash Boxes, International Journal of Crashworthiness, 5, No. 4, pp. 381-392, (April, 2000).

5. Hanssen, A.G., M. Langseth and O.S. Hopperstad, Optimum Design for Energy Absorption of Square Aluminium Columns with Aluminium Foam Filler, International Journal of Mechanical Sciences, 43, No. 1, pp. 153-176, (January, 2001).

6. Alusion – Aluminum foam architecture and design
www.alusion.com

7. Körner, C and R.F. Singer, Processing of Metal Foams – Challenges and Opportunities, Advanced Engineering Materials, 2, No. 4, pp. 159-165, (2000)

8. Cymat – Stabilized aluminum foam manufacturer
www.cymat.com

9. Hanssen, A.G., O.S. Hopperstad and M. Langseth, Design of Aluminium Foam-Filled Crash Boxes with Square and Circular Cross Sections, International Journal of Crashworthiness, Volume 6, No. 2, pp. 177-188, (March, 2001).

10. Hanssen, A.G., M. Langseth and O.S. Hopperstad, Static Crushing of Square Aluminium Extrusions with Aluminium Foam Filler, International Journal of Mechanical Sciences, 41, No. 8, pp. 967-993, (August, 1999).

11. Gradinger, R., M. Seitzberger, F.G. Rammerstorfer, H.P. Degischer, M. Blaimschein, and Ch. Walch, Aluminium Foam Filled Steel Tubes As Composite Shock Absorbers

12. Langseth, M., O.S. Hopperstad and A.G. Hanssen, Crash Behaviour of Thin-Walled Aluminium Members, Thin-Walled Structures, 32, No. 1-3, pp. 127-150, (September, 1998).

13. Santosa, S., J. Banhart and T. Wierzbicki, Bending Crush Resistance of Partially Foam-Filled Sections, Advanced Engineering Materials, 2, No. 4, (2000).

14. Santosa, S., J. Banhart and T. Wierzbicki, Experimental and Numerical Analyses of Bending of Foam-Filled Sections, Acta Mechanica, 148, pp. 199-213, (2001).

15. Sei Jin Machinery Co. Ltd. – Wire braid machine manufacturer www.seijinbraid.co.kr

16. Qiu, Y., Y. Wang, J.Z. Mi, M.A. Laton and C. Zhang, A Novel Approach for Measurement of Fiber-on-Fiber Friction, F98S-09, National Textile Center Annual Report, Wilmington, Delaware, (November, 1998)

17. Chen, J., R.A. DaSilva, S. Warner and A. Lewis, High Stress Elastic Materials, M98-D03, National Textile Center Annual Report, Wilmington, Delaware, (November, 1999).

18. Chen, J., R.A. DaSilva, S. Warner and A. Lewis, High Stress Elastic Materials, M98-D03-A1, National Textile Center Annual Report, Wilmington, Delaware, (November, 2001).

19. Harte, A.M. and N.A. Fleck, On the Mechanics of Braided Composites in Tension, European Journal of Mechanics A. Solids, 19, No. 2, pp. 259-275, (March, 2000).

20. Harte, A.M., N.A. Fleck and M.F. Ashby, Energy Absorption of Foam-Filled Circular Tubes with Braided Composite Walls, European Journal of Mechanics A. Solids, 19, No. 1, pp. 31-50, (January, 2000).

21. Matweb – Materials information www.matweb.com

10.2 Bibliography

1. Andrews, E.W., J.S. Huang and L.J. Gibson, Creep Behaviour of a Closed-Cell Aluminum Foam, Acta Metallurgica, 47, No. 10, pp. 2927-2935, (October, 1999).

2. Andrews, E.W. and L.J. Gibson, The Influence of Crack-Like Defects on the Tensile Strength of an Open-Cell Aluminum Foam, Scripta Materialia, 44, No. 7, pp. 1005-1010, (2001).

3. Boeman, R.G. and A.G. Caliskan, A Novel Capability for Crush Testing Crash Energy Management Structures at Intermediate Rates, 2002-01-1954, Society of Automotive Engineers, Inc., Warrendale, Pennsylvania, (February, 2002).

4. Budynas, R.G., Advanced Strength and Applied Stress Analysis, pp. 63-66, McGraw-Hill Book Company, New York, (1977).

5. Daxner, T., H.J. Böhm and F.G. Rammerstorfer, Mesoscopic Simulation of Inhomogeneous Metallic Foams with Respect to Energy Absorption, Computational Materials Science, 16, pp. 61-69, (1999).

6. Deshpande, V.S. and N.A. Fleck, Isotropic Constitutive Models for Metallic Foams, University of Cambridge, Cambridge, United Kingdom, (November, 1998).

7. Flesher, N., Braided Composite Tubes for Crash Energy Absorption, Stanford University, Stanford, California, (2003). http://structure.stanford.edu/Project/ResearchProjects/flesher/Flesher%20Research%20Brief.ppt

8. Hanssen, A.G., L. Enstock and M. Langseth, Close-Range Blast Loading of Aluminium Foam Panels, International Journal of Impact Engineering, 27, No. 6, pp. 593-618, (July, 2002).

9. Hearle, J.W.S, P. Grosberg and S. Backer, Structural Mechanics of Fibers, Yarns, and Fabrics, Volume 1, pp. 6-322, Wiley-Interscience, John Wiley & Sons, Inc., New York, (1969).

10. Hibbeler, R.C., Mechanics of Materials, Volume 1, pp. 325-416, pp. 631-660, pp. 685-722, Macmillan Publishing Company, New York, (1991).

11. Ip, S.W., Y. Wang and J.M. Toguri, Aluminum Foam Stabilization by Solid Particles, Canadian Metallurgical Quarterly, 38, No. 1, pp. 81-92, (January, 1999).

12. Kanahashi, H., T. Mukai, Y. Yamada, K. Shimojima, M. Mabuchi, T.G. Nieh and K. Higashi, Dynamic Compression of an Ultra-Low Density Aluminium Foam, Materials Science and Engineering, A280, pp. 349-353, (2000).

13. McCormack, T.M., R. Miller, O. Kesler and L.J. Gibson, Failure of Sandwich beams with Metallic Foam Cores, International Journal of Solids and Structures, 38, No. 28-29, pp. 4901-4920, (July, 2001).

14. Mukai, T., H. Kanahashi, T. Miyoshi, M. Mabuchi, T.G. Nieh, and K. Higashi, Experimental Study of Energy Absorption in a Close-Celled Aluminum Foam Under Dynamic Loading, Scripta Matierialia, 40, No. 8, pp. 921-927, (1999).

15. Raczy, A., Foam Filled Tubes as Energy Absorbers in Automotive Applications, University of Windsor, Windsor, Ontario, (2002).

16. San Marchi, C. and A. Mortensen, Deformation of Open-Cell Aluminum Foam, Acta Materialia, 49, No. 19, pp. 3959-3969, (November, 2001).

17. Santosa S.P., T. Wierzbicki, A.G. Hanssen and M. Langseth, Experimental and Numerical Studies of Foam-Filled Sections, International Journal of Impact Engineering, 24, No. 5, pp. 509-534, (May, 2000).

18. Santosa, S. and T. Wierzbicki, Crash Behaviour of Box Columns Filled with Aluminum Honeycomb or Foam, Computers & Structures, 68, No. 4, pp. 343-367, (August, 1998).

19. Santosa, S. and T. Wierzbicki, Effect of an Ultralight Metal Filler on the Bending Collapse Behavior of Thin-Walled Prismatic Columns, International Journal of Mechanical Sciences, 41, No. 8, pp. 995-1019, (August, 1999).

20. Santosa, S. and T. Wierzbicki, On the Modeling of Crush Behavior of a Closed-Cell Aluminum Foam Structure, Journal of Mechanics and Physics of Solids, 46, No. 4, pp. 645-669, (1998).

21. Singletary, J. and C. Pastore, Finite Element Modeling of 3-D Braided Carbon Fiber/Urethane Elastomer Tubes, Fiber Architects, www.fiberarchitects.com/aerospace/braidtubes.html

22. Thornton, P.H. and C.J. Amberger, The Effect of Foam Filling Upon the Energy Absorption of Spot Welded Sheet Metal Tubes, Journal of Engineering Materials and Technology, 107, pp. 334-337, (October, 1985).

23. Van Vlack, L.H., Elements of Materials Science and Engineering, Sixth Edition, pp. 504-517, Addison-Wesley Publishing Company, Don Mills, Ontario, (1989).

APPENDIX A

Physical Properties of Foam Specimens

Table A-1: Foam specimens used in quasi-static tensile testing

Specimen #	Average Length (mm)	Width (mm)	Height (mm)	Volume (m^3)	Mass (g)	Mass (kg)	Density (kg/m^3)	Notes
1	304.80	49.85	73.46	0.001116	310.8	0.3108	278.48	Test 3 Tested - 20030516
2	304.80	49.90	73.05	0.001111	275.5	0.2755	248.90	Test 2 Tested - 20030516
3	304.80	49.49	73.59	0.001110	414.5	0.4145	373.35	Test 6 Tested - 20030524
4	304.80	48.12	73.65	0.001080	312.2	0.3122	288.24	Test 4 Tested - 20030524
5	303.74	49.90	73.54	0.001115	332.4	0.3324	298.21	Test 5 Tested - 20030524
6	304.80	49.13	73.59	0.001102	250	0.25	226.87	Test 1 Tested - 20030516

Table A-2: Foam specimens used in preliminary dynamic impact testing

Specimen #	Length (mm)	Metric Width (mm)	Height (mm)	Volume (m^3)	Mass (g)	Mass (kg)	Density (kg/m^3)	Notes
7	150.8	49.2	49.2	0.000365	81.33	0.08133	222.7	Test #1 - 20030709
8	154.0	50.8	49.2	0.000385	90.14	0.09014	234.1	Test #1 - 20030709
9	153.2	52.4	50.0	0.000401	96.66	0.09666	240.9	Test #1 - 20030709
10	102.4	48.4	74.6	0.000370	95.32	0.09532	257.7	Test #2 - 20030709
11	150.8	49.2	74.6	0.000554	184.5	0.1845	333.2	Test #2 - 20030709
12	150.8	49.2	74.6	0.000554	186	0.186	335.9	Test #2 - 20030709
13	304.8	63.5	66.7	0.001290	284.4	0.2844	220.4	Test #3 - 20030709
14	304.8	63.5	66.7	0.001290	289.95	0.28995	224.7	

Dimensions and masses for preliminary dynamic impact tests - July 9, 2003

Table A-3: Foam specimens used for dynamic impact testing

Specimen #	Length (mm)	Metric Width (mm)	Height (mm)	Volume (m^3)	Mass (g)	Mass (kg)	Density (kg/m^3)	Notes
15	304.8	63.5	68.3	0.001321	327.3	0.3273	247.7	
16	304.8	63.5	68.3	0.001321	330.07	0.33007	249.8	
17	100.0	63.5	67.5	0.000428	98.05	0.09805	228.8	
18	102.4	63.5	67.5	0.000439	104.45	0.10445	238.1	
19	100.8	63.5	67.5	0.000432	101.97	0.10197	236.1	
20	100.8	63.5	62.7	0.000401	164.13	0.16413	408.9	Test 2 - 20030717
21	103.2	63.5	62.7	0.000411	176.54	0.17654	429.7	Test 3 - 20030717
22	100.0	63.5	62.7	0.000398	169.28	0.16928	425.1	Test 2 - 20030717
23	100.0	63.5	66.7	0.000423	102.17	0.10217	241.3	
24	101.6	63.5	67.5	0.000435	104.86	0.10486	240.9	
25	102.4	63.5	67.5	0.000439	107.24	0.10724	244.5	
26	96.8	63.5	67.5	0.000415	97.03	0.09703	233.9	Used for Stress/Strain
27	101.6	63.5	67.5	0.000435	104.21	0.10421	239.4	Used for Stress/Strain
28	102.4	63.5	67.5	0.000439	100.95	0.10095	230.1	Used for Stress/Strain
29	100.0	63.5	62.7	0.000398	171.13	0.17113	429.7	Test 3 – 20030717
30	100.8	63.5	62.7	0.000401	214.8	0.2148	535.1	Test 1 – 20030717
31	100.8	63.5	62.7	0.000401	187.12	0.18712	466.2	Test 1 – 20030717
32	101.6	63.5	62.7	0.000405	169.68	0.16968	419.4	Used for Stress/Strain
33	100.8	63.5	62.7	0.000401	165.87	0.16587	413.2	Used for Stress/Strain
34, 35	100.8	63.5	62.7	0.000401	170.72	0.17072	425.3	Used for Stress/Strain
36	304.8	63.5	62.7	0.001214	595.08	0.59508	490.3	Test 2 - 20030717
37	304.8	63.5	62.7	0.001214	592.35	0.59235	488.1	Test 1 - 20030717
38	304.8	63.5	62.7	0.001214	645.4	0.6454	531.8	Test 3 - 20030717

Dimensions and masses for dynamic test July 17, 2003

Table A-4: Foam specimens used for stress-strain and plateau stress analysis

Specimen #	Metric Length (mm)	Metric Width (mm)	Metric Height (mm)	Average Length (mm)	Average Width (mm)	Average Height (mm)	Volume (m^3)	Mass (kg)	Density (kg/m^3)	Notes
26	96.98	63.58	66.90	96.41	63.44	66.72	0.00041	0.09703	237.8	
	96.64	63.22	66.87							Used teflon pads top & bottom to reduce friction
	96.11	63.47	66.67							Tested at 15 000N setting
	95.90	63.47	66.72							Approx. 10 minute duration for test
			66.43							* Test requires 60 000N setting - Results no good
27	102.15	63.50	66.92	102.33	63.54	66.78	0.00043	0.10421	240.0	
	102.43	63.41	66.76							Used teflon pads top & bottom to reduce friction
	102.37	63.65	66.77							Tested at 60 000N setting
	102.37	63.58	66.67							Approx. 10 minute duration for test
28	102.55	63.61	67.09	102.78	63.56	66.85	0.00044	0.10095	231.1	
	102.64	63.49	66.86							No teflon pads used
	102.94	63.62	66.59							Tested at 60 000N setting
	102.99	63.53	66.87							Approx. 10 minute duration for test
32	102.32	63.56	62.13	102.36	63.68	62.19	0.00041	0.16968	418.6	
	102.13	63.66	62.24							No teflon pads used
	102.43	63.75	62.24							Tested at 150 000N setting
	102.56	63.73	62.15							Approx. 10 minute duration for test
33	100.67	63.60	62.38	100.14	63.58	62.55	0.0004	0.16587	416.5	
	99.95	63.62	62.63							No teflon pads used
	99.65	63.56	62.97							Tested at 150 000N setting
	100.30	63.55	62.23							Approx. 10 minute duration for test
34	48.44	63.57	61.95	47.58	63.69	61.90	0.00019	0.08007	426.9	
	47.20	63.73	61.87							No teflon pads used
	47.29	63.76	61.84							Tested at 150 000N setting
	47.38	63.68	61.92							Approx. 10 minute duration for test
35	52.85	63.65	62.28	52.58	63.64	62.53	0.00021	0.08830	422.0	
	52.68	63.64	62.48							No teflon pads used
	52.17	63.68	62.47							Tested at 150 000N setting
	52.63	63.57	62.88							Approx. 10 minute duration for test

APPENDIX B

Annular Wedge Clamp Drawings

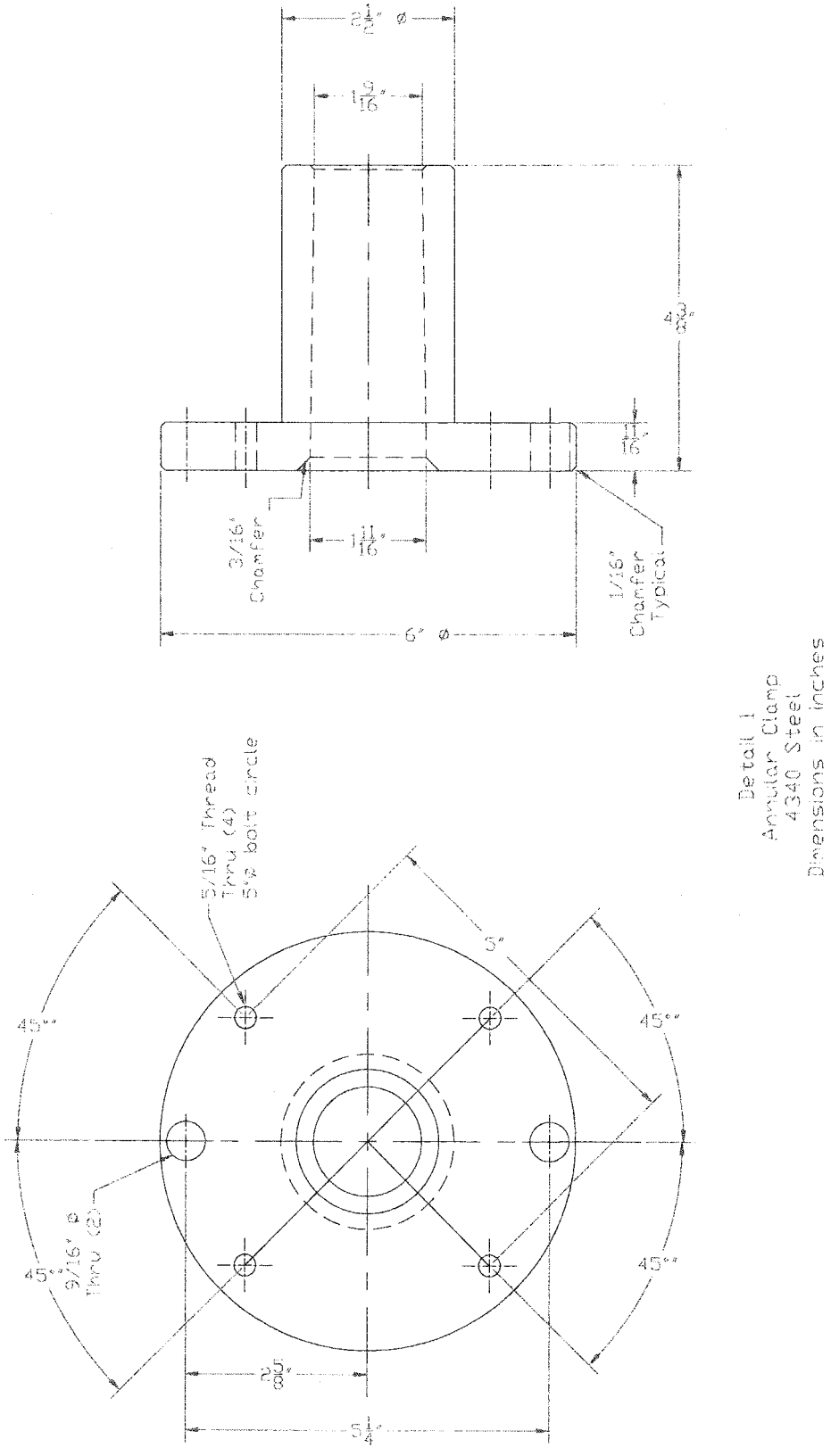

Figure B-1: Annular clamp drawing

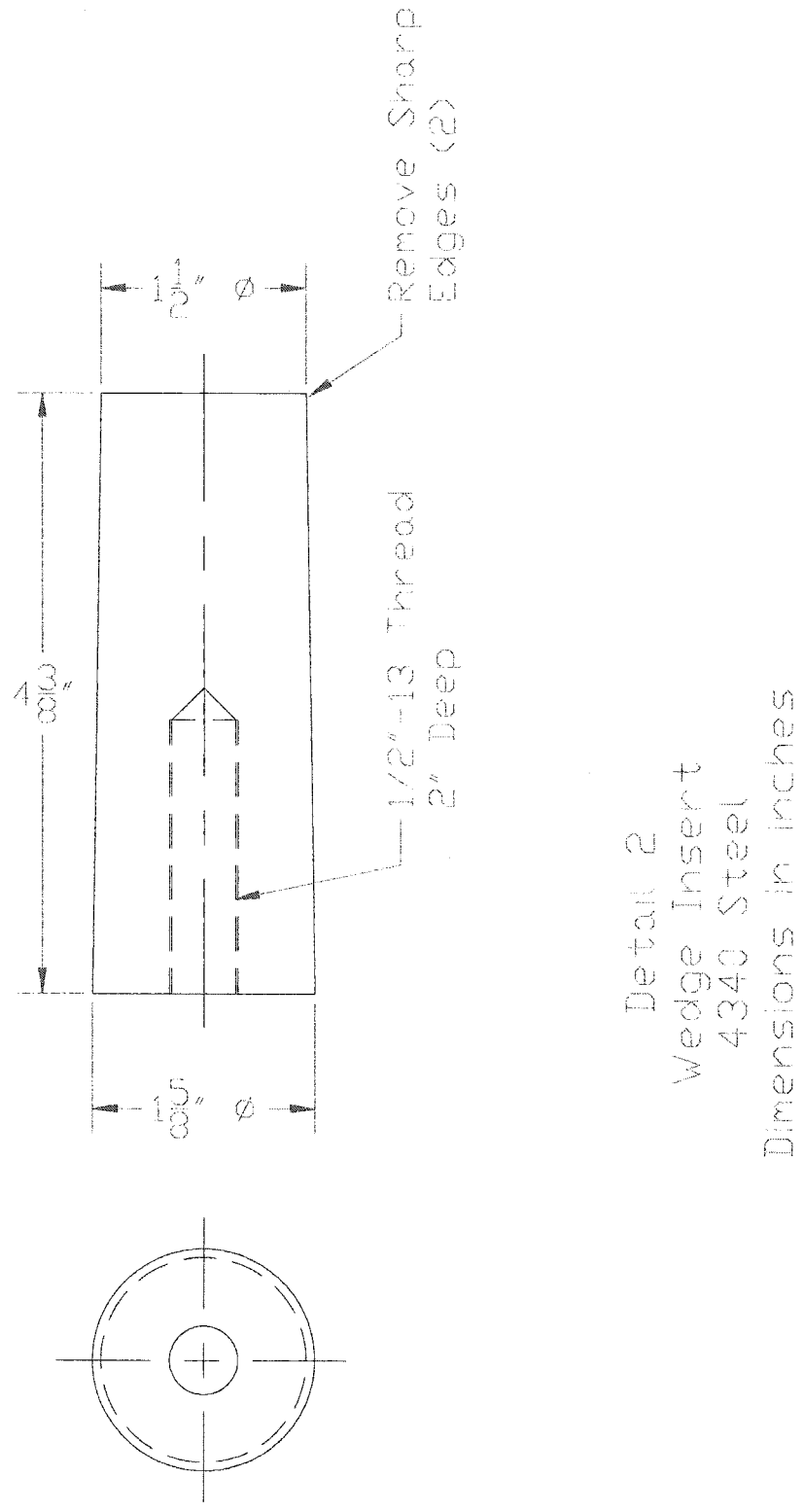

Figure B-2: Wedge insert drawing

APPENDIX C

Material Properties for 304 Stainless Steel

Table C-1: Material properties of 304 stainless steel

(Source: Matweb, materials property database, www.matweb.com [21])

304 Stainless Steel

Ultimate Tensile Strength	505	MPa (minimum)
Yield Strength	215	MPa (at 0.2% offset)
Elongation at Break	70%	
Modulus of Elasticity	193-200	GPa
Charpy Impact	325	J
Poisson's Ratio	0.29	
Shear Modulus	86	GPa
Hardness, Knoop	138	
Hardness, Rockwell B	70	
Hardness, Vickers	129	
Density	8000	kg/m^3

Composition – Percent by Weight

Carbon	Max 0.08
Chromium	18-20
Iron	66.345 – 74
Manganese	Max 2
Nickel	8 – 10.5
Phosphorus	Max 0.045
Sulphur	Max 0.03
Silicon	Max 1

Source for 2 inch stainless steel braided tubing:

Flex Pression Ltd.
6590 Abrams
Ville St Laurent, Quebec
H2S 1Y2

Telephone: (514) 334-9888
Fax: (514) 334-1044

www.flexpression.com

APPENDIX D

Detailed Quasi-Static Tensile Test Procedure

Test Procedure – Braided Tube Quasi-Static Tensile Testing

1. Remove all gripper jaws from upper and lower plate of Tinius Olsen test fixture.
2. Fasten outer wedge clamp to lower plate of test fixture and feed end of specimen through the centre of the wedge clamp – See Figure D-1 for details of Tinius Olsen test fixture.

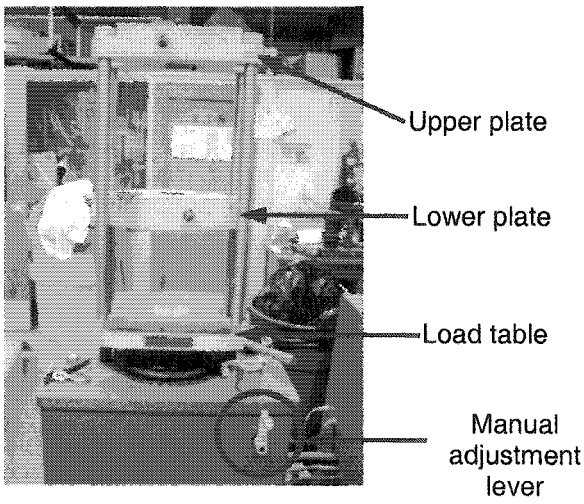

Figure D-1: Tinius Olsen test fixture details

3. Insert wedge inside braided tube and place steel block below wedge.
4. Start Tinius Olsen test machine and set scale range to 15 000 Newtons – see Figure D-2 for details of control panel.
5. Ensure no load on the fixture and zero load cell with adjustment dial – see Figure D-2 for details of control panel.

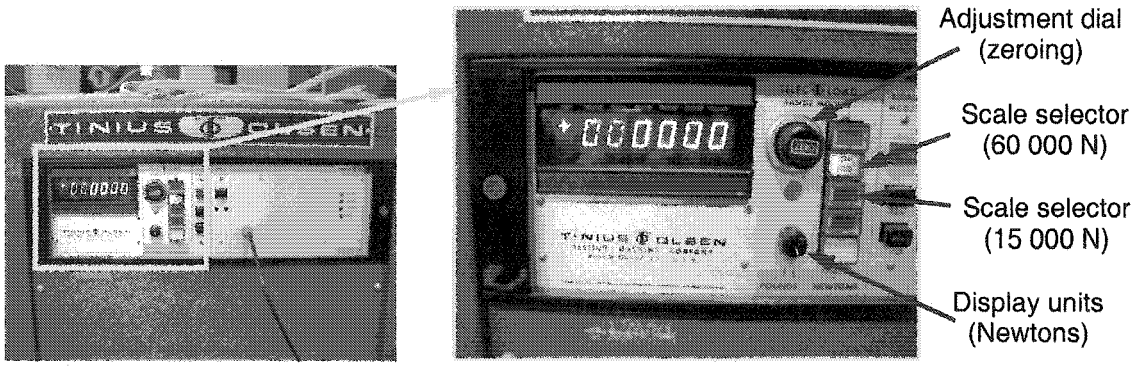

Figure D-2: Tinius Olsen control panel

6. Raise load table to make contact between lower wedge and steel block.

7. Continue raising load table until reading of 1 500 Newtons on the display is obtained.

8. Remove load from the test fixture – the locked assembly should be similar to Figure D-3.

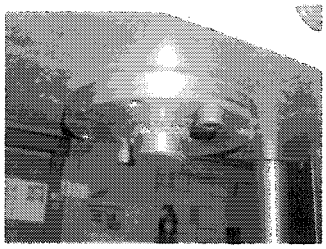

Figure D-3: Lower wedge clamp assembly

9. Fasten wedge clamp to upper plate.

10. Adjust lower plate of test fixture to allow the feed of the opposite end of the specimen through the centre of the wedge clamp and upper plate.

11. Insert wedge into the braided tube and secure in the upper clamp using mallet to secure as shown in Figure D-4.

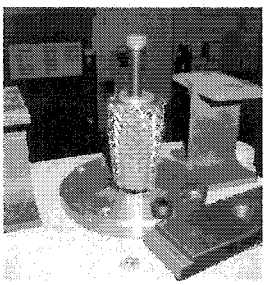

Figure D-4: Upper wedge clamp assembly

12. Reset load table of test fixture to a height of 172 mm (6 $^{7}/_{8}$ in) from the top of the load table to the base of the machine.
13. Using the manual adjustment lever, move the lower plate on the test fixture until the load sensor display reads 500 Newtons.
14. Start data collection software at the Tinius Olsen workstation shown in Figure D-5.

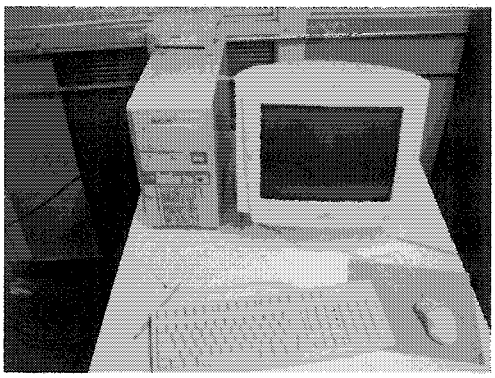

Figure D-5: Tinius Olsen data collection computer

15. Start tensile tester – note that the maximum travel of the test fixture is 150 mm.

*** If test is stopped, the data collection software must be re-started to ensure that data collection occurs ***

16. Stop tester when maximum travel is reached.
17. Remove load from test fixture and reset data collection computer for next trial.
18. Remove bolts from upper clamp.
19. Repeat Steps 12 – 17 for the 108 mm (4 ¼ in) and 171.45 mm (6 ¾ in) spacers under the upper wedge clamp and a setting of 60 000 N on the Tinius Olsen control panel.

APPENDIX E

Comparison of Theoretical and Quasi-Static
Experimental Test Results

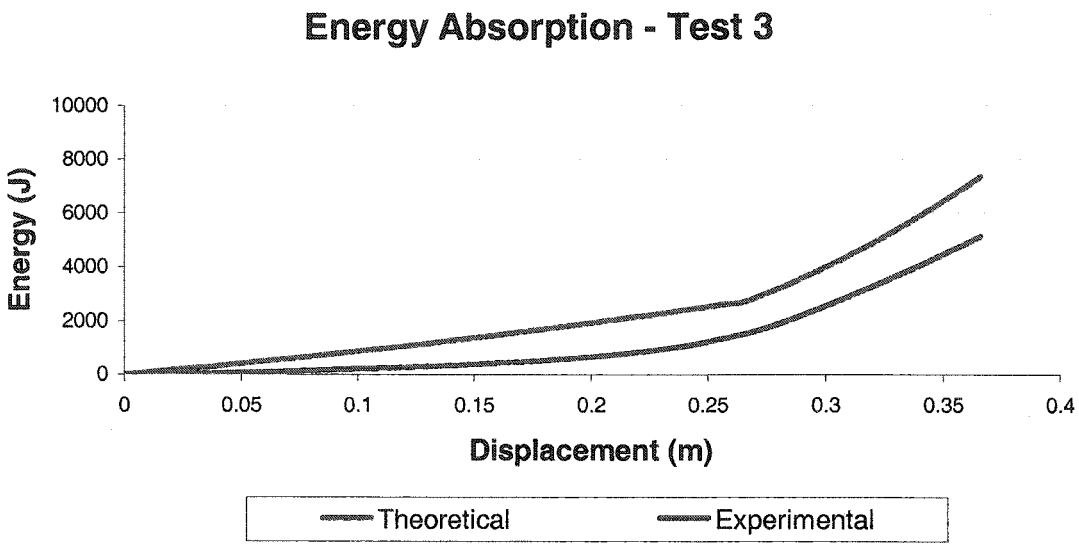

Figure E-1: Comparison between theoretical and experimental results for Test 3

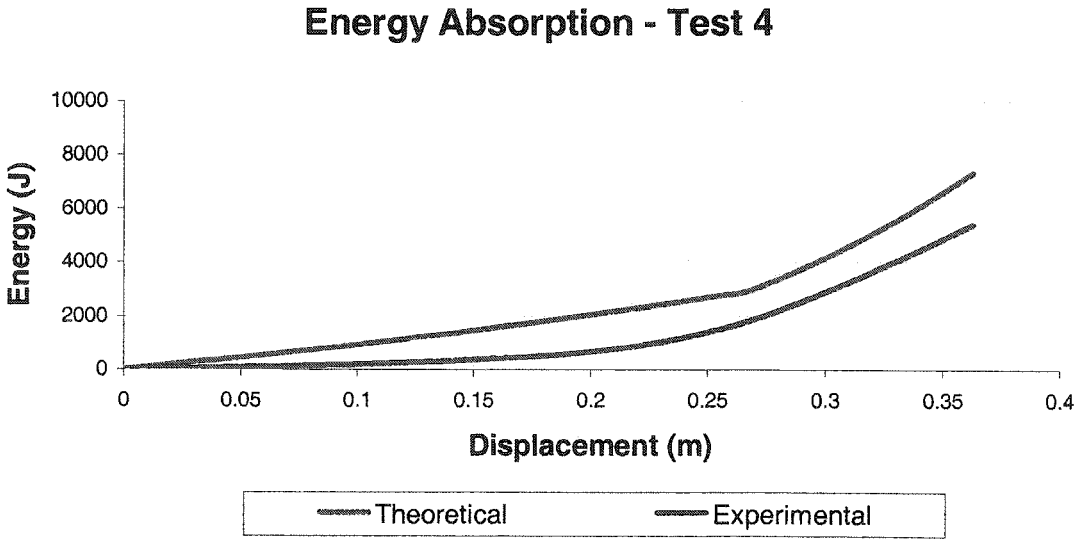

Figure E-2: Comparison between theoretical and experimental results for Test 4

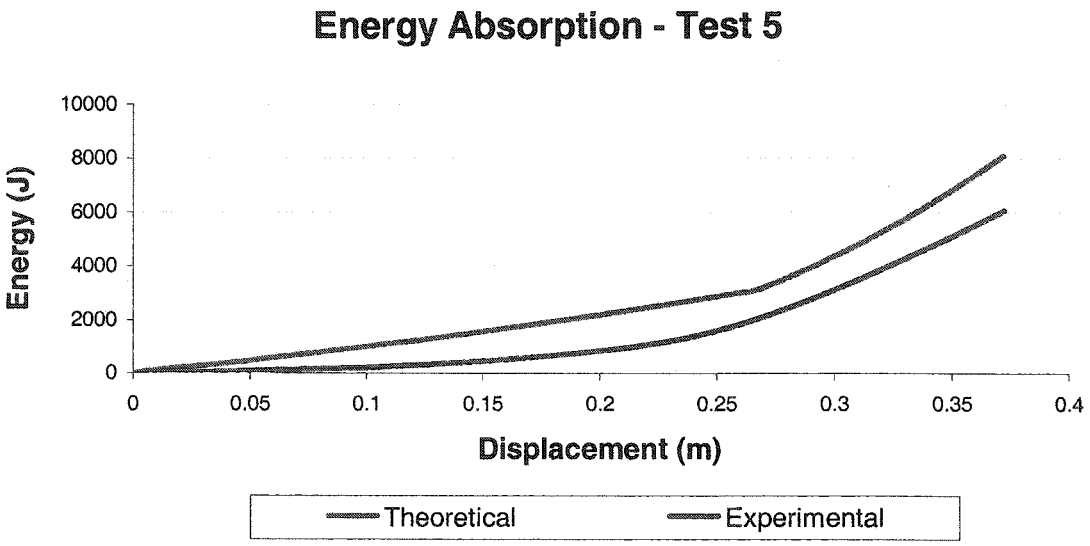

Figure E-3: Comparison between theoretical and experimental results for Test 5

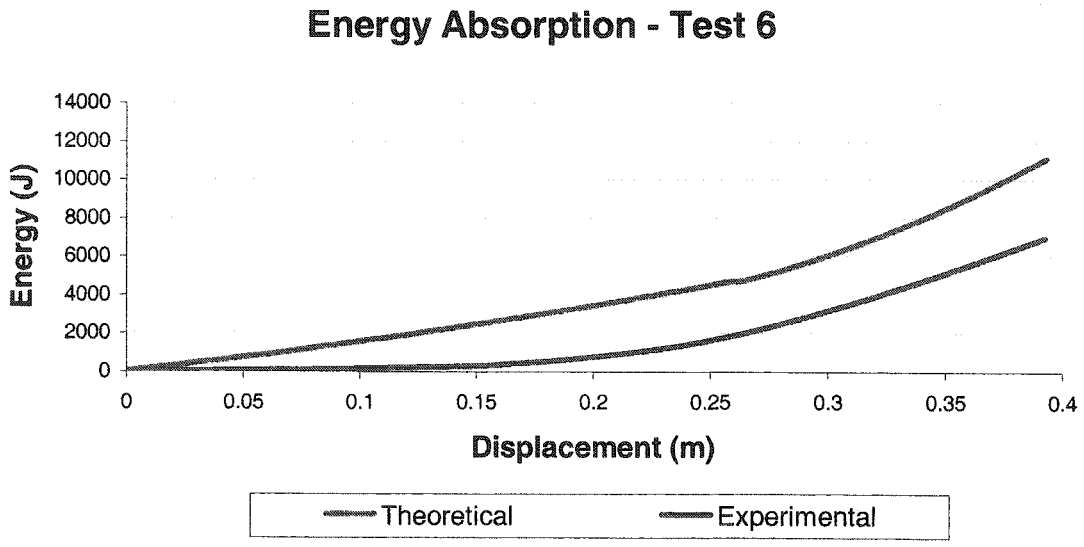

Figure E-4: Comparison between theoretical and experimental results for Test 6

APPENDIX F

Impact Nosepiece Drawings

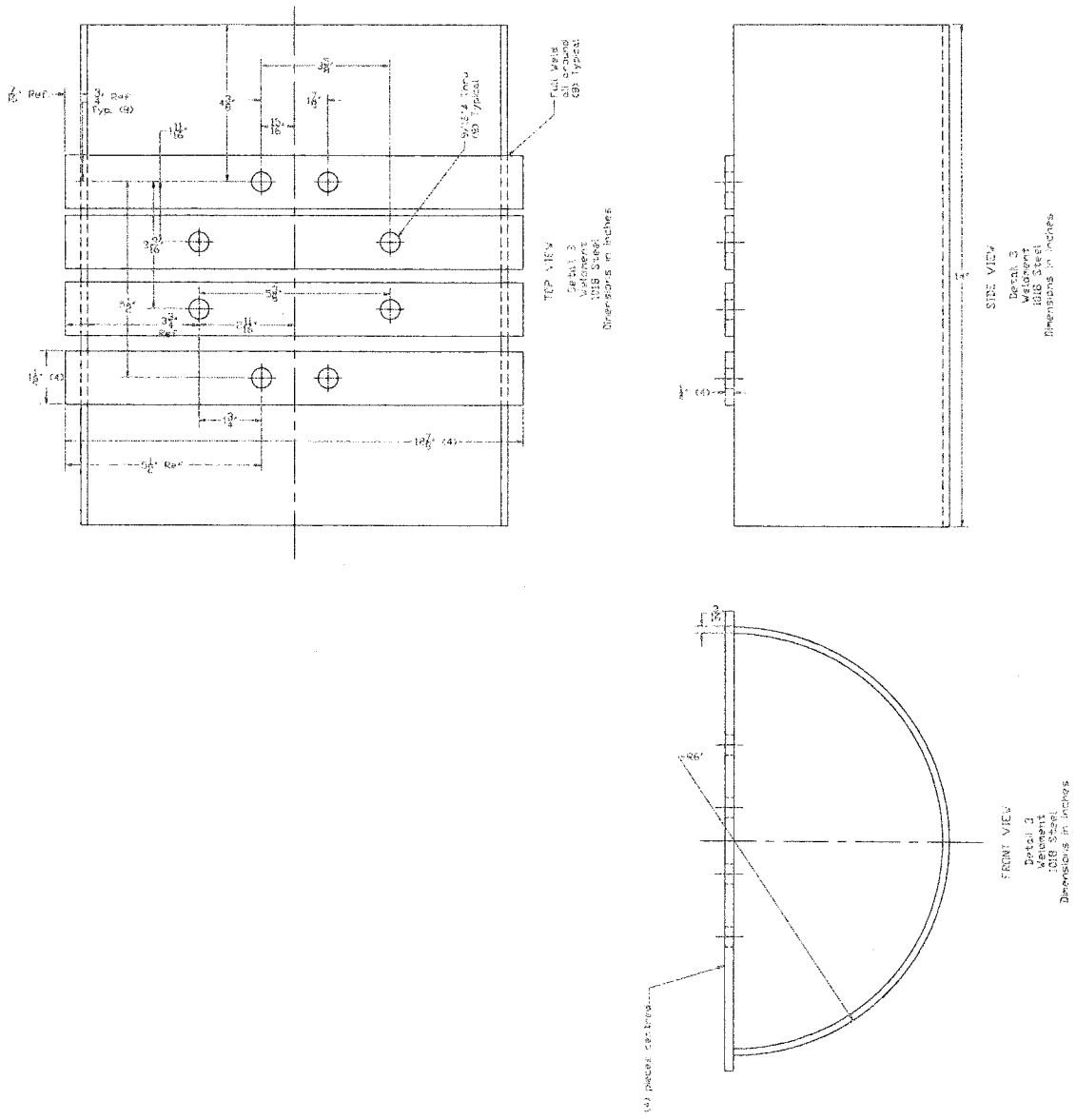

Figure F-1: Drawing overview of impact nosepiece

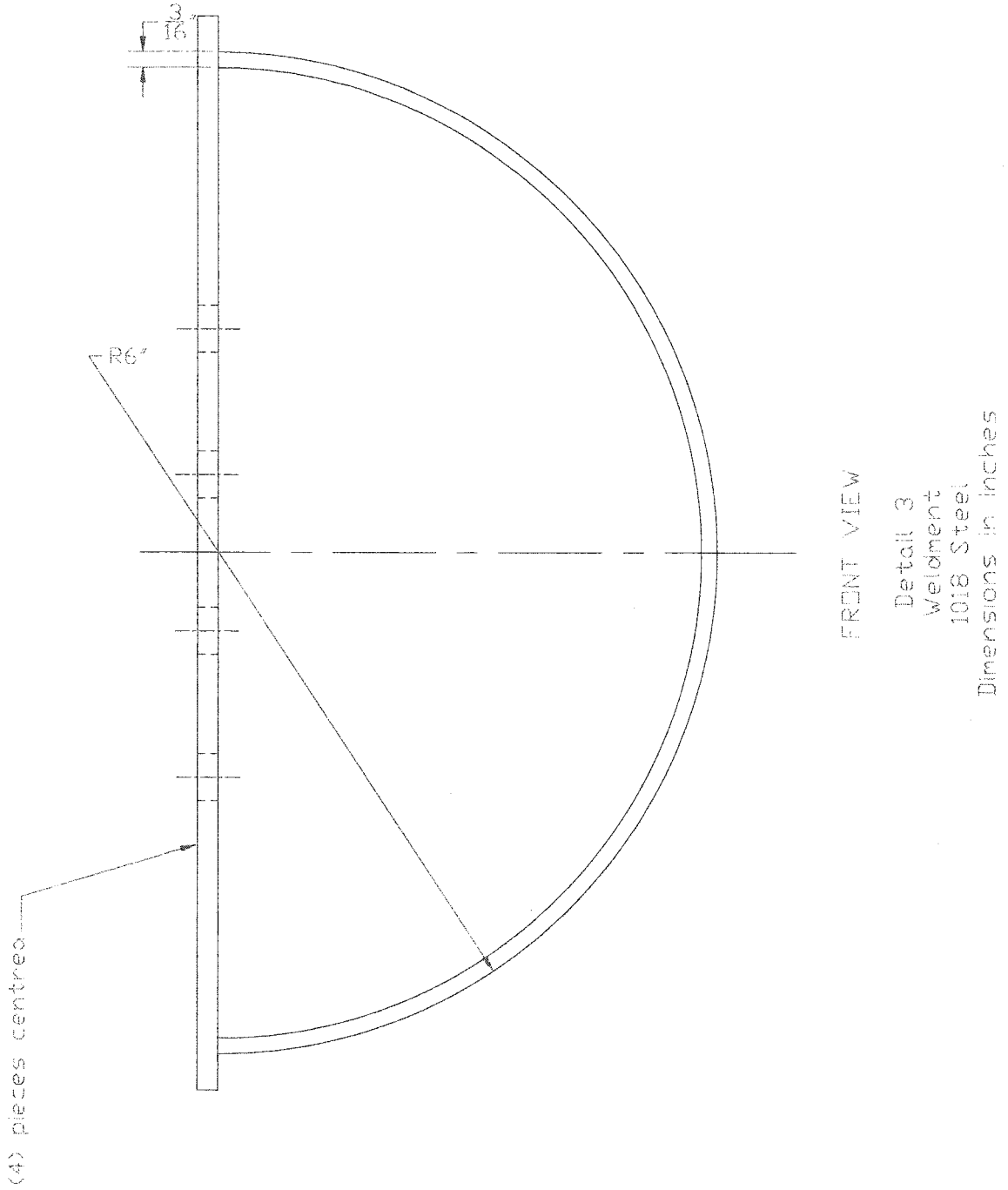

Figure F-2: Impact nosepiece – front view

Figure F-3: Impact nosepiece – side view

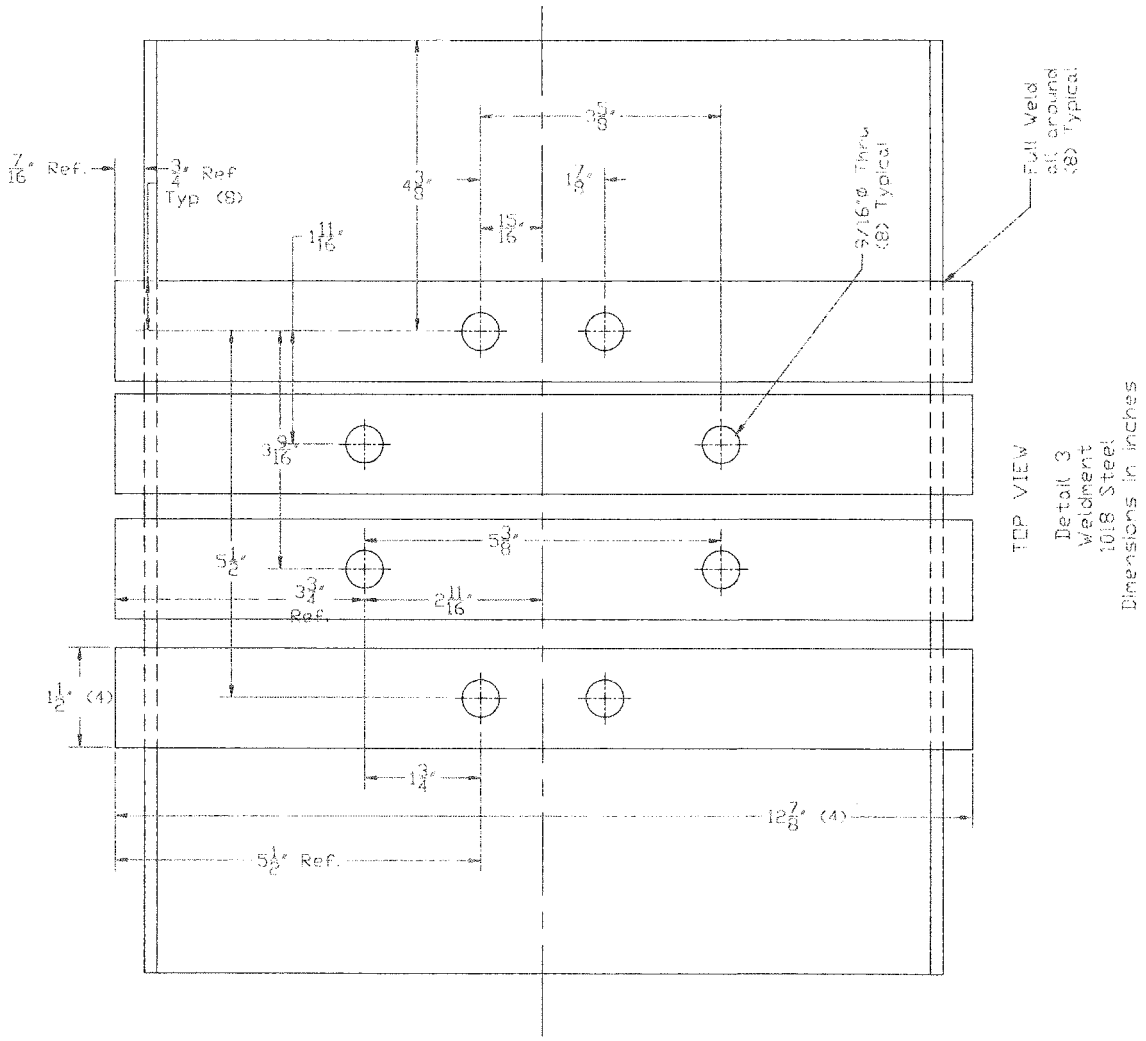

Figure F-4: Impact nosepiece – top view

VITA AUCTORIS

1971	Born in Canada
1994	Bachelor of Applied Science in Mechanical Engineering from the University of Windsor, Windsor, Ontario
1998	Member, Professional Engineers of Ontario
1994 - 2000	Manufacturing Engineer with Ford Motor Company of Canada - Windsor Engine Plant, Windsor, Ontario
2000 - 2003	Lead Manufacturing Engineer with Ford Motor Company of Canada, Windsor Engine Plant, Windsor, Ontario
2003	Currently a candidate for the degree of Master of Applied Science in Mechanical Engineering at the University of Windsor, Windsor, Ontario